Epigenetic and transcriptional regulation of neural development: Scml2 and Ezh2, new functions in health and disease

Inauguraldissertation

Zur Erlangung der Würde eines Doktors der Philosophie vorgelegt der

Philosophisch-Naturwissenschaftlichen Fakultät der Universität Basel

Von

Alberto Loche aus Italien

Basel, 2016

Genehmigt von der Philosophisch-Naturwissenschaftlichen Fakultät auf Antrag von

Prof. Dr. Filippo M. Rijli, (Dissertationsleiter)

Prof. Dr. Paolo Sassone-Corsi, (Korreferent)

Basel, 10 November 2015 Prof. Dr. Jörg Schibler

(Dekan)

Table of Content

Summary **4**

Chapter 1 ..... **6**

Introduction **6**

1.1 Epigenetic and transcriptional regulation in the brain 6

1.2 Basic mechanisms of epigenetic regulation by Polycomb 7

1.3 Epigenetic mutations and human brain pathologies 13

1.4 Genetic and epigenetic basis of epileptic syndromes 19

1.5 Pathways to epileptic syndromes 21

1.6 From brain insult to Polycomb proteins: the first insights 24

References **27**

Chapter 2 ..... **30**

Aim of the thesis **30**

Chapter 3 ..... **31**

Submitted manuscript: Mutations in the Polycomb protein *SCML2* cause a novel human epileptic syndrome by disrupting the inhibitory drive on excitatory neurons. **31**

Methods 54

Supplementary Information 62

Chapter 4 ..... **73**

Published article: EZH2 orchestrates topographic migration and connectivity of mouse precerebellar neurons **73**

Original Article 75

Conclusion and outlook 105

Summary

Neuronal activity is one of the most fascinating and complex properties of living cells, in which a quickly dissolving signal, or a pattern of them, is used to transfer a tremendous amount of information at any given time. This ensemble of signals must be fine tuned through the coupling of this activity patterns with a cell memory system that can ensure neuronal homeostasis and synaptic plasticity in response to mutating stimuli. Epigenetic processes provide an efficient way to transform activity dependent neuronal information into lasting effects on gene expression. Among others, the modification of histones at conserved critical residues is a well described epigenetic mechanism. Polycomb group proteins are some of the major cellular machineries mediating such regulation, and their function has been extensively studied during early phases of development. Nevertheless, their function in post-mitotic neurons is less understood. The broad aim of the present work is to investigate Polycomb protein function in the context of specialized neuronal functions, such as migration and proper establishment of inhibitory synapses. We therefore focused our attention on two proteins, *Ezh2* (a Polycomb Repressive complex 2 subunit) and *Scml2* (a Polycomb Repressive complex 1 variant member).

Epilepsy represents one of the most prevalent and detrimental neurological diseases, characterized by a disregulation of neuronal activity resulting into unpredictable synchronized waves, or seizures, spreading throughout the central nervous system. Evidences from both animal models and from human brain tissue have started to unveil that epilepsy and epileptogenesis can be associated with epigenetic changes. Aim of this work is to describe a novel epileptic syndrome, that opens a door to a new possible mechanism at the basis of activity disregulation in the brain. *SCML2* is a poorly studied gene, which translates into a member of the Polycomb Repressive Complex 1, a master regulator of gene repression and chromatin compaction. By generating mutant mice lacking the SCML2 functional protein, we discovered that its function is important to ensure proper inhibitory inputs onto excitatory neurons. A similar mechanism may be acting in the cortex as well as in the spinal cord, leading to

hyperexcitability and the development of synchronous activity upon challenge. Our analysis provides the first case of a Polycomb protein involved in the pathogenesis of human epilepsy and shed some light into a possible whole new field of investigation, where a deeper understanding of such epigenetic processes will likely lead to exciting new discoveries and possible new treatment options for a highly unmet medical need.

Chapter 1

Introduction

1.1 Epigenetic and transcriptional regulation in the brain

Mammalian transcription is a highly complex process, which controls fundamental aspects of cell diversity and organismal adaptation. Neurons, in particular, exhibit remarkable specialization and plasticity, which is mediated, in part, by activity dependent changes in gene expression[1]. One method to control activity-dependent gene expression is modulating the accessibility of genes to the transcriptional machinery via alterations in chromatin structure, the mechanisms of which are still poorly understood[2]. The exploration of brain epigenomes, which consist of various types of DNA methylation and covalent histone modifications, as well as high order chromatin structures and topologically organized domains, is providing new and unprecedented insights into the mechanisms of neural development, neurological disease and aging[3]. Chromatin regulators contribute to dynamic changes in gene expression but also maintain cell fates by providing stable, heritable states of gene expression. Many chromatin regulators have been demonstrated to be essential for developmental processes, including the development of the brain[4].

Several major events and processes must be precisely orchestrated during normal brain development and failure to properly regulate these processes, due to a genetic or environmental insult, can result in cognitive deficits and other features of neurodevelopmental disorders. A consensus is emerging on the role of chromatin regulatory mechanisms as key players in several of the major events during neural development. In this context, the repressive function mediated by the Polycomb protein family, forming functional complexes named Polycomb Repressive

Complexes (PRCs), is a well-established necessary function that enables embryonic mouse development as well as maintenance of stem cell identity and execution of differentiation programs. At the present time, several studies have described neuronal specific functions of Polycomb group proteins at the early stages of life, and an increasing body of literature begin to unveil their specialized role during adulthood in complex processes, such as puberty[5] or synaptic plasticity[6].

1.2 Basic mechanisms of epigenetic regulation by Polycomb

A fast increasing body of evidences point at a crucial role for Polycomb Group Proteins in a wide variety of molecular mechanisms, ultimately impacting the vast majority of physiological processes in health and disease.

Polycomb Group Proteins have been classically characterized as epigenetic repressors, acting through their biochemical activity on histone proteins. Polycomb proteins have been divided in two major Repressive Complexes, the Polycomb Repressive Complex 1 (PRC1) and the Polycomb Repressive Complex 2 (PRC2). PRCs are etero-multimeric protein complexes with a core cathalitical component and several variable accessory proteins. A key feature of these complexes is that their gene targeting depends on previously established chromatin states at that locus[7]. In particular PRCs catalyze the chemical modification of histone tails at different residues, and these modifications, in turn, are fundamental for subsequent binding of downstream effectors or simply modify the overall chemical properties of chromatin, therefore being key to its compaction and accessibility. The two major groups of PcG protein complexes exhibit distinct enzymatic activities: Polycomb repressive complex 2 (PRC2) catalyses di- and tri-methylation of histone H3 at lysine 27 (H3K27me2/3), and Polycomb repressive complex 1 (PRC1) catalyses monoubiquitination of histone

H2A at lysine 119 (H2AK119ub1) and/or compacts chromatin.

Polycomb repressive complex 1 (PRC1) has a core of four proteins. In Drosophila melanogaster, these components are: Polycomb (Pc), with trimethylated histone H3 lysine 27 (H3K27me3) binding activity, Polyhomeotic (Ph), *Sex combs extra* (*Sce*) and Posterior sex combs (Psc). PcG complexes are generally simpler in *Drosophila* than in mammalian cells, where alternate subunit compositions create larger families of related PRC1-type and PRC2-type complexes. There are at least six distinct groups of mammalian PRC1 complexes, PRC1.1–1.6, each comprising one of six Polycomb group RING fingers (PCGFs), and the E3 ligase RING1A/B[8].

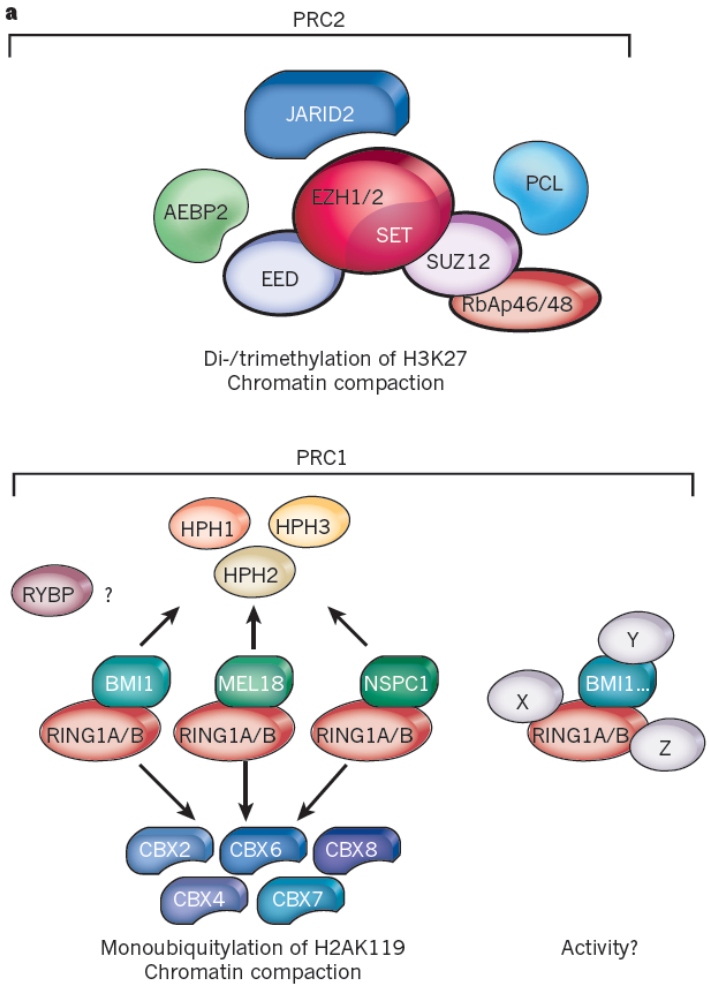

Figure 1. **Schematic representation of the subunit composition of the mammalian**

This complexity presents an ongoing challenge to sort out precisely which biochemical functions depend upon which subunits and family members. The same scenario is true for the PRC2, where the core PRC2 complex, which is conserved from *Drosophila* to mammals, comprises four components: EZH1/2, SUZ12, EED and RbAp46/48 (also known as RBBP7/4). Notably, the PRC2 components, in contrast to those of PRC1, underwent little duplication in mammals, with vertebrates containing two copies of enhancer of zeste homologue, EZH1 and EZH2. They target the same genes and are thought to contribute to the repression of the same pathway[9]. In addition to the four core members, other proteins transiently interact with PRC2 (for example, DNMTs, HDAC1, SIRT1and SCML2), but their effect on PRC2 function is unclear and needs further investigation.

Nevertheless, certain core PcG complex activities, conserved from flies to humans, have been defined (as Sce in Drosophila, see table 1). Studies conducted in flies provide evidences that PRC1 basic molecular mechanism of gene repression, is more complex and variable than what proposed in the classical model of H2AK119ub1 deposition. In fact, it has been shown that repression does not always require H2A ubiquitylation. The repressive activity associated with PRC1 is therefore far more heterogeneous than expected. Moreover, the canonical PRC1 multimer can be partially disassembled without necessarily losing its repressive function as it is demonstrated by the fact that the repression of some genes occurs in the absence of the Pc component, which binds to trimethylated H3K27 (H3K27me3)[10,11]. This evidence also questions the classical vision of the two complexes, PRC1 and PRC2

working together and opens the possibility of many new targets where the several differentially assembled complexes may exert their exclusive and specific H3K27me3 independent gene regulation[12].

As mentioned, the variable components present in mammalian genomes confer to these complexes a great flexibility in carrying out their function onto differential sets of target genes within many different cell types and at different times of development[7].

Drosophila melanogaster subunits	Characteristic domains	Homologous subunits in humans
Polycomb repressive complex 1 (PRC1)		
E3 ubiquitin-protein ligase RING1 (also known as Sce)	RING	RING2 (also known as RING1B and RNF2) and RING1 (also known as RING1A and RNF1)
Posterior sex combs (Psc) and Suppressor of zeste 2 (Su(z)2)	RING	BMI1 (also known as PCGF4) and MEL18 (also known as PCGF2)
Polyhomeotic-proximal (Ph-p) and Polyhomeotic-distal (Ph-d)	Sterile α-motif (SAM) and zinc-finger	Polyhomeotic-like protein 1 (PHC1; also known as EDR1), PHC2 (also known as EDR2) and PHC3 (also known as EDR3)
Polycomb (Pc)	Chromodomain	Chromobox protein homologue 2 (CBX2), CBX4, CBX6, CBX7 and CBX8
Sex comb on midleg (Scm)	Malignant brain tumour (MBT), SAM and zinc-finger	Sex comb on midleg homologue 1 (SCMH1) and Sex comb on midleg-like protein 2 (SCML2)
Polycomb repressive complex 2 (PRC2)		
Enhancer of zeste (E(z))	SANT, CXC and SET (Su(var)3-9–Enhancer of zeste–Trithorax)	Enhancer of zeste homologue 2 (EZH2; also known as KMT6) and EZH1
Extra sex combs (Esc) and Extra sex combs-like (Escl)	WD40	EED
Suppressor of zeste 12 (Su(z)12)	Zinc-finger and VEFS (VRN2–EMF2–FIS2–Su(z)12) box	SUZ12
Chromatin assembly factor 1 subunit Caf1	WD40	Histone-binding protein RBBP4 (also known as RBAP48) and RBBP7 (also known as RBAP46)
Jing	Zinc-finger	Zinc-finger protein AEBP2

Table 1. **PRC1 and PRC2 core complex components in Drosophila melanogaster and humans** (from Schwartz and Pirrotta, Nature Reviews Genetics, 2013)**.**

The understanding of how the recruitment of Polycomb is carried out to target specific genomic sites is of primary importance to understand its several functions. In *D. melanogaster,* recruitment happens due to direct DNA – Protein interactions at the level of discrete and defined sites called Polycomb Response Elements (PREs). Intense investigation has failed to discover a similar mechanism in vertebrates, where

PREs where not found. In contrast, the vertebrate Polycomb complex seems to be directed to target genes by locus-specific interactions or by a more generalized targeting mechanism[13]. Nevertheless. Only few examples provide an unbiased evidence that a locus-specific mechanism, based on transcription factor's DNA binding or on long-non-coding RNA molecules, really exist (ie. E2F, MGA, MAX, JARID2, Xist, etc.) [14-17]. The current model seems to consider this specific interactions as a very specialized function, whereas more general mechanisms of targeting play a role in broader genomic domains. Indeed, in vertebrates seems that Polycomb occupancy very often occurs at CpG rich regions, so called CpG islands (CGIs), which are usually 1 to 2 kb long[18]. Polycomb recruitment at CGIs has been extensively investigated in regard to KDM2B-containing PRC1 complexes, even though several observations suggest that other alternative targeting mechanisms are also in place. Recent advances are also questioning the hierarchical model by which PRC1 complexes would be recruited to chromatin in a PRC2 dependent manner[13,19]. In fact, Blackledge and colleagues have reported that several subtypes of variant PRC1 complexes, artificially targeted to engineered genomic locations, were able to recruit PRC2 complexes, leading to new H3K27me3 deposition in a H2AK119ub1-dependent mechanism *in vivo*. In conclusion, our understanding of Polycomb function is rapidly evolving to a very complex and sophisticated system of several molecular mechanisms that specific cell types in different conditions use to achieve fine tuned gene regulation. Non canonical complexes generate a wide variety of functions that may well be used as alternative strategies for a coordinated regulation of different gene pools.

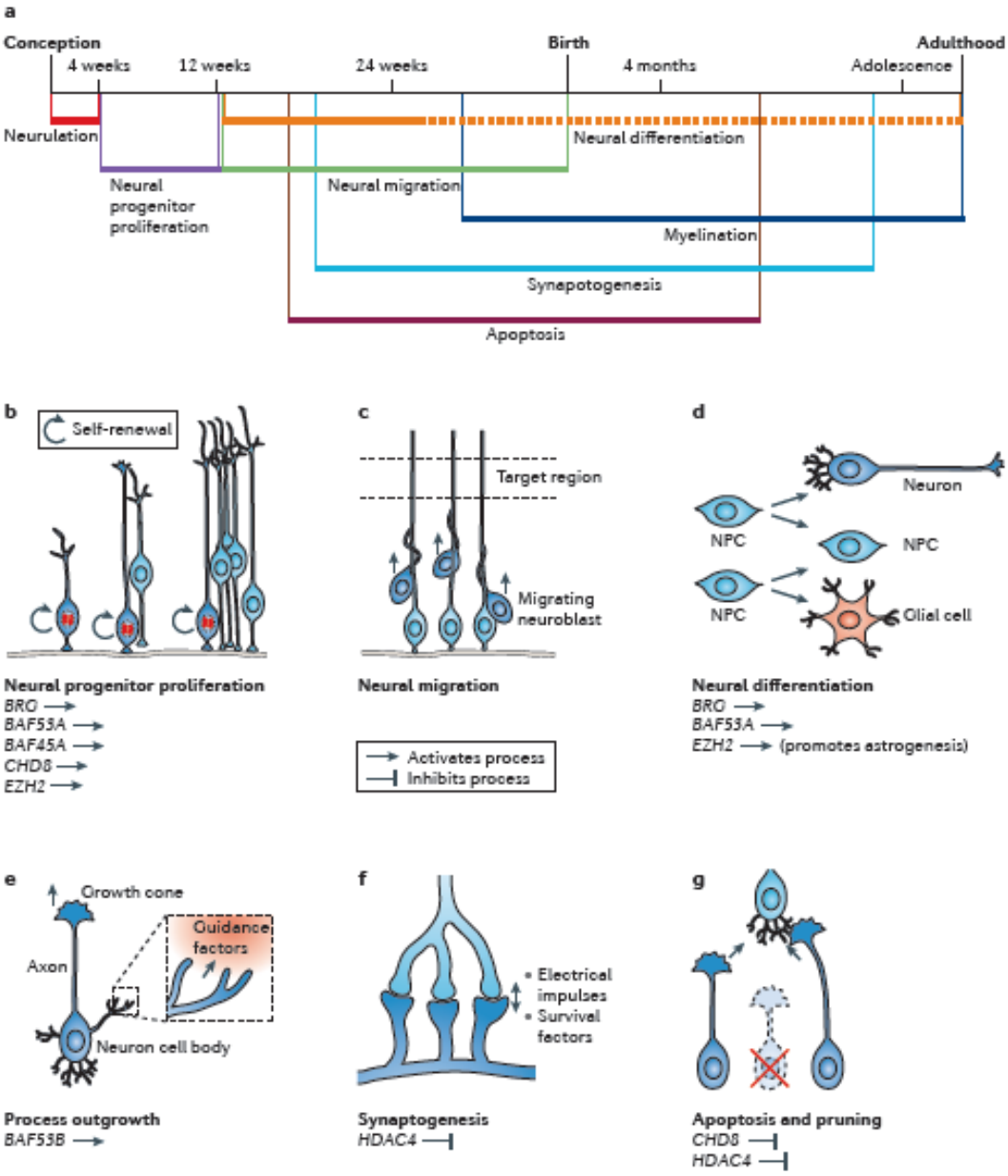

Figure 2. **Chromatin regulators have essential roles throughout neural development.** The fundamental processes of neural development are illustrated. Chromatin regulators discussed in this review are noted under the processes in which they have important roles. The key indicates whether a particular regulator promotes or inhibits each neurodevelopmental process. **a** | A timeline of human neural development. **b** | The development of the vertebrate nervous system begins during gastrulation. In the early embryo, neural progenitor cells undergo symmetrical proliferative division. **c** | With the expansion of the number of cell types and the size

of the nervous system, the cell bodies of both neural progenitors and resulting postmitotic neurons migrate away from their birthplace to appropriate regions in response to environmental cues. **d** Neural progenitors asymmetrically divide to give rise to neurons, glial cells or intermediate progenitors. Neural differentiation generates enormous numbers of diverse cell types in the nervous system. **e** After migrating neurons have reached their destinations, they extend axonal and dendritic processes, which are guided by intricate cellular interactions and guidance molecules to appropriate target regions, where they further elaborate processes to cover receptive fields and innervate targets. **f** Mature synapses are formed between neurons that are connected to each other. Synaptogenesis begins during embryonic development, but subsequent synaptic stabilization and plasticity occur throughout life and are adaptive to learning experiences and other activity-dependent environmental inputs. **g** Active apoptosis and local degenerative pruning events maintain and refine established neuronal morphologies and neural circuit assembly. NPC, neural progenitor cell. (from Ronan et al., Nature Reviews Genetics, 2013)

1.3 Epigenetic mutations and human brain pathologies

Next Generation Sequencing technologies and new analytical tools are driving at a fast pace the transition to a new way of moving from the leads offered by human pathologies to the generation and study of the causal links that current model organisms offer. Thanks to these advancements, the roles of chromatin and chromatin remodelers in neural development are rapidly emerging from human disease studies. [4]. In fact, several pathological brain conditions and psychiatric disorders have been linked to mutated chromatin regulators such as autism spectrum disorder (ASD) and schizophrenia, not to mention the many other complex syndroms. Tables 1[3] and 2[4]

provide a good example of the diversity of epigenetic regulators involved in such disorders. These lists include embryonic defects, multiorgan disorders and neurological syndromes that show symptom onset at very different stages of life. This observation implies that, either brain-specific, neuron-specific or even neuronal subpopulation-specific epigenetic mechanisms function, is crucial for proper brain function at post developmental stages and/or the disruption of such mechanisms early in an individual's life leads to pathologic manifestation only many years later. This may be due to the long lasting intrinsic feature of many epigenetic modifications, such as DNA methylation or high order permissive or repressive chromatin domains. Once in place they may well be responsible for long lasting effect on proper gene expression and regulation in the nervous system. DNA methylation has been long studied in the context of some neurodevelopmental syndromes, the most relevant example being the Rett Syndrome, caused by mutations in the gene MeCP2[20]. It is beyond the scope of the present work to review the broad literature about the involvement of defective DNA methylation in neural developmental defects, nevertheless it represents the first example of the involvement of epigenetic regulation in the etiopathology of a cognitive disease.

If we consider instead the role of histone covalent modifications in neurodevelopmental syndromes, we see examples of a early childhood diseases, such as Coffin-Lowry syndrome[21], or neurodegeneration and regression beginning after adolescence (as in Kleefstra syndrome)[22] or other examples occurring very in life, as hereditary sensory and autonomic neuropathy type 1, (HSAN1) with early-onset dementia[3]. It is indeed only recently that evidences accumulated about the remarkable plasticity that chromatin epigenetic states retain even long after the exit of the neuronal cells from the cell cycle[23,24]. This observation clearly explains why

mutations in chromantin regulators that are redundant and/or dispensable for early development may acquire unique and specific functions in the adult nervous system, and their mutations selectively affect only some neuronal populations or specific circuits. Even though it is believed that all the epigenetic modifications are reversible, available data show an accumulation of repressive epigenetic marks in the aging brain. This phenomenon is accompanied by the progressive downregulation of neuronal genes[25,26]. It is therefore not hard to imagine a role for Polycomb repressive complexes during this process, which we just begin to understand. In fact, an age dependent modulation of epigenetic state has been reported also with respect to histone covalent modifications, such as H3K4me3 and the PRC2 mark H3K27me3[27]. Importantly, global levels of repressive Polycomb mediated histone marks did not correlate with transcription, but were nonetheless increased in the aging brain[27] as well as in another model of accelerated brain senescence with cognitive abnormalities(Chun Mei Wang et al.). The dissection of epigenetically driven molecular cascades involving the role of key histone modifiers in post mitotic neurons has shed light on some of their notable function. As key events in the life of a post mitotic neuron, we will consider its migration from the birthplace to its final location, as well as the establishment of proper synaptic connectivity in order to form functional circuits. Mutations affecting both mechanisms have been linked to several neurological and psychiatric disorders. Interestingly, inactivation of the chromatin remodeler ATRX in the mouse was found responsible of a striking increase in neuronal apoptosis during early stages of corticogenesis[28]. In human patients, mutations of ATRX leads to severe cognitive impairment and autism. Nevertheless, the molecular cascade that link, on one side, *ATRX* disfunctions in the nucleus to, on the other side, the observed neurological phenotypes, remains to be elucidated[3]. The

problem exemplified by ATRX is common to several of the chromatin regulators found mutated in other neurodevelopmental disorders (Table 1 and Table 2). It is now evident the lack of understanding of the pathways that, downstream of epigenetic regulators, control in a cell specific manner the connectivity and function of sub-circuit elements which ultimately represent the causal knot of the underlying pathology. Interestingly, mutations of several chromatin regulators playing a role in a neurodevelopmental context are also involved in human cancer. BRG *and* BRM*, in example, two highly homologous members of the BAF complex,* are found frequently mutated in different tumors, such as medulloblastoma, which is a brain cancer as well as in neurodevelopmental syndromes (reviewed in ref. 17). It seems that BRM and BRG, even though mostly found co-expressed in the same tissues and cell types, may carry out different functions in neural development, since similar mutations cause different disorders. Moreover, mutations in EZH2, a member of the PRC2, identified in patients with Weaver's syndrome, a disease characterized by general overgrowth and several neurological abnormalities, such as speech delay, seizures, mental retardation, hypotonia or hypertonia, and behavioral problems, are, in other cases, leading to cancer. Although EZH1 and EZH2 are thought to be highly redundant, up to date no disease have been found caused by EZH1 mutations, underlying once again the cell specific functions that likely lay behind pathological mutations of these epigenetic regulators. The striking correlation, exemplified by EZH2 or by several members of the BAF complex, between cancers and neurological diseases once more points at the importance of the characterization of the common pathways leading to very diverse diseases.

The study of SCML2 (see Chapter 3), a component of variant PRC1 complexes, is well engraved in this paradigm. In fact, even though poorly studied, SCML2 has been

implicated, together with other MBT (Malignant Brain Tumor) containing homologues proteins, in medulloblastoma[29]. Nevertheless, its function was only investigated in the context of spermatogenesis, leaving unexplained the possible role that SCML2 may be playing in the brain.

Despite observations of dynamic PcG activity in postmitotic neurons, few studies have addressed the role of PcG-mediated repression in neurological disease, and none in epilepsy. Moreover, several mutations occurring in chromatin regulators leads to Autism Spectrum Disorders (see Table 1 and Table 2), which are well known to be often co-morbid with seizures and epilepsy. In the present work, we aim at shading some light into SCML2 function, starting from two rare mutations that we have found by whole-exome sequencing (described in Chapter 3) in severely affected patients with a novel epileptic syndrome.

Gene	OMIM (gene)	Function	Syndrome(s)	OMIM (phenotype)
ATRX (Xq21.1)	300032	Replication-independent nucleosome remodeling and histone H3.3 incorporation	ATRX; autism[40]	301040
CREBBP (16p13.3); *EP300* (22q13.2)	600140; 602700	Transcriptional coactivator; histone acetyltransferase	Rubinstein-Taybi syndrome (RSTS) 1 and 2 (ref. 105)	180849 (RSTS1); 613684 (RSTS2)
DNMT1 (19p13.2)	126375	DNA methyltransferase; disease mutations are associated with hypomethylated repeats and promoters	Hereditary sensory and autonomic neuropathy type 1 with adult-onset dementia[5]; ADCA-DN[6].	614116
DNMT3B (20q11.21)	602900	DNA methyltransferase; disease mutations are associated with hypomethylation of pericentric repeats	ICF1 mental-retardation syndrome[28,106]	242860
ZBTB24 (6q21)	614064	Transcriptional repressor and regulator of DNA methylation at pericentric repeats	ICF2 mental-retardation syndrome[28,29]	614069
KDM5C (Xp11.22)	314690	Histone H3K4 demethylase	X-linked mental retardation[107]; autism[108]	300534
EHMT1 (9q34.3)	607001	Histone H3K9 methyltransferase	Kleefstra syndrome (mental retardation)[109]; schizophrenia[110]; nonspecific psychiatric phenotypes and neurodegenerative disease in postadolescence period[111]	610253
NSD1 (5q35.2–q35.3)	606681	Histones H3K36 and H4K20 methyltransferase	Sotos syndrome (mental retardation)[112]	117550
PHF8 (Xp11.22)	300560	Histone H3K9 demethylase and transcriptional activator	X-linked mental retardation without cleft lip and/or palate (Siderius-Hamel)[113,114]	300263
RPS6KA3 (Xp22.12)	300075	Serine/threonine kinase (of both histones and nonhistone proteins)	Coffin-Lowry X-linked mental-retardation syndrome[115]	303600
MECP2 (Xq28)	300005	Methyl-CpG–binding protein	RTT and other neurodevelopmental syndromes; autism[116]	312750

Table 2. **Monogenic brain disorders associated with DNA methylation and histone-modification defects.** (from Jakovcevski and Akbarian, Nature Medicine, 2012)**.**

Table 1 | **Chromatin regulators mutated in human mental disorders**

Chromatin regulator*	Disease (or diseases)	Mutations	Chromatin regulator type	Refs
BAF250A (ARID1A; BAF complex)	Coffin–Siris syndrome	Nonsense, frameshift indel	Chromatin-remodelling complex subunit	29
BAF250B (ARID1B; BAF complex)	Intellectual disability, Coffin–Siris syndrome, autism, schizophrenia	Translocation, frameshift indel, nonsense, missense, microdeletion	Chromatin-remodelling complex member	32,33,34, 28,36
BRM (SMARCA2; BAF complex)	Coffin–Siris syndrome, Nicolaides–Baraitser syndrome, schizophrenia	Partial deletion, missense, intronic alteration	Chromatin-remodelling complex ATPase	31,30, 39,40
BRG1 (SMARCA4; BAF complex)	Coffin–Siris syndrome	Missense	Chromatin-remodelling complex ATPase	29
BAF47 (SMARCB1; BAF complex)	Coffin–Siris syndrome, Kleefstra's syndrome phenotypic spectrum	In-frame deletion, missense	Chromatin-remodelling complex subunit	29,108
BAF155 (SMARCC1; BAF complex)	Autism	Missense	Chromatin-remodelling complex subunit	35
BAF170 (SMARCC2; BAF complex)	Autism	Splice site mutation	Chromatin-remodelling complex subunit	35
BAF180 (PBRM; BAF complex)	Autism	Missense	Chromatin-remodelling complex subunit	36
CHD7	CHARGE syndrome, autism	Missense	Chromatin remodeller	36,109
CHD8	Autism	Nonsense, frameshift indel missense	Chromatin remodeller	35,36, 51,52
ATRX	X-linked α-thalassaemia/mental retardation syndrome	Missense	Chromatin remodeller	110
p300	Rubinstein–Taybi syndrome	Large deletions and duplications, missense	Histone acetyltransferase	111
CBP	Rubinstein–Taybi syndrome	Microdeletions, nonsense	Histone acetyltransferase	112
KAT6B (MYST4 or MORF)	Say–Barber–Biesecker–Young–Simpson syndrome (SBBYSS or Ohdo's syndrome)	Frameshift indel, missense	Histone acetyltransferase	113
HDAC4	Brachydactyly mental retardation syndrome	Balanced chromosomal translocation; deletion	Histone deacetylase	87,88
EZH2	Weaver's syndrome (learning disability)	Missense, frameshift indel	Histone methyltransferase	74,75
EHMT1	Kleefstra's syndrome phenotypic spectrum; autism	Microdeletions, nonsense, frameshift, missense	Histone methyltransferase	36,108, 114
MLL	Wiedemann–Steiner syndrome	Nonsense	Histone methyltransferase	115
MLL2	Kabuki's syndrome	Nonsense, frameshift	Histone methyltransferase	116,117
MLL3	Autism, Kleefstra's syndrome	Missense, nonsense	Histone methyltransferase	35,36,108
KDM5C (JARID1C)	Non syndromic X-linked mental retardation	Missense, frameshift, nonsense, intronic alteration	Histone lysine demethylase	118,119
PHF8	X-linked mental retardation	Missense mutation, nonsense	Histone lysine demethylase	120,121
HUWE1	XLMR Turner type	Duplications, missense, copy number gains	Histone ubiquitylation	122
MECP2	Rett's syndrome, Angelman's syndrome, nonsyndromic X-linked mental retardation, autism	Missense, nonsense, frameshift indel, duplication	DNA methylation binding protein	123,124
MBD5	Autism, Kleefstra's syndrome	Frameshift indel, nonsense	DNA methylation binding protein	35,36,108
MED12	Lujan–Fryns syndrome, FG syndrome (also known as Opitz–Kaveggia syndrome)	Missense	REST mechanism for disease, Mediator complex subunit	125,126
MED23	Non-syndromic intellectual disability	Missense	Mediator complex subunit	127
PHF21A (BHC80)	Intellectual disability, craniofacial anomalies	Translocation and deletion	Chromatin reader, histone deacetylase complex member	128

*Protein aliases are given in brackets; if the protein is a member of a complex, the complex name is also given in brackets. EZH2, enhancer of zeste 2; HDAC4, histone deacetylase 4.

Table 3. **Chromatin regulators mutated in human mental disorders.** (from Ronan et al., Nature Reviews Genetics, 2013)**.**

1.4 Genetic and epigenetic basis of epileptic syndromes

Epileptic encephalopathies are a group of partially overlapping neurological syndromes where patients are affected by psychomotor dysfunctions and severe clinical epilepsy, often with infantile spasms[30]. After for long time being considered a non genetic disease, it is now known that genetic mutations are the basis of most neurodevelopmental syndromes. Nevertheless an increased effort should be made to increase the number of studies, and samples within studies, in order to achieve a useful understanding of the pathogenesis of epileptic syndromes leading to possible cures. To complicate this effort, despite the steep advancement of molecular biology techniques, two main obstacles remain. The first one is the etherogeneity of human conditions characterized by the development of seizures and epilepsy, and the second one is the partial penetrance that many mutations display. De novo mutations often represent the cause of neurodevelopmental disorders, and offer the possibility for researchers to have an entry point into the investigation of molecular mechanisms of the disease. On the technical side, an additional hindrance is represented by the natural occurrence of de novo mutations also in healthy individual[30]. Only in recent years, our understanding has taken a leap forward thanks to novel research on mechanisms that regulate neuronal excitability or modulate circuit activity. The molecular deficiencies contributing to neuronal dysfunction in epilepsy are now beginning to be clarified but it is still missing a general approach to the study of altered function at the circuit level and a systemic investigation of the dysfunctional molecular pathways, likely arising in the cell nucleus, leading to the generation of seizures. Moreover, a big open question is how increased synchrony in local microcircuits, often undetectable, following an initial sensory input or an insult then is

able to travel throughout the cortex and reach distal regions of the brain[31]. A plethora of studies have shown the basic principles of seizures generation, as either caused by mechanisms that ultimately activate synaptic and voltage-gated excitatory currents, or, by contrast, down regulate synaptic and voltage-gated inhibitory currents. Not surprisingly, such impairments of the inhibitory/excitatory balance lead to seizures. The reality nevertheless show us that epilepsies are not characterized by permanent states of neuronal excitation but rather by a constant increased probability for a seizure to take place[32]. In fact, with the exception of the most severe cases, in the great majority of epileptic patients seizures represent less than 1% of the total nervous system activity[33]. The needed expansion of our theories describing epileptogenesys have therefore to take into account that such network imbalances are usually compensated for and not present at steady state, neither in animal models nor in the majority of epileptic patients. Although probably not causal for ictogenesis, the steady state of a brain's circuit might be a permissive factor that increase seizure probability, as exemplified by diseases such as autosomal dominant nocturnal frontal lobe epilepsy[34] or catamenial epilepsy[35]. If instead we have a look at the molecular level, mutations in both pre- and postsynaptic proteins indeed support the model in which an imbalance of inhibition versus excitation deriving from misregulated synaptic plasticity may lead to the transition from high, but physiological, levels of neural activity into epileptic activity. This model of synaptically driven activity-dependent disinhibition would have a similar effect of that of a dysregulation of ionic concentrations in the epileptic neurons, in fact supported by several studies reporting human epilepsies due to mutations affecting calcium, potassium, protons and/or chloride ionic gradients[36,37]. It is believed that in healthy people the activity-dependent modification of synapses (short term plasticity) or the dysregulation of ion gradients

never generate a self-reinforcing, positive feedback cycle of increased activity, disinhibition and consequent further increases in activity, therefore not resulting in seizures or ultimately, epilepsy.

1.5 Pathways to epileptic syndromes

If activity dependent shifts in short term synaptic plasticity may underlie the generation of seizures, it still needs to be discussed the case of abnormal excitation that may, alone or in combination with the aforementioned mechanisms, contribute to the epileptic phenotypes. With respect to the molecular mechanisms possibly leading to iperexcitability, data are available reporting a number of mutations in the PI3K, IGF and mTOR pathway (Fig.3). These mutations associate with complex brain malformations that usually come with epilepsy. Upregulation of this pathway may cause an excessive synaptic connectivity leading to epilepsy[38]. Similarly, several pathways controlling the proper specification and migration of inhibitory interneurons have been show to play a fundamental role in keeping excitation in check. Indeed, as it is the case for mutants in *ARX*, or aristaless related homeobox gene, failure to reach the final destination after migration and finally properly integrating into newly formed neural circuits, is crucial for keeping a correct inhibitory/excitatory balance[39]. In other cases, after proper migration, a specific subclass of inhibitory interneurons was found to be unable to carry out its function by properly inhibiting its target cells. An example of this kind of disorders affecting the class of Parvalbumin Interneurons is represented by mutations in *SCN1A*[40]. Proper inhibition is established by specialized neurons that, after being generated in the ganglionic eminences at prenatal stages of development, migrate to their final location and integrate themselves into newly

forming circuits. Different subclasses of inhibitory interneurons are known to target different excitatory neurons on either the cell soma, the axonal tract of the dendrites, in this way assuring a fine regulation of neural transmission.

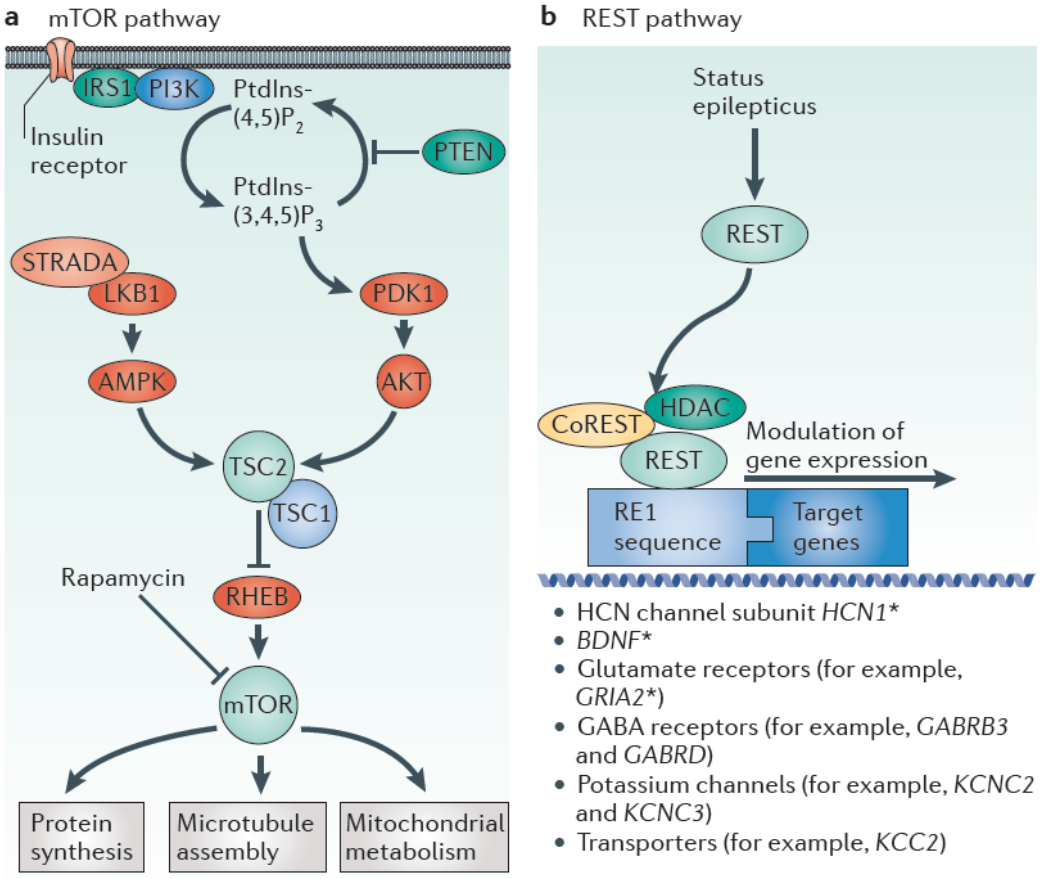

***Fig. 3* Schematic representation of the mTOR and thr REST pathways**

Ultimately, after proper specification, migration and connectivity, the neurons must retain the functional property of assuring a response to external excitatory and inhibitory stimuli by modulating several cellular parameters, such as neurotransmitter synthesis, vesicle trafficking, synapse stabilization or elimination etc. In this process, called homeostasis, the neuronal cell has to put in place feedback and signaling mechanisms in order to be able to fuction in a constantly changing network. Conditions that generate an excess of neuronal activity are thought to lead to

downregulation of excitatory current; on the other side an upregulation of inhibitory currents will occur under circumstances of persistent reduced excitation[41]. Several intracellular pathways have been shown to contribute to neuronal homeostasis. Aim of this introduction is to provide an overview of the known mechanisms that will allow for a deeper understanding of the following chapters. Attention will be therefore given to pathways that have discovered a possible epigenetic link in the context of neuronal homeostasis in an activity dependent manner. At the present time, two pathways have directly or indirectly been implicated in the epigenetic adaptive response of neuronal cells to prolonged excitation. The first pathway involving epigenetic regulators clearly playing a role in epileptogenesys is involving the repressor element 1 (RE1)- silencing transcription factor (REST; also known as neuron-restrictive silencer factor (NRSF). REST negatively regulates the expression of many neuronal genes in non- neuronal cells and neuronal precursor cells. It also regulates neuronal gene expression in mature neurons[2]. REST binds to the co-repressors CoREST and mSin3A, which in turn recruit histone deacetylase 1 (HDAC1) and HDAC2. By regulating chromatin structure these deacetylases repress the expression of hundreds of neuronal genes. About 2,000 genes have REST-binding motifs, nevertheless REST could potentially bind many more sites, including ~10% of all neuronally expressed genes, some of which encode proteins that are fundamental regulators of neuronal excitability and have been independently associated to epileptic mechanisms. These genes include several key components of the inhibitory post-synaptic structure, such as type A GABA ($GABA_A$) receptor β3 subunit (*GABRB3*), $GABA_A$ receptor δ-subunit (*GABRD*) or other channels such as the ionotropic AMPA2 glutamate receptor (*GRIA2*). Also *BDNF* and genes encoding hyperpolarization-activated cyclic nucleotide-gated (HCN) channel subunits 1–4

(*HCN1–HCN4*) have been reported as targeted by REST following status epilepticus. Evidences are accumulating, in fact, that status epilepticus could account for the reactivation of REST in order to suppress important mediators of neuronal excitability. The REST pathway, as well as the mTOR pathway, are very exciting new potential targets for intervention in the epileptogenic process. The most prominent unanswered question is indeed to determine if activation of the REST or mTOR pathways are a primary mechanisms of epileptogenesis or rather just a consequence of this pathological process. Either way, epigenetic targets may well represent the new avenue to treatments for a number of unresponsive cases of epilepsy.

1.6 From brain insult to Polycomb proteins: the first insights

In the recent years, some insights have been provided into the role that epigenetic regulators of the Polycomb family may play in neurological diseases, including epilepsy. In fact, few hints from a handful of studies are starting to call for a deeper understanding of these mechanisms. The lead begins from the existing remarkable link between stroke and epilepsy. From the point of view of the epigenetic mechanisms, it needs to be noted that the REST pathway is a common response to neural insults. Indeed, both ischemic insults and seizures have been shown to activate the otherwise silent REST transcription[42].

REST have been shown to repress the expression of miR9 and miR124[43], which in turn is necessary to drive the transition to a neurogenic BAF complex[44] (Fig. 6) (reviewed in Ronan and Crabtree, 2013). But where are the Polycomb Complexes, (PRC1 and PRC2) involved? Recent data show that occupancy of PRC1 and PRC2

complexes on chromatin inversely correlate with the presence of remodeling complex such as REST or BAF[45]. In addition to this observation, more direct evidence are arising from in vivo model stroke and epilepsy. In a model of Ischemic Tolerant brain, SCMH1, a member of the Polycomb Repressive complex 1, was unbiased found upregulated by quantitative mass spectrometry[46]. The same study shows that SCMH1 and BMI1 (another member of the same complex) bind to the promoter of two notable potassium channels, Kcna5 and Kcnab2. Moreover, knockdown or overexpression of either of the PRC1 proteins shows a significant alteration in potassium currents. Both Kcna5 and Kcnab2 have been found mutated in human pathologies, and specifically Kcnab2 was found mutated in a epileptic syndrome, the so called Monosomy 1p36[47]. Homozygous mutations of this channel in the mouse have shown cognitive defects in the form of impaired learning and amygdala hyperexcitability[48]. In another study, found that Polycomb proteins were ether iper- or hypomethylated after intraperitoneal injection of Kainic Acid, a wifely used model of induced status epilepticus[49]. Included in a rather short list of differentially methylated genes were *PhC2, Suz12 and sfmbt2*. Independently, it has been shown PRC1 and PRC2 genes respond to Kainic Acid administration in the murine hippocampus. In fact, effects on transcripts levels of PRC1 and 2 were already visible after 1 hour from the treatment. The genes where firstly upregulated after 1 hour, then downregulated in following measurements after 2, 8 and 12 hours. These data altogether suggest an involvement of Polycomb Group Proteins in mechanisms related to either the genesis of status epilepticus or the tolerance to brain insults. Again, the fundamental question of whether certain epigenetic states act in favor of the subsequent development of hyper synchronous neural activities, characteristics of status epilepticus, or they represent a consequence of such activities, deriving from altered neural networks remain unanswered. Either way, Polycomb proteins, and more in general epigenetic mechanisms may well represent new targets for the many

untreatable forms of human epilepsies. Further work is needed to precisely elucidate these epigenetic mechanisms. In the work presented in this thesis, the role of another member of the PRC1, *SCML2*, homologous to the previously mentioned *SMCH1* and *Sfmbt2*

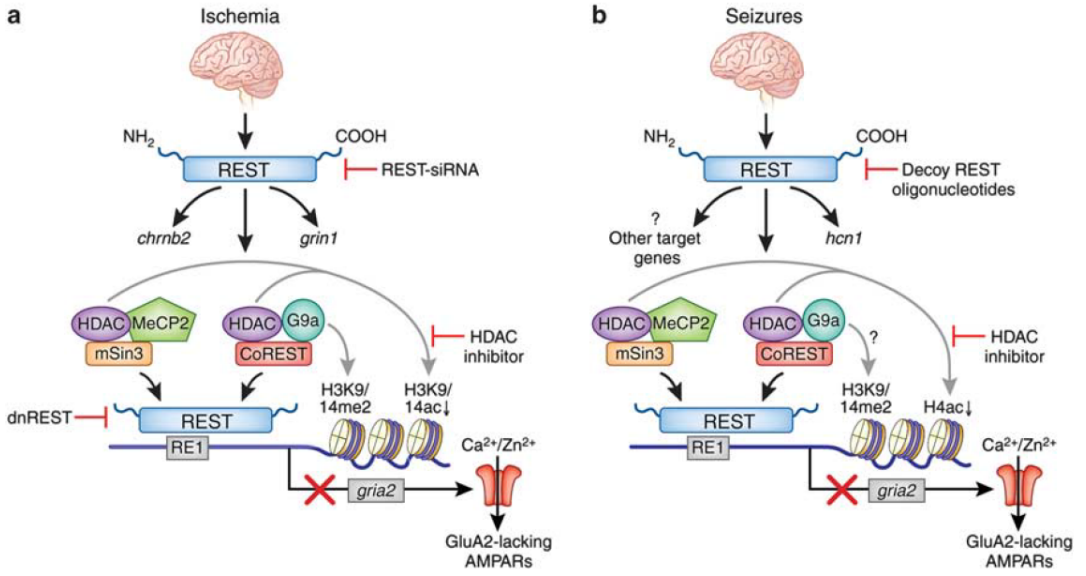

***Fig. 4* Epigenetic mechanisms of stroke and epilepsy.** Model showing REST-dependent epigenetic remodeling of the gria2 promoter in response to ischemic stroke or seizures. Global ischemia (left) or seizures (right) activate REST. REST binds to the RE1 element within the promoter of its target gene *gria2* and recruits mSin3A and CoREST, HDACs-1/2, G9a and MeCP2. The REST-corepressor complex promotes epigenetic remodeling of core histone proteins at the *gria2* promoter. This, in turn, represses GluA2 expression, leading to formation of GluA2-lacking, Ca^{2+}-permeable AMPARs. (from Hwang et al., *Neuropsychopharmacology Reviews*, 2013).

References

1. Greer, P. L. & Greenberg, M. E. From Synapse to Nucleus: Calcium-Dependent Gene Transcription in the Control of Synapse Development and Function. *Neuron* **59,** 846–860 (2008).
2. Borrelli, E., Nestler, E. J., Allis, C. D. & Sassone-Corsi, P. Decoding the Epigenetic Language of Neuronal Plasticity. *Neuron* **60,** 961–974 (2008).
3. Jakovcevski, M. & Akbarian, S. Epigenetic mechanisms in neurological disease. *Nat. Med.* **18,** 1194–1204 (2012).
4. Ronan, J. L., Wu, W. & Crabtree, G. R. From neural development to cognition: unexpected roles for chromatin. *Nature Publishing Group* **14,** 347–359 (2013).
5. Lomniczi, A. *et al.* Epigenetic control of female puberty. *Nat Neurosci* **16,** 281–289 (2013).
6. Södersten, E. *et al.* Dopamine Signaling Leads to Loss of Polycomb Repression and Aberrant Gene Activation in Experimental Parkinsonism. *PLoS Genet* **10,** e1004574 (2014).
7. Schwartz, Y. B. & Pirrotta, V. A new world of Polycombs: unexpected partnerships and emerging functions. *Nature Publishing Group* **14,** 853–864 (2013).
8. Gao, Z. *et al.* An AUTS2–Polycomb complex activatesgene expression in the CNS. *Nature* **516,** 349–354 (2014).
9. Shen, X. *et al.* EZH1 Mediates Methylation on Histone H3 Lysine 27 and Complements EZH2 in Maintaining Stem Cell Identity and Executing Pluripotency. *Molecular Cell* **32,** 491–502 (2008).
10. Gutierrez, L. *et al.* The role of the histone H2A ubiquitinase Sce in Polycomb repression. *Development* **139,** 117–127 (2011).
11. Leeb, M. *et al.* Polycomb complexes act redundantly to repress genomic repeats and genes. *Genes & Development* **24,** 265–276 (2010).
12. Schwartz, Y. B. *et al.* Genome-wide analysis of Polycomb targets in Drosophila melanogaster. *Nat. Genet.* **38,** 700–705 (2006).
13. Blackledge, N. P., Rose, N. R. & Klose, R. J. Targeting Polycomb systemsto regulate gene expression: modifications to a complex story. *Nature Publishing Group* 1–7 (2015). doi:10.1038/nrm4067
14. Ogawa, H., Ishiguro, K.-I., Gaubatz, S., Livingston, D. M. & Nakatani, Y. A complex with chromatin modifiers that occupies E2F- and Myc-responsive genes in G0 cells. *Science* **296,** 1132–1136 (2002).
15. Gao, Z. *et al.* PCGF Homologs, CBX Proteins, and RYBP Define Functionally Distinct PRC1 Family Complexes. *Molecular Cell* **45,** 344–356 (2012).
16. da Rocha, S. T. *et al.* Jarid2 Is Implicated in the Initial Xist-Induced Targeting of PRC2 to the Inactive X Chromosome. *Molecular Cell* **53,** 301–316 (2014).
17. Sarma, K. *et al.* ATRX Directs Binding of PRC2 to Xist RNA and Polycomb Targets. *Cell* **159,** 869–883 (2014).
18. Deaton, A. M. & Bird, A. CpG islands and the regulation of transcription. *Genes & Development* **25,** 1010–1022 (2011).
19. Blackledge, N. P. *et al.* Variant PRC1 Complex-Dependent H2A Ubiquitylation Drives PRC2 Recruitment and Polycomb Domain Formation. *Cell* **157,** 1445–1459 (2014).
20. Amir, R. E. *et al.* Rett syndrome is caused by mutations in X-linked MECP2,

encoding methyl-CpG-binding protein 2. *Nat. Genet.* **23,** 185–188 (1999).
21. Pereira, P. M., Schneider, A., Pannetier, S., Heron, D. & Hanauer, A. Coffin-Lowry syndrome. *European Journal of Human Genetics* **18,** 627–633 (2010).
22. Kleefstra, T. *et al.* Further clinical and molecular delineation of the 9q subtelomeric deletion syndrome supports a major contribution of EHMT1 haploinsufficiency to the core phenotype. *J. Med. Genet.* **46,** 598–606 (2009).
23. Cheung, I. *et al.* Developmental regulation and individual differences of neuronal H3K4me3 epigenomes in the prefrontal cortex. *Proceedings of the National Academy of Sciences* **107,** 8824–8829 (2010).
24. Numata, S. *et al.* DNA Methylation Signatures in Development and Aging of the Human Prefrontal Cortex. *The American Journal of Human Genetics* **90,** 260–272 (2012).
25. Siegmund, K. D. *et al.* DNA methylation in the human cerebral cortex is dynamically regulated throughout the life span and involves differentiated neurons. *PLoS ONE* **2,** e895 (2007).
26. Hernandez, D. G. *et al.* Distinct DNA methylation changes highly correlated with chronological age in the human brain. *Human Molecular Genetics* **20,** 1164–1172 (2011).
27. Stadler, F. *et al.* Histone methylation at gene promoters is associated with developmental regulation and region-specific expression of ionotropic and metabotropic glutamate receptors in human brain. *J. Neurochem.* **94,** 324–336 (2005).
28. Bérubé, N. G. *et al.* The chromatin-remodeling protein ATRX is critical for neuronal survival during corticogenesis. *J. Clin. Invest.* **115,** 258–267 (2005).
29. Northcott, P. A. *et al.* Multiple recurrent genetic events converge on control of histone lysine methylation in medulloblastoma. *Nat. Genet.* **41,** 465–472 (2009).
30. Novarino, G., Baek, S. T. & Gleeson, J. G. The Sacred Disease:The Puzzling Genetics of Epileptic Disorders. *Neuron* **80,** 9–11 (2013).
31. Focus on epilepsy. **18,** 317–317 (2015).
32. Staley, K. Molecular mechanisms of epilepsy. *Nat Neurosci* **18,** 367–372 (2015).
33. Moran, N. F. *et al.* Epilepsy in the United Kingdom: seizure frequency and severity, anti-epileptic drug utilization and impact on life in 1652 people with epilepsy. *Seizure: European Journal of Epilepsy* **13,** 425–433 (2004).
34. Nobili, L. *et al.* Nocturnal frontal lobe epilepsy. *Curr Neurol Neurosci Rep* **14,** 424 (2014).
35. Herzog, A. G. Catamenial epilepsy: definition, prevalence pathophysiology and treatment. *Seizure: European Journal of Epilepsy* **17,** 151–159 (2008).
36. Veeramah, K. R. *et al.* Exome sequencing reveals new causal mutations in children with epileptic encephalopathies. *Epilepsia* **54,** 1270–1281 (2013).
37. Rajakulendran, S., Kaski, D. & Hanna, M. G. Neuronal P/Q-type calcium channel dysfunction in inherited disorders of the CNS. *Nat Rev Neurol* **8,** 86–96 (2012).
38. Lasarge, C. L. & Danzer, S. C. Mechanisms regulating neuronal excitability and seizure development following mTOR pathway hyperactivation. *Front Mol Neurosci* **7,** 18 (2014).
39. Kato, M. & Dobyns, W. B. X-linked lissencephaly with abnormal genitalia as a tangential migration disorder causing intractable epilepsy: proposal for a new term, "interneuronopathy". *Journal of Child Neurology* **20,** 392–397 (2005).

40. Yu, F. H. *et al.* Reduced sodium current in GABAergic interneurons in a mouse model of severe myoclonic epilepsy in infancy. *Nat Neurosci* **9,** 1142–1149 (2006).
41. O'Leary, T. & Wyllie, D. J. A. Neuronal homeostasis: time for a change? *J. Physiol. (Lond.)* **589,** 4811–4826 (2011).
42. Hwang, J.-Y., Aromolaran, K. A. & Zukin, R. S. Epigenetic Mechanisms in Stroke and Epilepsy. *Neuropsychopharmacology* **38,** 167–182 (2012).
43. Conaco, C., Otto, S., Han, J.-J. & Mandel, G. Reciprocal actions of REST and a microRNA promote neuronal identity. *Proc. Natl. Acad. Sci. U.S.A.* **103,** 2422–2427 (2006).
44. Yoo, A. S., Staahl, B. T., Chen, L. & Crabtree, G. R. MicroRNA-mediated switching of chromatin- remodelling complexes in neural development. *Nature* **460,** 642–646 (2009).
45. Ren, X. & Kerppola, T. K. REST Interacts with Cbx Proteins and Regulates Polycomb Repressive Complex 1 Occupancy at RE1 Elements. *google.com*
46. Stapels, M. *et al.* Polycomb group proteins as epigenetic mediators of neuroprotection in ischemic tolerance. *Sci Signal* **3,** ra15 (2010).
47. Heilstedt, H. A. *et al.* Loss of the potassium channel beta-subunit gene, KCNAB2, is associated with epilepsy in patients with 1p36 deletion syndrome. *Epilepsia* **42,** 1103–1111 (2001).
48. Perkowski, J. J. & Murphy, G. G. Deletion of the Mouse Homolog of KCNAB2, a Gene Linked to Monosomy 1p36, Results in Associative Memory Impairments and Amygdala Hyperexcitability. *Journal of Neuroscience* **31,** 46–54 (2011).
49. Miller-Delaney, S. F. C. *et al.* Differential DNA Methylation Patterns Define Status Epilepticus and Epileptic Tolerance. *Journal of Neuroscience* **32,** 1577–1588 (2012).

Chapter 2

Aim of the thesis.

Aim of the present work is to describe and characterize two newly discovered pathways, involving the two epigenetic regulator SCML2 and EZH2. The first one in the context of a novel human epileptic syndrome, and the second in its key role as regulator of neuronal migration during precerebellar system development.

Chapter 3

Submitted manuscript: Mutations in the Polycomb protein *SCML2* cause a novel human epileptic syndrome by disrupting the inhibitory drive on excitatory neurons.

Mutations in Polycomb group gene *SCML2* cause a novel infantile epileptic syndrome by disrupting the inhibitory drive on excitatory neurons

Alberto Loche[1,2,*], Claudia Compagnucci[3,*], Federico Esposti[1], Paolo Botta[1], Mary Ellen Ahearn[4], Jesse M. Hunter[4], Fabiana Fattori[3], Andrea Ciolfi[5], Massimiliano Valeriani[6], Federico Vigevano[6], Bruno Dallapiccola[7], Laura Crisponi[8], Heintz Gut[1], Andreas Lüthi[1], Botond Roska[1], Marco Tartaglia[5,7], Francesco Roselli[9,10], Lisa Baubach-Reardon[5], Enrico Bertini[3,11], and Filippo M. Rijli[1,2,11]

1 Department of Neurobiology, Friedrich Miescher Institute for Biomedical Research, Basel, Switzerland

2 University of Basel, Switzerland

3 Department of Neurosciences, Unit of Neuromuscular and Neurodegenerative Disorders, Laboratory of Molecular Medicine, Bambino Gesù Children's Research Hospital, Rome, Italy

4 Translational Genomics Research Institute, Phoenix, Arizona, USA Dept. of Neurosciences, Division of Pediatric Neurology, Bambino Gesù Children's Research Hospital, Rome, Italy

5 Department of Hematology, Oncology and Molecular Medicine, Istituto Superiore di Sanità, Rome, Italy

6 Department of Neurosciences, Division of Pediatric Neurology, Bambino Gesù Children's Research Hospital, Rome, Italy

7 Ospedale Pediatrico Bambino Gesù-Istituto di Ricovero e Cura a Carattere Scientifico, Rome, Italy

8 Istituto di Ricerca Genetica e Biomedica, Consiglio Nazionale delle Ricerche, Cittadella Universitaria di Monserrato, SS 554 km 4500, Monserrato, 09042, Italy.

9 Department of Neurology, University of Ulm Medical School, Ulm, Germany

10 Department of Anatomy and Cell biology, University of Ulm Medical School, Ulm, Germany

* These authors have equally contributed to this work

11 Correspondence should be addressed to ESB (enricosilvio.bertini@opbg.net) or FMR (filippo.rijli@fmi.ch)

Homeostatic regulation of excitation/inhibition balance is a fundamental feature of healthy neuronal ensembles[1,2] whose alteration may underlie complex psychiatric and neurological diseases such as epilepsy, autism and cognitive disabilities[3-5]. Inhibitory synapses are main cellular elements controlling the excitability of principal excitatory neurons in the central nervous system (CNS)[6], and deficits in inhibitory signaling can cause pathological hyperexcitability[7,8]. Here, we found that mutations in *Sex Comb on Midleg-Like 2* (*SCML2)*, a X-linked member of Polycomb Repressive complex 1 (PRC1), cause a novel human neurological syndrome of neuronal excitability resulting in multiple muscle contractures and early onset infantile epilepsy. Analysis of *Scml2* mutant mice provided insights into the etiology of the human syndrome, revealing spontaneous cortical hyperexcitability, impairment of inhibitory currents and synapses on cortical excitatory neurons associated with reduction of postsynaptic Gephyrin and Neuroligin 2, increased susceptibility to seizures, and impaired inhibitory synapses in spinal motor neurons. Thus, *SCML2* is a novel postsynaptic inhibitory synapse regulator and its mutation may lead to previously unrecognized neurodevelopmental conditions of neuronal hyperexcitability.

GABAergic and glycinergic inhibitory synapses are main cellular elements keeping in check excitability of principal neurons in the CNS[9]. Severe deficits in inhibitory input during development and in adulthood cause pathological hyperexcitability, resulting in the clinical features of epilepsy[7,10,11]. Many of the genes that have been linked to epilepsy regulate inhibitory interneuron development and function, with only a handful of post-synaptic molecules regulating inhibitory response of excitatory neurons[7,8]. Moreover, to date no chromatin writer has been involved in the regulation of the inhibitory synapse program during normal development, whose mutation may lead to alteration of the proper excitation/inhibition balance and epilepsy.

By whole exome-sequencing of two independent families (Fig. 1; Methods; Supplementary Note), we identified two segregating pathogenic mutations in the coding sequence of *SCML2*. *SCML2* is located on chromosome Xp.22[15] and is a non-canonical member of the Polycomb Repressive complex 1 (PRC1)[5,12,13]. SCML2 is associated with the PRC1.2 and 1.4 sub-complexes and with the catalytic subunit RING1B which in turn ubiquitinates the histone H2A at K119[12,13]. SCML2 interacts with other Polycomb subunits via its C-terminal SAM domain[14], and binds methylated histones through its MBT domains[15] (Fig. 1a). SCML2 generally represses target gene expression *in vitro* and *in vivo*[13,14], although an alternative role in preventing gene silencing through its association with the USP7 deubiquitinase has been described during mouse spermatogenesis[13,16,17].

The affected individuals came from two non-consanguineous families of Mexican (hereafter, family *M*) and Italian (*I*) origins (Fig. 1; Supplementary Note). Inheritance modality showed a recessive X-linked neurodevelopmental syndrome, with affected males in both families. All patients in the two families shared a clinical condition of congenital multiple joint contractures (arthrogryposis), with clenched

hands and rocker bottom/club feet. In family *M*, two miscarriages, two stillborn or neonatal deaths and one termination at 24 weeks gestation carried the start codon loss mutation p.M1V resulting in loss of SCML2 protein function (Fig. 1b, Supplementary Table 1; Supplementary Note). One boy was born alive, but expired within fifteen minutes of birth. Brain abnormalities were found in two patients (Supplementary Note), consisting of hypoplasia of the vermis with a dilated fourth ventricle and partial agenesis of the corpus callosum in one patient, and cerebellar hypoplasia with underdevelopment of the cortex in the other. Since the phenotype in family M resulted in fetal or neonatal death it is unknown if the affected children would have developed further neurological abnormalities.

In the I family, the affected boy carried instead a missense mutation within the conserved MBT1 domain of *SCML2* (Fig. 1c, Supplementary Note, Supplementary Table 2). Variant filtering and prioritization allowed to identify the c.349C>A missense substitution (p.Pro117Thr) in *SCML2* as the candidate causative event underlying the trait in the family I (Fig. 1a, c; Methods; Supplementary Table 2; Supplementary Note). The mutation was inherited from the mother and not found in the healthy sibling brother (Fig. 1c). *In silico* modeling based on the solved crystal structure of human SCML2 MBT1/MBT2 domains[18], suggested that mutation of the highly conserved P117 residue (Fig. 1h) results in the disruption of the hydrophobic stacking interaction between P117 and F160 (Fig. 1g) likely disruptive of protein function.

The affected child (Fig. 1d) shared a similar phenotype with the affected children of family M, including multiple joint contractures, club feet and clenched fists. He survived until two years of age, thus allowing further evaluation of the

impact of the *SCML2* mutation. He presented hypogonadism and an intellectual disability. A brain MRI showed no gross brain anatomical abnormalities (Fig. 1f). At one month, the child started to manifest frequent tonic fits during the day (Fig. 1e; Supplementary Note) which had no correlation with EEG abnormalities and were characterized by raising and abduction of upper limbs, eyes staring, and prolonged cyanosis (Extended data, video 1). At three months, a hemiclonic status epilepticus appeared on the right side corresponding to an ischemic brain lesion on the left parieto-temporal lobes. This episode followed a prolonged tonic fit with respiratory failure and cyanosis. Tonic fits and apneas increased in frequency and became almost ceaseless starting to associate with clusters of massive myoclonus of upper limbs and *palpebral myoclonus*, and did not respond to anticonvulsant therapy. The child died at the age of 2 years during one of such prolonged apnea episodes.

Human and murine *SCML2*/*Scml2* MBT domains share 77% of sequence homology (based on HHPRED alignment). To gain insights into the etiology of the human epilepsy syndrome, we generated a mouse model of *Scml2* targeted inactivation. We engineered a pair of targeted Transcriptional Activator Like Effector Nucleases (TALENs) (Methods) and generated a 11 base pair (bp) frame shift deletion in the *Scml2* exon 4 introducing a premature stop codon within the MBT1 domain (Supplementary Fig. 1). $Scml2^{Y/-}$ (hereafter referred to as $Scml2^{KO}$) mutant males and $Scml2^{+/-}$ heterozygous mutant females were viable although $Scml2^{KO}$ males had fertility defects, due to hypogonadism and spermatogenesis defects[12,13] (Supplementary Fig. 1b). By mating wild type males to $Scml2^{+/-}$ females, the mutant allele was inherited at the expected mendelian ratio ($Scml2^{Y/-}$ males n=54; $Scml2^{+/-}$ females n=49; and not shown). Brain size and anatomy appeared grossly normal in $Scml2^{KO}$ males (Supplementary Fig. 2a-e).

To analyze Scml2 expression, we generated an antibody against the protein C-terminus (Methods). In the testis, where Scml2 is normally expressed[12,13], we readily detected specific immunostaining signal in the nucleus of wild type undifferentiated spermatogonia[12,13] (Supplementary Fig. 1a). In contrast, no Scml2 signal was detected in *Scml2*^{KO} testis supporting antibody specificity and Scml2 protein impairment in mutants (Supplementary Fig. 1b). In the mouse cortex of *GAD67::eGFP* transgenic mice, expressing eGFP in inhibitory interneurons[18], Scml2 was mostly expressed in eGFP-negative pyramidal excitatory neurons at P0 (Fig. 2a, b, d-f) and at P60 (Supplementary Fig. 3a-e). Similarly, human SCML2 was expressed in infantile and adult cortical neurons (Fig. 2i-o). Moreover, Scml2 was expressed in spinal motor neurons and in subsets of dorsal horn sensory neurons (Fig. 2c, g-h and Supplementary Fig. 3f-g).

Next, we characterized the baseline cortical activity of *Scml2*^{KO} adult mice by *in vivo* local field potential recordings. We implanted 16-channel linear electrodes in the somatosensory cortex (Fig. 3a) and performed multiple recording sessions (n=4 of 300 seconds each/animal). In all (n=6) *Scml2*^{KO} mutant animals, baseline cortical activity was characterized by variable spontaneous episodes of fast ripple-like synchronous activity through all cortical channels, not observed in wild type littermates (n=4) (compare Fig. 3b and 3c-e). Moreover, one *Scml2*^{KO} mutant also displayed synchronous infraslow-like activity[17] at 0.1Hz (Supplementary Fig. 4a-d). Ripple-like and/or infraslow-like syncronous activities are indicators of inter-ictal discharges characteristic of epileptic syndromes[19,20].

Scml2^{KO} cortical hyperexcitability could be related to impaired spontaneous GABAergic inhibitory currents on excitatory pyramidal neurons. Whole-cell patch clamp recordings of excitatory cortical neurons in acute brain slices revealed

defective inhibitory transmission, resulting in reduced frequency (Fig. 3f-h), but not amplitude or decay time (Fig. 3i-l), of $GABA_A$ receptor-mediated miniature inhibitory postsynaptic currents (mIPSCs). Inhibitory interneuron and $NeuN^+$ neuron numbers were not decreased in mutant *Scml2^{KO};GAD67::eGFP* cortex (Supplementary Fig. 2b-e). However, we detected a significant reduction of perisomatic puncta of Gephyrin, a postsynaptic scaffold protein involved in stability of inhibitory synapses[21], in $CamKIIalpha^+$ *AAV1.CMV.TurboRFP.WPRE.rBG (AAV-RFP)*-labeled excitatory *Scml2^{KO}* pyramidal neurons (Fig. 4a, b), whereas presynaptic inhibitory VGAT puncta were unaffected (Fig. 4c). We also observed a reduction of apposed pairs of perisomatic postsynaptic puncta for the inhibitory synapse adhesion protein Neuroligin 2 (Nlgn2) (Sudhof, 2008) and presynaptic synaptotagmin 2 (Syt2) puncta (Fig. 4b). Moreover, presynaptic $Syt2^+$ puncta were present at inhibitory parvalbumin $(PV)^+$ basket cell terminals even in the absence of postsynaptic Nlgn2 (Fig. 4). Together with the observed mIPSC frequency reduction (Fig. 3f-h), these data indicate a reduction of functional postsynaptic sites at inhibitory synapses without affecting synaptic transmission at remaining functional synapses in *Scml2^{KO}* cortical excitatory neurons, which may result in their hyperexcitability (Fig. 3).

Since human *SCML2* mutations result in multiple muscle spasms and contractures, we next analysed *Scml2*-expressing spinal motor neurons (Fig. 2). Similar to excitory cortical neurons, in *Scml2^{KO}* motor neurons we found a reduction of perisomatic Gephyrin as well as glycin receptor GliR1a puncta, whereas apposed presynaptic GlyT2 puncta were unaffected (Fig. 4d, f-g) supporting a selective defect of the inhibitory postsynapse.

We next measured susceptibility to pilocarpine-induced seizures[22] by multiphoton imaging of *Scml2^{KO}* adult somatosensory cortex, as compared to wild

type (WT) littermates (Fig. 5a). In WT mice, pilocarpine-induced epilepy is triggered above 250 mg/kg[23]. Notably, in *Scml2*^{KO} mutants prolonged synchronous cortical activation was already triggered in response to 100 mg/kg (Fig. 5a), displaying typical activity alterations observed in high dose-treated WT mice[23]. Moreover, in analogy to the family *I* patient, *Scml2*^{KO} mice failed to recover from pilocarpine-induced seizures after treatment with an antiepileptic drug (midazolam) with GABAergic agonist activity (Fig. 5b). Thus, *Scml2*^{KO} mice showed spontaneous ectopic baseline hyperactivity (Fig. 3), a feature of epileptic brains, and, in addition, a higher susceptibility than wild type brains to pilocarpine-induced seizures.

We report here a novel neurological syndrome characterized by hyperexcitability of cortical and spinal neurons, due to mutation of the X-linked epigenetic regulator SCML2/Scml2. A series of deletions and duplications of the Xp22.13 region were reported in patients with severe neurodevelopmental disorder characterized by early-onset seizures, infantile spasms, anti-epileptic drug resistance, and motor impairment[24,25]. The pathogenic potential of the deletions was attributed to the involvement of *CDKL5*[16], whereas the *SCML2* gene was not investigated. *Scml2*^{KO} mutant mice display several critical elements of the human condition, providing a fundamental entry point into the syndrome etiology. In particular, mutant mice developed morphological and functional alterations of the postsynaptic component of inhibitory synapses on excitatory neurons, underlying their increased spontaneous excitability and susceptibility to seizures (Figs. 3-5).

Homeostatic regulation of excitation/inhibition balance is tightly controlled by the interaction of integrated synaptic input with cell-autonomous transcriptional programs[26]. Chromatin remodeling factors are crucial for normal transcriptional regulation of neuronal development, and their potential role in epileptogenesis has

been postulated[21]. However, to date no chromatin factor has been associated with epileptic syndromes, leaving unexplored the possibility of epigenetic deregulation of gene expression as a potential primary cause of this disease.

Recent advances have furthered our understanding of PRC1 function in the brain. For example, a SCML2 paralogue, Sex Comb on Midleg Homolog 1 (SCMH1), is required to induce ischemic tolerance through its association with the promoter regions of two voltage-gated potassium channel genes, whose expression is decreased in ischemic-tolerant neurons[27]. Furthermore, mutations in AUTS2, whose association to PRC1 results into transcriptional activation[23], were causally linked to autism spectrum disorders (ASD)[28]. Thus, aberrant function of a non-canonical member of the PRC1 complex can lead to a neurological syndrome by interfering with normal gene expression during brain development.

A number of genes directly regulated by SCML2 is involved in synaptogenesis, such as for instance *protocadherin-10* (*PCDH10*)[14]. Here, we additionally show that *Scml2*^{KO} excitatory pyramidal and spinal motor neurons display a selective reduction of the inhibitory post-synapse proteins Gephyrin and Nlgn2 (Fig. 4), whose mutations have been associated with an increased risk for autism, schizophrenia, and epilepsy[29]. These findings raise the possibility that SCML2-dependent epigenetic sub-programs might exist that result in the fine-tuning of the number and/or maturation of inhibitory synapses. Epileptic syndromes are highly heterogeneous and recent developments in whole exome sequencing techniques have led to the identification of many causative genes[8]. Here we show that SCML2-dependent epigenetic regulation of gene expression can also influence neuronal excitation/inhibition balance eventually resulting in epilepsy. These findings underscore the central role of epigenetic regulation in health and disease. Our mouse

model provides insights into the neurophysiological consequences of detrimental pathological rare mutations affecting SCML2 in humans leading to a previously uncharacterized neurodevelopmental syndrome including early-onset infantile epilepsy. Moreover, it is conceivable that mutations in SCML2 might be additionally involved in other so far unrecognized neurodevelopmental conditions involving neuronal hyperexcitability.

Author contributions

AL, CC, ESB and FMR conceived the project and designed the experimental approach. AL generated the mouse model, carried out the histological analysis, antibody design and experimental validation, discovered the phenotype, helped during the electrophysiological and imaging experiments, analysed the results together with FMR. CC discovered the SCML2 mutation in family I and JMH, LBR, and MEA discovered the SCML2 mutations in families M, CC carried out the human brain histological analysis for patient I. FE carried out and FE and BR analyzed *in vivo* multi-electrode recording and two-photon imaging experiments. PB carried out and PB and AL analyzed *ex vivo* slice recordings. MV and FV carried out MRI and EEG recordings of patient I. MT, JMH, MEA, LBR, and AC analyzed exome sequencing results. FF sequenced *CRFL1* in the atypical Crisponi Syndrome patients. HG performed *in silico* protein analysis and modeling. FR carried out the spinal cord analysis. AL, ESB and FMR wrote the manuscript; all authors contributed to the manuscript.

Acknowledgements

We are grateful to P. Scheiffele for discussion and reagents. We thank Jean-Francois Spetz, Sandrine Bichet, and Matyas Flemr for their valuable technical help. LBR laboratory was supported by Muscular Dystrophy Association Grant Number 186435, the Flinn Foundation of Arizona and the Translational Genomics Research Institute. FMR laboratory was supported by the Swiss National Science Foundation (31003A_149573), ARSEP, and the Novartis Research Foundation.

References

1. Peng, Y. R. *et al*. Postsynaptic Spiking Homeostatically Induces Cell-Autonomous Regulation of Inhibitory Inputs via Retrograde Signaling. *Journal of Neuroscience* **30,** 16220–16231 (2010).
2. Nelson, S. B. & Valakh, V. Excitatory/Inhibitory Balance and Circuit Homeostasis in Autism Spectrum Disorders. *Neuron* **87,** 684–698 (2015).
3. Jeste, S. S. & Geschwind, D. H. Disentangling the heterogeneity of autism spectrum disorder through genetic findings. *Nat Rev Neurol* **10,** 74–81 (2014).
4. Lee, B. H., Smith, T. & Paciorkowski, A. R. Epilepsy & Behavior. *Epilepsy & Behavior* **47,** 191–201 (2015).
5. Åndell, E. *et al*. The incidence of unprovoked seizures and occurrence of neurodevelopmental comorbidities in children at the time of their first epileptic seizure and during the subsequent six months. *Epilepsy Research* **113,** 140–150 (2015).
6. Isaacson, J. S. & Scanziani, M. How Inhibition Shapes Cortical Activity. *Neuron* **72,** 231–243 (2011).
7. Staley, K. Molecular mechanisms of epilepsy. *Nat Neurosci* **18,** 367–372 (2015).
8. Noebels, J. Pathway-driven discovery of epilepsy genes. *Nat Neurosci* **18,** 344–

350 (2015).

9. Moss, S. J. & Smart, T. G. Constructing inhibitory synapses. *Nat Rev Neurosci* **2,** 240–250 (2001).

10. Consortium, E., Project, E. P. G., Consortium, E. & Project, E. P. G. De novo mutations in epileptic encephalopathies. *Nature* **501,** 217–221 (2013).

11. Poduri, A. & Lowenstein, D. Epilepsy genetics — past, present, and future. *Current Opinion in Genetics & Development* **21,** 325–332 (2011).

12. Gao, Z. *et al*. PCGF Homologs, CBX Proteins, and RYBP Define Functionally Distinct PRC1 Family Complexes. *Molecular Cell* **45,** 344–356 (2012).

13. Hasegawa, K. *et al*. SCML2 Establishes the Male Germline Epigenome through Regulation of Histone H2A Ubiquitination. *Developmental Cell* 1–16 (2015). doi:10.1016/j.devcel.2015.01.014

14. Bonasio, R. *et al*. Interactions with RNA direct the Polycomb group protein SCML2 to chromatin where it represses target genes. *Elife* **3,** e02637 (2014).

15. Santiveri, C. M. *et al*. The Malignant Brain Tumor Repeats of Human SCML2 Bind to Peptides Containing Monomethylated Lysine. *Journal of Molecular Biology* **382,** 1107–1112 (2008).

16. Bello-Espinosa, L. E. Epilepsy & Behavior. *Epilepsy & Behavior* 1–5 (2015). doi:10.1016/j.yebeh.2015.04.031

17. Luo, M. *et al*. Polycomb Protein SCML2 Associates with USP7 and Counteracts Histone H2A Ubiquitination in the XY Chromatin during Male Meiosis. *PLoS Genet* **11,** e1004954 (2015).

18. Sathyamurthy, A., Allen, M. D., Murzin, A. G. & Bycroft, M. Crystal Structure of the Malignant Brain Tumor (MBT) Repeats in Sex Comb on Midleg-like 2 (SCML2). *J. Biol. Chem.* **278,** 46968–46973 (2003).

19. Wendling, F., Bartolomei, F., Mina, F., Huneau, C. & Benquet, P. Interictal spikes, fast ripples and seizures in partial epilepsies - combining multi-level computational models with experimental data. *European Journal of Neuroscience* **36,** 2164–2177 (2012).

20. Rodin, E., Constantino, T. & Bigelow, J. Clinical Neurophysiology. *Clinical*

Neurophysiology **125,** 919–929 (2014).

21. Choii, G. & Ko, J. Gephyrin: a central GABAergic synapse organizer. **47,** e158–10 (2015).

22. Turski, W. A. *et al*. Seizures produced by pilocarpine in mice: a behavioral, electroencephalographic and morphological analysis. *Brain Res*. **321,** 237–253 (1984).

23. Gröticke, I., Hoffmann, K. & Löscher, W. Behavioral alterations in the pilocarpine model of temporal lobe epilepsy in mice. *Experimental Neurology* **207,** 329–349 (2007).

24. Bahi-Buisson, N. *et al*. Epileptic encephalopathy in a girl with an interstitial deletion of Xp22 comprising promoter and exon 1 of the CDKL5gene. *Am. J. Med. Genet.* **9999B,** n/a–n/a (2009).

25. Tiwari, V. N., Sundaram, S. K., Chugani, H. T. & Huq, A. H. M. M. Infantile Spasms Are Associated With Abnormal Copy Number Variations. *Journal of Child Neurology* **28,** 1191–1196 (2013).

26. Hong, E. J., West, A. E. & Greenberg, M. E. Transcriptional control of cognitive development. *Curr. Opin. Neurobiol.* **15,** 21–28 (2005).

27. Stapels, M. *et al*. Polycomb group proteins as epigenetic mediators of neuroprotection in ischemic tolerance. *Sci Signal* **3,** ra15 (2010).

28. Sultana, R. *et al*. Identification of a Novel Gene on Chromosome 7q11.2 Interrupted by a Translocation Breakpoint in a Pair of Autistic Twins. *Genomics* **80,** 129–134 (2002).

29. Südhof, T. C. Neuroligins and neurexins link synaptic function to cognitive disease. *Nature* **455,** 903–911 (2008).

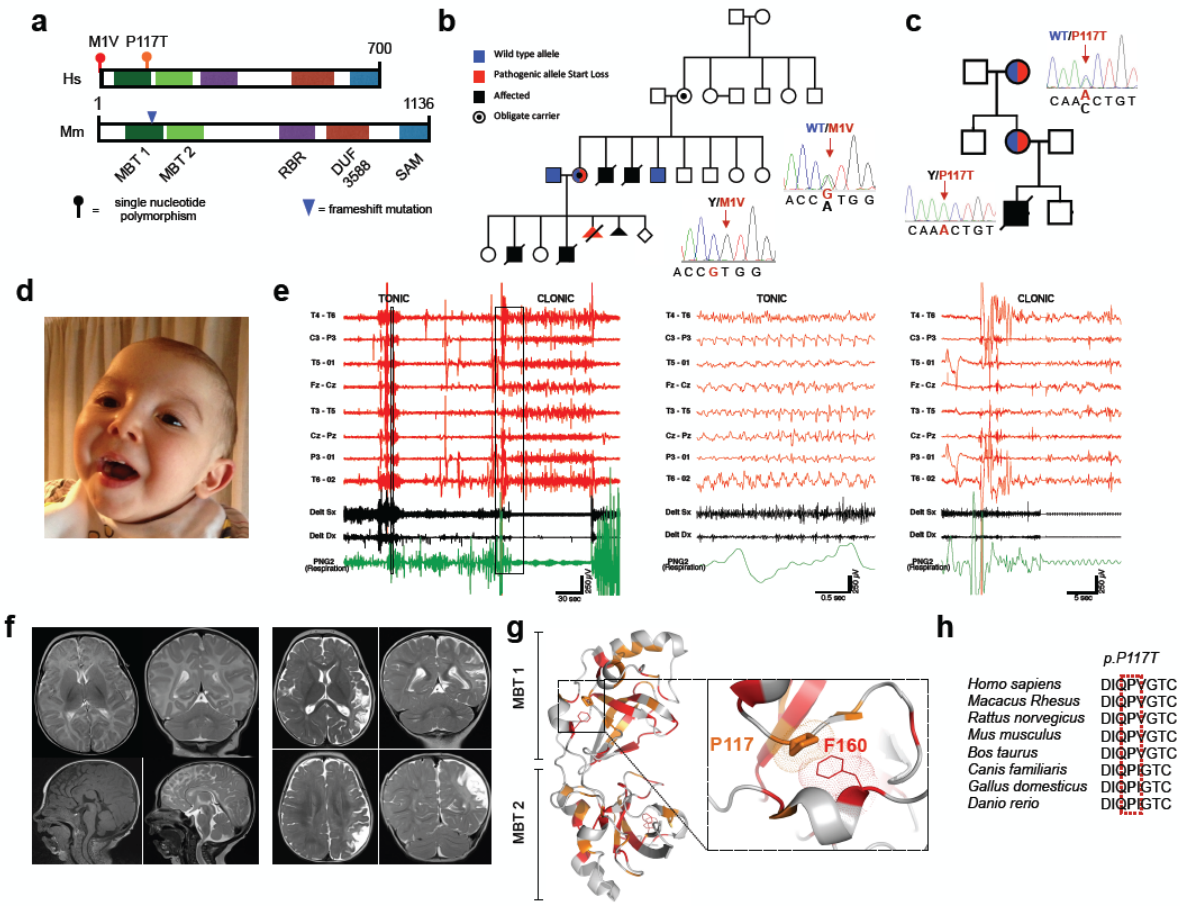

Figure 1. *SCML2* is mutated in a novel human infantile syndrome. a, Schematic representations of Homo sapiens (Hs) and Mus musculus (Mm) SCML2 homologue proteins with their malignant brain tumor (MBT)1 and MBT2, ring between ring fingers (RBR), domain of unknown function (DUF) 3588, and sterile alpha motif (SAM) functional domains. In the top diagram are indicated the positions of M1V and P117T mutations from the mexican (M) and italian (I) families, respectively, whereas in the bottom diagram is shown the position of the frameshift deletion engineered in the mouse Scml2 MBT1 introducing a premature stop codon. **b-c,** Pedigrees, segregation analysis, and Sanger sequencing of the two pathogenic *SCML2* single nucleotide variants identified in the M (b) and I families (c), respectively. **d**, Picture of the patient from family I at 1 year of age. **e,** EGG/EMG example trace recording

during the occurrence of a tonic/clonic seizure. **f,** Brain MRI images of the patient in (d) showing no gross brain anatomical abnormalities at 1 month of age. **g,** Crystal structure of the MBT domains highlighting conserved residues (color coded) and showing that the P117 mutated residue in family I normally makes a pairing stack with F160. **h**, P117 mutated residue is conserved among vertebrates and occurs within a highly conserved motif.

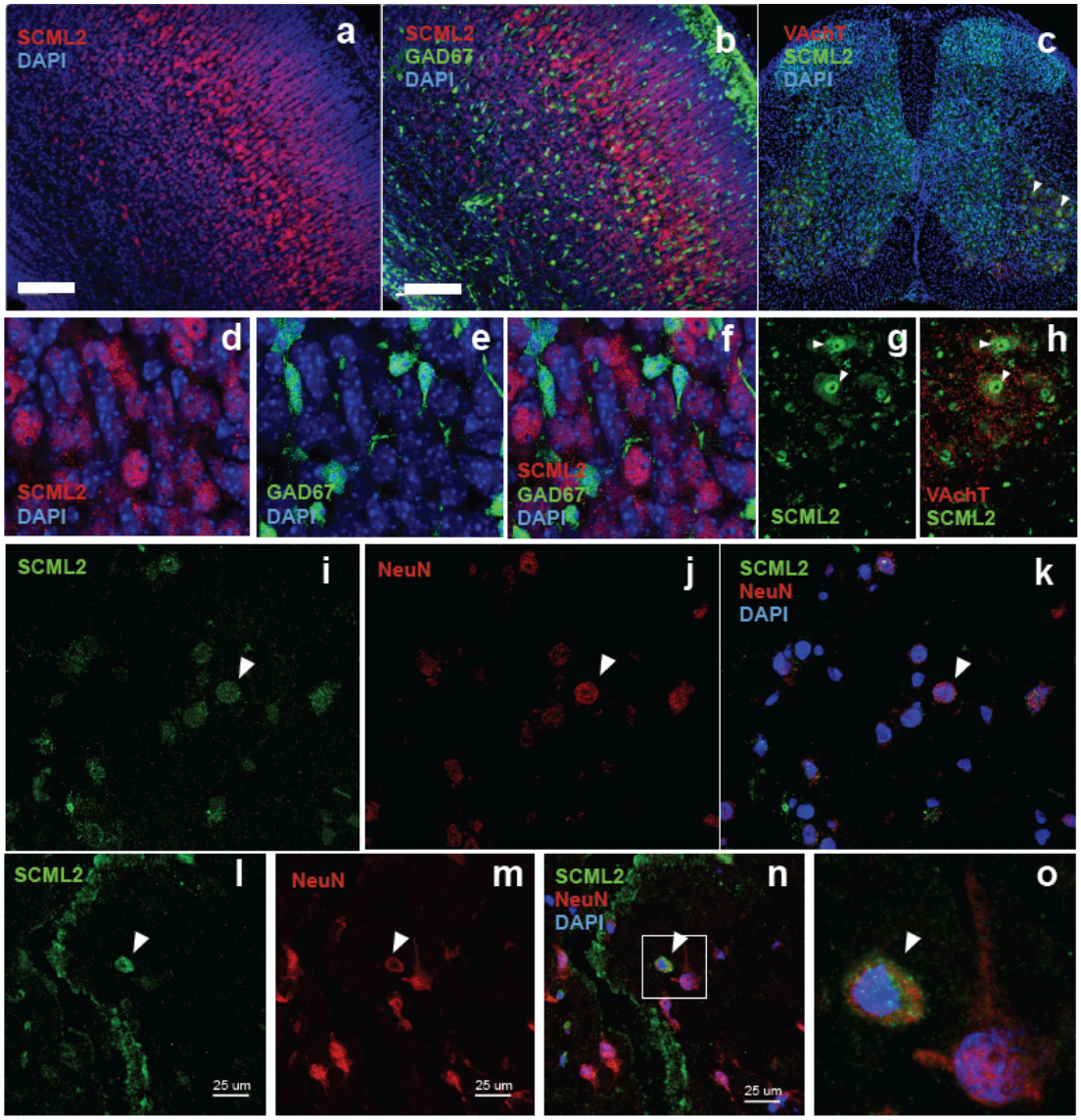

Figure 2. Scml2/SCML2 expression in mouse and human cortical and spinal cord neurons a-b, **d-f,** Anti-Scml2 immunostaining (red signal) of P0 *GAD67::eGFP* murine cortex shows expression mainly in eGFP(green signal)-negative, excitatory, cortical neurons. **c, g, h** Anti-Scml2 (green signal) immunostaining in spinal motor neurons (arrowheads), as identified by vesicular acetylcholine transporter (VAChT) staining (red signal). **i-o**, Anti-SCML2 immunostaining (green signal) shows co-localisation (arrowheads) with NeuN (red signal) in postnatal (6 months) and adult (17 years) human cortical samples. DAPI, 4',6-diamidino-2-phenylindole.

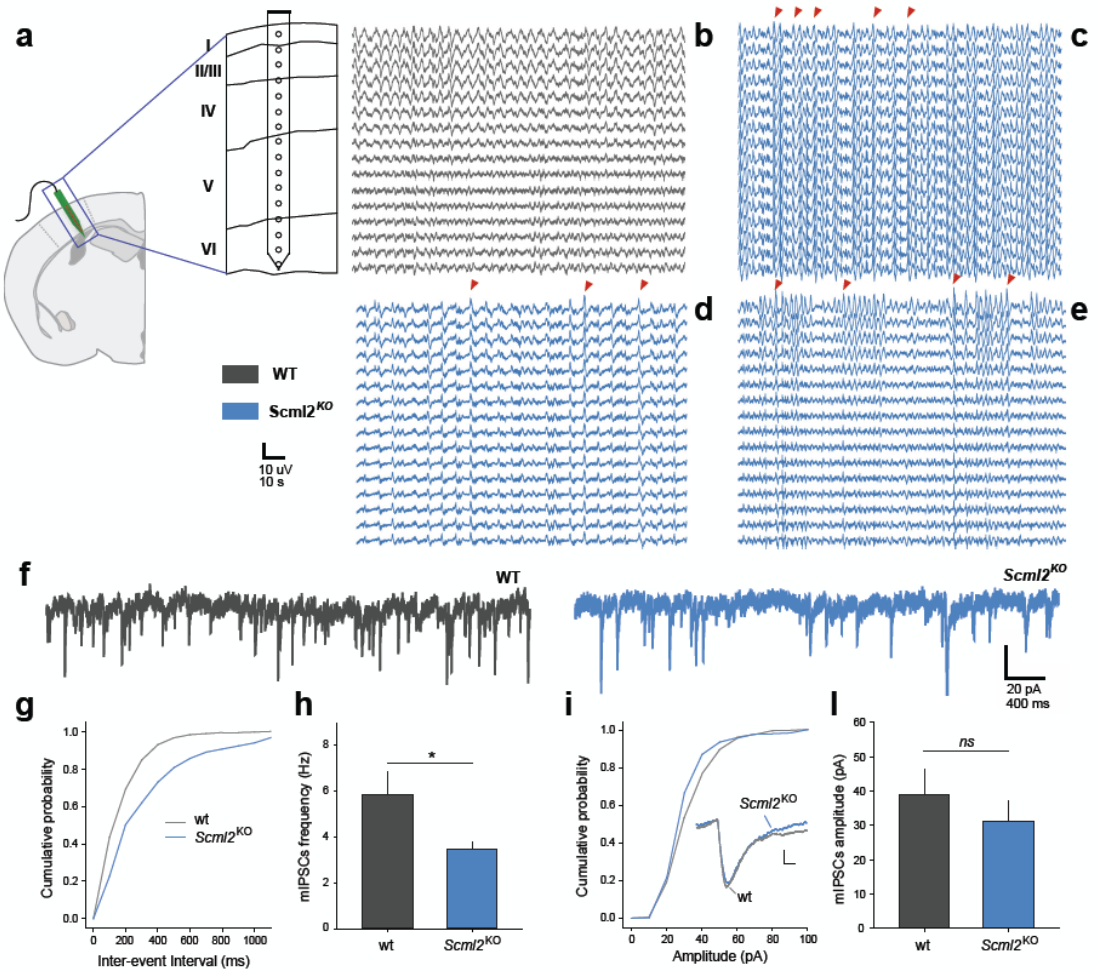

Figure 3. Abnormal cortical activity and reduced GABAergic transmission on excitatory neurons in *Scml2*^{KO} mice. a-e, *In vivo* local field potential recorded by a multi-channel electrode implanted in sensory cortex (diagram in a) of mildly anesthetized wild type (b) and *Scml2*^{KO} mutant (c-e) mice. *Scml2*^{KO} mice show frequent and syncronous ectopic ripple-like episodes through cortical layers (red arrowheads), not present in wild type littermates. **f-l**, Whole cell recording of miniature inhibitory post-synaptic currents (mIPSCs) of somatosensory cortex pyramidal neurons (layer 2/3) in acute brain slices. **f,** Representative traces showing reduced mIPSC frequency in *Scml2*^{KO} mutant (blue) as compared to wild type (WT) pyramidal cortical neurons. **g**, Difference in cumulative probability of mIPSC inter-event interval (ms) in wild type (wt) (grey line) and *Scml2*^{KO} mutant (blue line)

pyramidal neurons. **h**, Quantification of mIPSC frequency (Hz) showing a statistically significant reduction in *Scml2*^{KO} mutant (n=9) as compared to wt (n=8) cortical pyramidal neurons (*p < 0.05 by unpaired t-test). **i**, Representative cumulative probability of mIPSC amplitude (pA). **l**, Bar graph of mIPSC amplitude (pA) of wt and *Scml2*^{KO} mutant cortical pyramidal neurons showing non-significant (ns) statistical difference between the two groups (p > 0.05 by unpaired t-test). All data are shown as mean ± s.e.m.

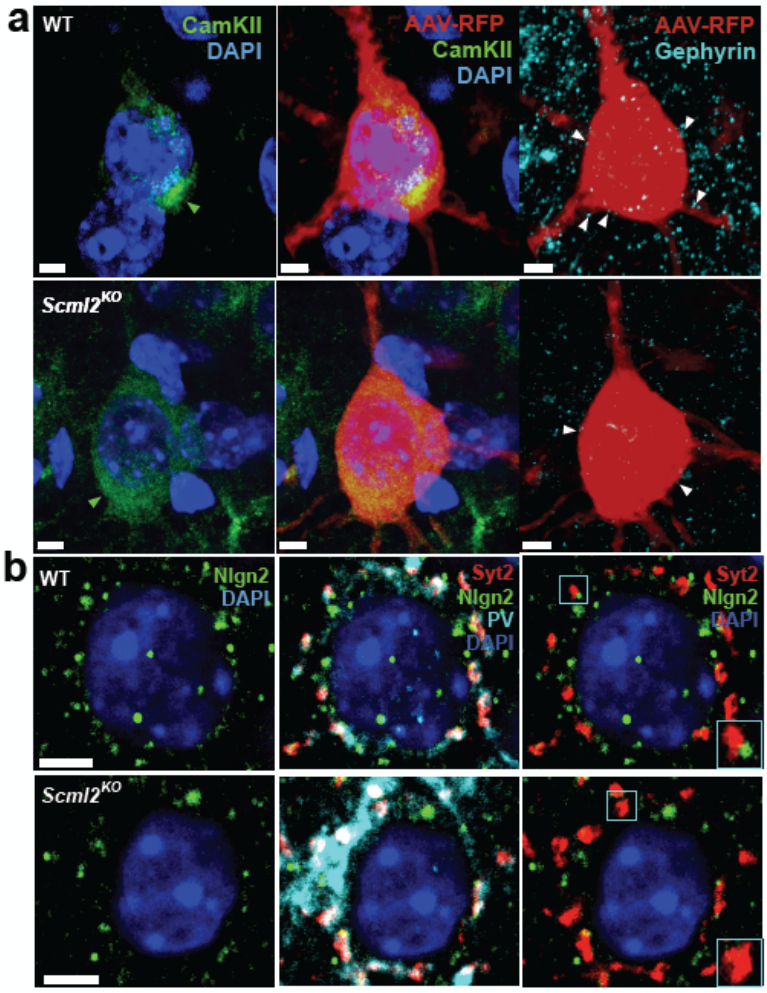
a
WT
CamKII
DAPI
AAV-RFP
CamKII
DAPI
AAV-RFP
Gephyrin
Scml2KO
b
WT
Nlgn2
DAPI
Syt2
Nlgn2
PV
DAPI
Syt2
Nlgn2
DAPI
Scml2KO

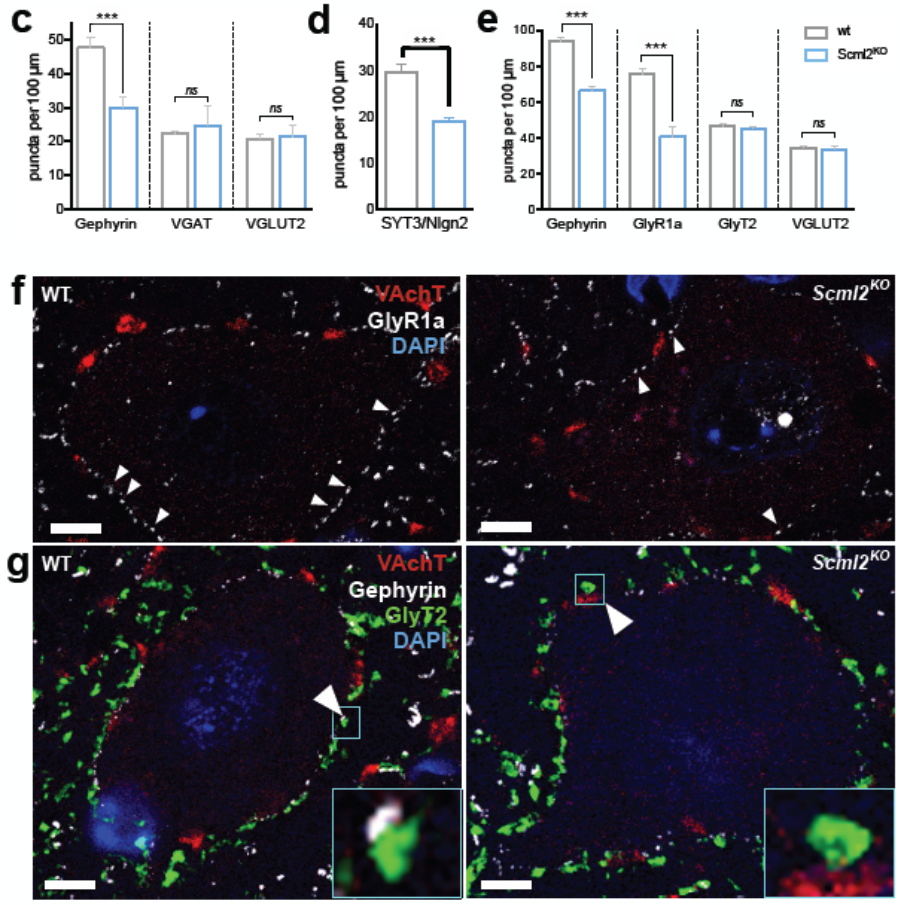

Figure 4 Impairment of inhibitory postsynapses in *Scml2*^{KO} mice. **a-b,** Immunostaining showing reduced perisomatic puncta (arrowheads) of Gephyrin in CamKIIalpha^{+} *AAV1.CMV.TurboRFP.WPRE.rBG (AAV-RFP)*-labeled excitatory *Scml2*^{KO} (b), as compared to wild type (WT) (a), cortical pyramidal neurons. **c**, Immunostaining showing lack (insets) of postsynaptic Neuroligin 2 (Nlgn2) (green) apposed to synaptotagmin 2 (Syt2) presynaptic (red) puncta at parvalbumin (PV) inhibitory terminals. **d-e,** Quantification and statistical significance of reduction of synaptic Nlgn2/Syt2 pair (d), and (e) Gephyrin, vesicular GABA transporter (VGAT), and vescicular glutamate transporter 2 (VGLUT2), in wild type (grey bars) and *Scml2*^{KO} (blue bars) cortical neurons. **f-g,** Immunostaining showing (f) perisomatic

reduction of glycine receptor 1a (GlyR1a) puncta (white signal, arrowheads), and (g) lack (arrowhead, insets) of postsynaptic Gephyrin puncta (white signal) apposed to presynaptic Glycine transporter 2 (GlyT2) (green) puncta in *Scml2*^{KO} mutant as compared to wild type (WT) spinal motor neurons. **h,** Quantifications and statistical significance of reduction of Gephyrin, GlyR1a, GlyT2, and VGLUT2 in wild type (grey bars) and *Scml2*^{KO} (blue bars) spinal motor neurons; non-significant, *ns*= $p>0.05$; ***=$p<0.001$ paired t-test. All data are shown as mean ± s.e.m. VAChT, vesicular acetylcholine transporter.

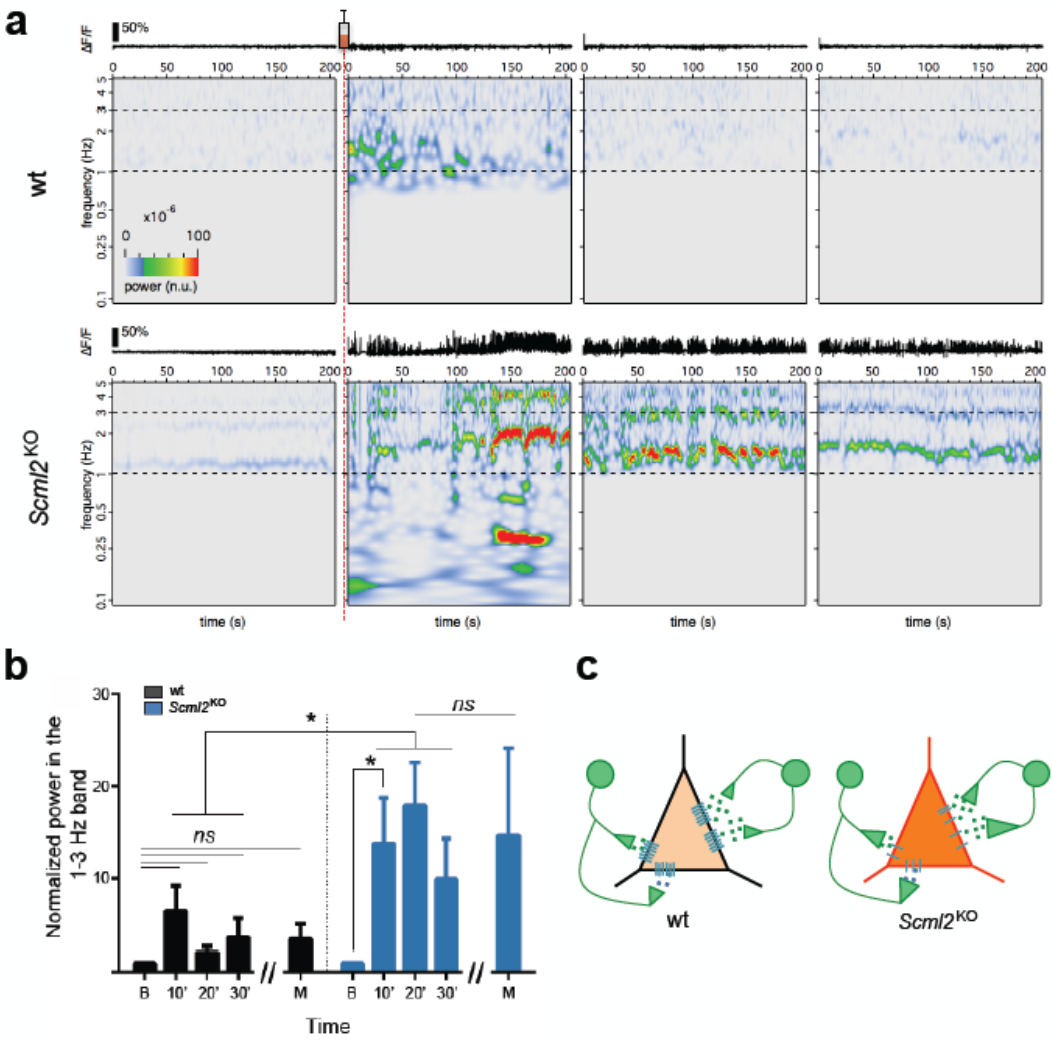

Figure 5 *Scml2*^{KO} mice display increased seizure susceptibility. a, Wavelet time-frequency plots representative of *in vivo* neuronal activity measured by two-photon imaging of somatosensory cortex loaded with the fluorescent calcium indicator X-Rhod1 AM. Comparison of baseline activity and recording 10, 20, 30, and 40 minutes after sub-threshold (100mg/kg) intra-peritoneal administration of pilocarpine (syringe) in wild type (wt) and *Scml2*^{KO} mice. Note that *Scml2*^{KO}, unlike wt, mice induce and maintain strong prolonged synchronous (1-2Hz) cortical activation. **b**, Quantification of normalized activity in wt (n = 3) (black bars) and *Scml2*^{KO} (n = 3) (blue bars) pilocarpine-induced somatosensory cortex (ns, non-significant = $p > 0.05$; *=$p<0.05$). Pilocarpine-induced activity cannot be brought back to baseline by

administration of anti-epileptic drug midazolam (M). **c**, Summary diagram of the selective postsynaptic impairment of inhibitory synapses on excitatory cortical pyramidal neurons, underlying the SCML2-dependent epilepsy syndrome.

Methods

Animals

The following mouse strain was used: G42 GAD67-GFP (JAX Laboratory, number 007677). All animal procedures were performed in accordance with the Swiss Veterinary Law guidelines and were approved by the Veterinary Department of the Canton of Basel-Stadt.

EEG recording

All video-EEG recordings were performed by using 21 scalp electrodes, placed according to the 10-20 International system. The polygraphic examinations included also electromyographic recordings from different muscles. Bipolar and monopolar montages of the scalp electrodes were analysed (SystemPlus, Micromed, Mogliano Veneto, Italy).

Brain MRI

All images were obtained by using a 1.5T Magnetom Vision scanner (Siemens, Erlangen, Germany). Nitrous oxide was administered for sedation by an anesthesiologist after parental consent. Sleeping child was scanned with a quadrature knee coil under constant cardiorespiratory monitoring. The MR imaging protocol included coronal and axial SE T1-weighted sequences (TR/TE/excitations = 400/15

ms/2), axial SE T2-weighted sequences (TR/TE/excitations = 3800/81–120 ms/1), and axial IR sequences (TR/TE/TI = 8416/60/350 ms), acquired with a 4-mm sec- tion thickness with no gap.

Whole Exome Sequencing of patients

Targeted enrichment and massively parallel sequencing were performed on genomic DNA extracted from circulating leukocytes of a single affected subject and his parents (family I). Exome capture was carried out using Nimblegen SeqCap EZ v.2.0 (Roche) or TruSeq v.2 (Illumina) capture kits, and sequenced on a HiSeq2000 platform (Illumina). WES data analysis was performed using an in-house implemented pipeline. Paired-end reads were aligned to the human genome (UCSC GRCh37/hg19) with the Burrows-Wheeler Aligner (BWA V. 0.7.10). Presumed PCR duplicates were discarded using Picard tools' MarkDuplicates (http://broadinstitute.github.io/picard/). The Genome Analysis Toolkit (GATK V.3)[1] was used for realignment of sequences encompassing INDELs and for base quality recalibration. SNPs and small INDELs were identified by means of the GATK's HaplotypeCaller used in gVCF mode, followed by family-level joint genotyping and phasing (see https://www.broadinstitute.org/gatk/guide/best-practices?bpm=DNAseq).

Variant call files were annotated with data from numerous databases using in-house tools and databases as well as publicly available software and databases (see Supplementary Note). Variants in each family were custom filtered based on family inheritance patterns, allele frequencies, predicted deleterious effects of variants, and other annotation information (see Supplementary Note). Exome sequencing results were confirmed by Sanger sequencing. PCR primers were designed for the variants

and purified products sequenced using Big Dye V3.1 chemistry and the Applied Biosystems 3730XL Sequence Analysis Instrument.

Scml2 antibody generation

A custom antibody against the C-terminal domain of SCML2 was generated by Eurogentec s.a. (Seraing, Belgium). In brief, a synthetic 16 AA peptide was synthetized (Aa 891-905: h- C+ SSKVPRKSGQASKGN –oh) and used to immunize rabbits, resulting in polyclonal antisera. The antibody was affinity purified and used for immunostaining at a dilution of 1:250.

TALEN-mediated generation of *Scml2*^{KO} mice and genotyping

The 11bp frame-shift mutation produced in intron 4 was performed using specific TALEN designed to recognize DNA sequences upstream and downstream of the deletion point as described in Flemr et al., 2015[2]. In brief, TALENs targeting *Scml2* were assembled using the Golden Gate cloning system for TALEN assembly (Addgene TALEN Kit No. 1000000024). The following repeat variable diresidue repeats were used to generate individual TALENs: SCML2_FWD_TAL1-ELD NN-NN-NI-NN-NI-HD-NG-NG-NN-NG-NN-NN-NI-NG-NG-HD-NI-NG-HD-NI, SCML2_REV_TAL1-KKR HD-NG-HD-HD-NG-HD- HD-NG-NG-NN-NG-NG-HD-NI-HD-NN-NG. Each TALEN-encoding plasmid was linearized with NotI and transcribed in vitro using the mMESSAGE mMACHINE T7 Kit (Ambion). The RNAs were then polyadenylated using the Poly(A) Tailing Kit (Ambion) and purified on RNeasy Mini columns (Qiagen). A dilution for microinjection was prepared by mixing the two TALEN RNAs in ultrapure water at concentration of 20 ng/ml each.

Fertilized oocytes were injected and re-implanted. Progeny was genotyped using the following primers: fwd- ggtgtgtgttgcttcggt; rev- cccagtggaggctgaagta. An heterozygous female carrying an 11bp frame-shift mutation, resulting in a premature STOP codon in exon 4, was selected as founder and used for subsequent crossings.

In vivo local field potential recordings

Local field potentials were recorded from light-anesthetized WT and *Scml2*^{KO} mice (fentanyl 0.05 mg/kg, medetomidine 0.5 mg/kg, midazolam 5.0 mg/kg). A 3 mm-diameter cranial window was performed over the mouse primary somatosensory cortex; after removal of the skull flap, the cortical surface was kept moist with a cortex buffer, containing: 125 mM NaCl, 5 mM KCl, 10 mM glucose, 10 mM HEPES, 2 mM $MgSO_4$ and 2 mM $CaCl_2$. After surgery, a linear multichannel electrode (Neuronexus®, 16 electrodes with 50 μm spacing) was implanted in the primary somatosensory cortex. In the configuration employed, the most superficial electrode laid on the cortical surface (after *dura mater* removal), while the deepest electrode laid at a depth of 750 μm from the cortical surface. Data were collected at 25 kHz from all electrodes for 300 seconds time windows. Spectral analysis was performed in Matlab® on the module of the Hilbert Transform of recorded data, after downsampling (1:100).

Ex vivo electrophysiological recordings

Coronal slices of P60 mice were transferred to an interface chamber containing ACSF equilibrated with 95% O2/5% CO2 containing the following: 124 mM NaCl, 2.7 mM

KCl, 2 mM CaCl2, 1.3 mM MgCl2, 26 mM NaHCO3, 0.4 mM NaH2PO4, 18 mM glucose, 4 mM ascorbate. Recordings were performed with ACSF in a recording chamber at a temperature of 35°C at a perfusion rate of 1-2 ml/min. Neurons were visually identified with infrared video microscopy using an upright microscope equipped with a 40X objective (Olympus, Tokyo, Japan). Patch electrodes (3–5 MΩ) were pulled from borosilicate glass tubing. For voltage clamp experiments to record miniature inhibitory post-synaptic currents (mIPSCs), patch electrodes were filled with a solution containing the following (in mM): 110 CsCl, 30 K-gluconate, 1.1 EGTA, 10 HEPES, 0.1 CaCl2, 4 Mg-ATP, 0.3 Na-GTP (pH adjusted to 7.3 with CsOH, 280 mOsm) and 4 N-(2,6-Dimethylphenylcarbamoylmethyl)triethylammonium bromide (QX-314; Tocris-Cookson, Ellisville, MO). To exclude AMPA receptor and NMDA receptor-mediated inputs, CNQX (6-cyano-7-nitroquinoxaline-2,3-dione, 10 μM: AMPA receptor antagonist) and (R)-CPP (NMDA recetor antagonist) were added to the ACSF. To exclude action potential dependent IPSCs, tetrodotoxin (TTX, 1 μM) was added to the ACSF. Whole cell patch-clamp recordings were excluded if the access resistance exceeded 13 MΩ and changed more than 20% during the recordings. Data were recorded with a MultiClamp 700B (Molecular Devices) amplifier, filtered at 0.2 kHz, and digitised at 10 kHz. Data were acquired and analysed with Clampex 10.0, Clampfit 10.0 (Molecular Devices) and the Mini Analysis Program (Synaptosoft, Decatur, GA). All chemicals for the internal and external solutions were purchased from Fluka/Sigma (Buchs, Switzerland). Glutamatergic blockers were purchased from Tocris Bioscience (Bristol, UK). TTX was from Latoxan (Valence, France).

Viral injections and immunostainings

In order to visualize cortical pyramidal neurons, we delivered AAV-RFP virus (AAV1.CMV.TurboRFP.WPRE.rBG, Penn Vectors, USA) through stereotaxic injections in Isofluorane anesthetized adult mice (P60-P90). After 10 days, mice were perfused with 4% PFA and sacrificed. Brains were equilibrated in 30% sucrose, frozen in OCT and preserved at -80°C. Immunohistochemistry was performed on free floating brain sections. Antibodies used were the followings: SCML2 (custom made, Eurogentec S.A., Seraing, Belgium), NeuN (Millipore, 1:1000), Gephyrin (Synaptic Systems, 1:200), VGAT (Millipore, 1:500), VGluT2 (Milipore, 1:500), GlyR1a (1:500), GlyT2 (1:500), VAchT (1:500), Parvalbumin (Swant Inc., 1:250), Syt2 (Sigma Aldrich, 1:500), Nlgn2, (Santa Cruz, 1:200). Overview imaging for cell visualization and count was performed with a confocal laser scanning microscope (LSM700, Zeiss) equipped with a 10x objective. Imaging for synapsis visualization was carried out using a confocal laser scanning microscope (LSM700, Zeiss) equipped with 488 nm and 555 nm laser diodes. Images of Soma were obtained with a 63× objective.

Calcium imaging recordings

Craniotomy for calcium imaging was performed on anesthetized WT and *Scml2*^{KO} mice (fentanyl 0.05 mg/kg, medetomidine 0.5 mg/kg, midazolam 5.0 mg/kg). A 3 mm-diameter cranial window was performed over the mouse primary somatosensory cortex; after removal of the skull flap, the cortical surface was kept moist with a cortex buffer, containing: 125 mM NaCl, 5 mM KCl, 10 mM glucose, 10 mM HEPES, 2 mM $MgSO_4$ and 2 mM $CaCl_2$. After *dura mater* removal, 3µl of AM X-

Rhod-1 1 mM (solution in 20% Pluronic F-127 in DMSO) was injected at 400 μm from the cortical surface. The skull window was then sealed with a 3mm-diameter glass coverslip. A thin iron ring and a metal bar were attached to the skull with a mixture of dental cement and Super Glue to allow for head fixation during calcium imaging.

Thirty minutes after injection we performed calcium imaging by means of a two-photon laser scanning microscope equipped with a 16 X water immersion objective (0.8 NA) attached to a laser adjusted to 920 nm. During imaging, mice were anesthetized with 0.25% isoflurane and sedated with 2.5 mg/kg chlorprothixene. An area of 300 × 400 μm was imaged at 300 μm below the pial surface. Images were collected at 10 Hz for 200 seconds time windows. For both WT and *Scml2*^{KO} mice, images were collected in baseline conditions, and after 10, 20 and 30 min from intraperitoneal injection of Pilocarpine (100 mg/kg). Time-frequency analysis of the data was performed by Wavelet analysis in Igor Pro®.

Statistics

All data are presented as mean +/- s.e.m. All statistical analysis were performed in Excel or Graphpad Prism 6.0, using unpaired Student's t-tests. Significance in the time-frequency domain (Fig. 5) was assessed by comparing the power integrals in the 1-3 Hz band among different animals with unpaired T tests or among different treatments with paired T tests.

References

1. McKenna, A. *et al*. The Genome Analysis Toolkit: A MapReduce framework for analyzing next-generation DNA sequencing data. *Genome Research* **20,** 1297–

1303 (2010).

2. Flemr, M. & Bühler, M. Single-Step Generation of Conditional Knockout Mouse Embryonic Stem Cells. *Cell Rep* **12,** 709–716 (2015).

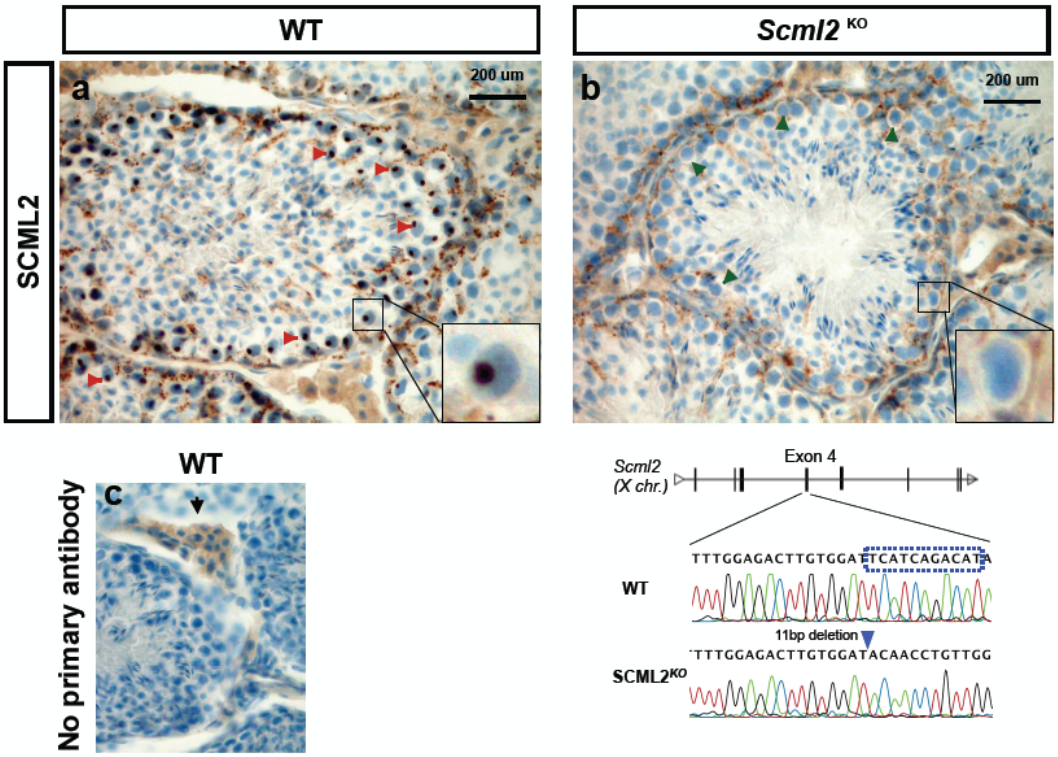

Supplementary Figure 1 Validation of custom produced antibodies demonstrates the loss of native Scml2 protein in *Scml2*^{KO} mice In order to validate the specificity of the rabbit polyclonal custom antibody, we performed immunohistochemistry on PFA perfused wild-type and *Scml2*^{KO} mice testicular sections. **a, b**, Staining displays an identical pattern compared to previously published data in the wt tissue, with a strong subnuclear localisation in undifferentiated spermatogonia (red arrows). The C-terminus targeting specific antibody shows high specificity. Staining in the *Scml2*^{KO} is negative for Scml2. **c**, A test without primary antibody is shown to demonstrate the endogenous unspecific peroxidase activity of sertoli cells. Nuclei were counterstained (light blue).

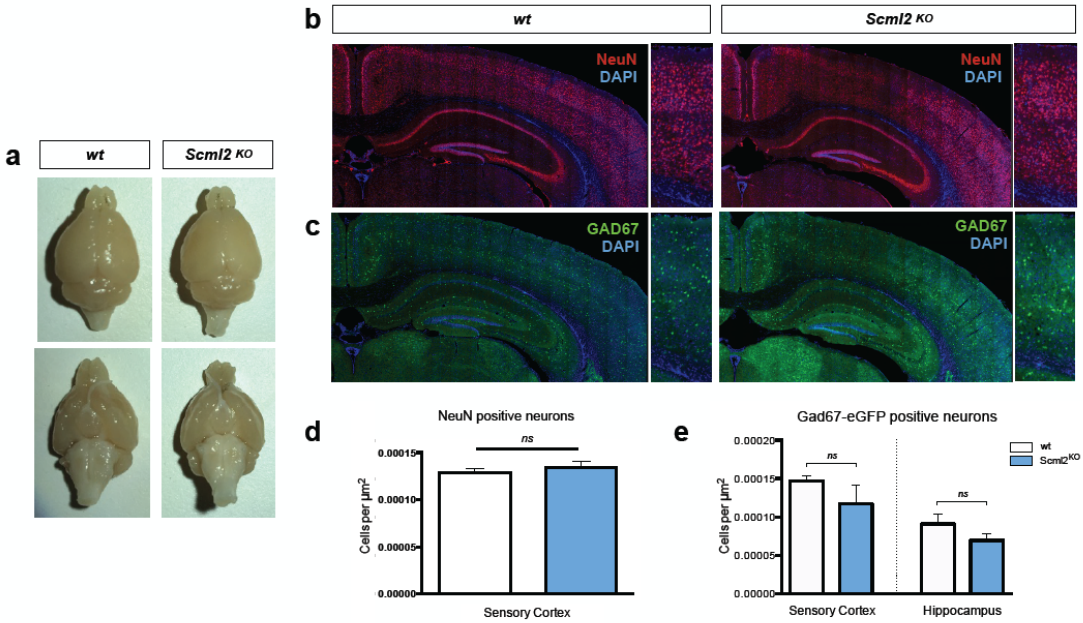

Supplementary Figure 2 *Scml2*^{KO} mice do not display significant brain alterations. a, Mutant *Scml2*^{KO} mice do not show striking brain abnormalities as shown by a comparable size and comparable general anatomy of the brain. Quantification of NeuN positive neurons in the cortex as well as Gad67-eGFP positive neurons in the cortex and hippocampus show no significant differences between *Scml2*^{KO} mice and littermate controls (n=3-5 per group, unpaired t-test $p>0.05$).

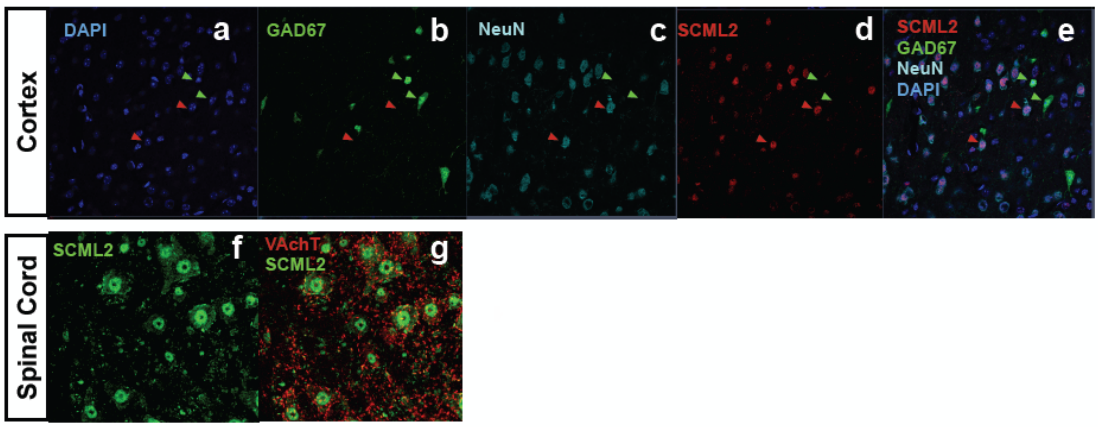

Suplementary Figure 3 SCML2 protein is detectable in excitatory neurons of adult mouse brain. Immunohistochemistry showing the presence of SCML2 in NeuN-positive adult cortical neurons (a-e) and motor neurons (f-i).

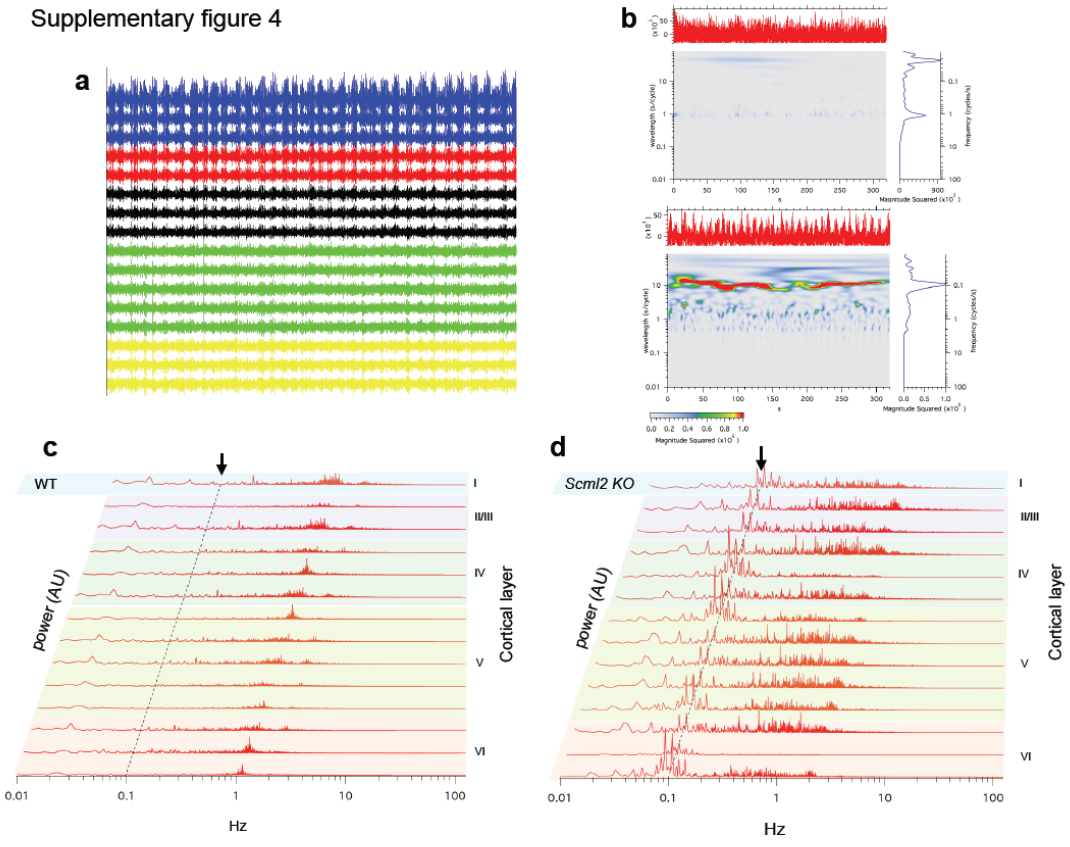

Supplementary Figure 4. Example of infra slow electrical activity in *Scml2*^{KO} mouse. **a,** Spectral analysis of the 16 electrode electrode traces (as in figure 3a-b) for a mutant mouse. **b**, Wavelets transform of the top trace from Fig. 3b **c**, wavelets

transform of the top trace from a. **d,** Please note the persistent ectopic activity at 0.1 Hz in b and d (infra slow activity).

Supplementary Table 1. Whole exome sequencing data output (family S).

Target region coverage, 2x	96.8%	96.2%
Target region coverage, 10x	93.6%	91.1%
Target region coverage, 20x	90.3%	82.7%
Average sequencing depth on target	103.5	53.3
Variants after pre-filtering (based on depth, quality, and MAF)		4687
Functional family variants, pre filtered, start, stop, missense, insertions, deletions, splice, near splice, rare		661
X-linked variants		10
Functionally relevant X-linked variants		1, *SCML2*

Supplementary Table 2. Whole exome sequencing data output (family I).

Target region coverage, 2x[1]	99.0%
Target region coverage, 10x[1]	96.6%
Target region coverage, 20x[1]	92.8%
Average sequencing depth on target[1]	99x
Number of variants with predicted functional effect	11,617
Novel, clinically associated, and unknown/low frequency variants[2]	325

De novo variants[3,4]	3
Functionally relevant *de novo* variants[5]	1, *CACNA1C*[6]
Autosomal recessive variants[7]	4
Functionally relevant Autosomal recessive variants [5]	1, *CACNA1C*[6]
X-linked variants[8]	4
Functionally relevant X-linked variants[5]	1, *SCML2*

[1]Referred to Nimblegen SeqCap EZ Library v.2.0 (Roche).

[2]MAF <0.1% in dbSNP142 and ExAC V. 0.3 databases, and with frequency <2% in our *in-house* database.

[3]Only *de novo* changes are considered as both parents are unaffected.

[4]*CACNA1C* (chr12:2717781, CCTT>C), *GAGE12J* (chrX:49179739, A>G, rs201649497) and *ZNF880* (chr19:52888377, C>G).

[5]Filtering retained functionally relevant variants (*i.e.*, nonsynonymous and splice site changes, excluding variants predicted as benign by CADD and metaSVM algorithms).

[6]Heterozygous mutations in this gene cause Brugada Syndrome type 3 (MIM 611875), and Timothy syndrome (MIM 601005). Sanger sequencing of exon 27 and exon 42 of CACNA1C (NM_000719.6) confirmed the presence of p.F1155del and p.V1707I variants in heterozygosis. The p.V1707I (rs147896322, MAF<0.01), classified as a likely benign variant in dbSNP, has been inherited from mother and has also been found in brother of patient I. The p.F1155del variant has not been reported before and has a de novo occurrence in patient I. This mutation affects one of two conserved contiguous phenylalanine residues in one of the transmembrane domains of

the Cav1.2 channel. Patient I did not show signs of Brugada or Timothy syndromes (see Supplementary Note).

[7]*CACNA1C* (chr12:2717781, CCTT>C *de novo*; chr12:2788637, G>A, rs147896322), *PCNT* (chr21:47746327, A>G; chr21:47786930, A>G), *SCRIB* (chr8:144886866, G>A; chr8:144892761, C>T) and *SYNE1* (chr6:152737729, C>A; chr6:152623079, C>G, rs368601212).

[8]*SCML2* (chrX:18342027, G>T), *SHROOM2* (chrX:9900348, C>T, rs200219705), *STARD8* (chrX:67937855, G>A, rs200219705) and *USP26* (chrX:132160047, T>G).

Supplementary Note

Additional information on variant annotation and filtering

Variant call files were annotated with information from the Genetic variant annotation and effect prediction toolbox (SnpEff)[1], then further annotated with information from numerous databases such as ClinVar (www.ncbi.nlm.nih.gov/clinvar/), Polyphen-2[2], FATHMM[3], SIFT[4], Clinical Genomic Database[5], and the National Heart, Lung, and Blood Institute's GO Exome Sequencing Project (ESP) (ESP 2013). Allele counts from ExAC (Exome_Aggregation_Consortium 2014) and CADD[6] scores were also obtained. Called variants were next filtered by applying the following thresholds: variants with quality >100 and quality-by-depth score >1.5 were retained; variants below these thresholds or resulting from four or more reads having ambiguous mapping (this number being greater than 10% of all aligned reads) were discarded. Variants identified in each family were custom sorted based on allele frequency, family inheritance patterns, predicted deleterious functional effects of variants, and other annotations. For the I family, data annotation predicted 11,617 high-quality variants having functional impact (*i.e.*, non-synonymous and splice site changes). Among them, 325 private and rare changes were retained for further analyses. Only changes predicted to be deleterious by Combined Annotation Dependent Depletion (CADD) (score >15.0) and Database for Nonsynonymous SNPs' Functional Predictions (dbNSFP) Support Vector Machine (SVM) (radial score >0.0) algorithms were retained, and prioritized on the basis of the functional relevance of genes, taking into account X-linked, autosomal dominant, and autosomal recessive inheritance models. Variant filtering and prioritization allowed to identify the c.349C>A missense substitution (p.Pro117Thr) in *SCML2* as the only excellent candidate as causative

event underlying the trait.

Clinical summary for family I (Italian)

This boy was the first born child to a unrelated Italian couple. There was no family history of miscarriages or infertility. The child was born by TC at 39 weeks of gestation, weight at birth was 2.710 kg, Apgar score of 8-8. Before birth a fetal echography detected bilateral clubfoot which was confirmed postnatally. At birth the child in addition was hypotonic and hyporeactive against gravity and showed arthrogryposis of hands with medially overlapping fingers and clenched fists, suggesting a stiff baby syndrome. The club feet were corrected with plaster casts. At the age of one month the child started to manifest frequent tonic fits during the day. The tonic fits had no correlation with EEG abnormalities and were characterized by raising and abduction of his upper limbs and eyes staring. A brain MRI at age 1 months was normal. In the following months the child swallowed slowly and suck with difficulty and sluggishly and had failure to thrive. When he was uncomfortable for any reason and when crying he frequently had tonic fits with apnea and cyanosis. At age 3 months following a prolonged episode of apnea and cyanosis, the child started to manifest a hemiclonic status epilepticus on the right side which corresponded at a control MRI to an ischemic brain lesion on the left parieto-temporal lobes. During the follow-up spontaneous tonic fits or reactive to any uncomfortable condition recurred daily together with myoclonus. Tonic fits increased in frequency with time and started to associate with clusters of massive myoclonus of upper limbs and palpebral myoclonus, and did not respond to any anticonvulsant therapy. Moreover, tonic and myoclonic fits together with episodes of trismus, excessive salivation, apnea and cyanosis became almost ceaseless preventing feeding and the

child needed gastrostomy. Repeated video-EEG monitoring sessions showed that the tonic fits had no corresponding EEG correlate and did not record any abnormalities of the *cardiac rhythm* during prolonged apnea. This patient also carried two heterozygous variant mutations of *Cacna1c* (Supplementary Information). However, repeated EKGs (electrocardiograms) did not disclose any prolongation of the QT interval and, with the exception of an intellectual disability, this patient had no signs of Brugada or Timothy syndromes (Venetucci et al., 2012) that is characterized by multi-organ dysfunction including arrhythmias, syndactyly, congenital heart disease, and immune deficiency. The child died at the age of 2 years during an episode of tonic fit and prolonged apnea.

Clinical summary for family M (Mexican)

Family F009, non-consanguineous-family from Mexico, demonstrated a history of apparent X-linked inheritance with a strong maternal family history of perinatal lethal disease seen only in males. The proband in this family was a woman with previous history of miscarriage and loss of two male children with the birth of two healthy female children. The first male died approximately fifteen minutes after birth and was suggested to have trisomy 18 although no karyotype was performed. Autopsy reported numerous abnormalities including micrognathia, abnormal helices, clenched hands, overlapping digits, rocker-bottom feet, microcephaly, dysplasia of the inferior olivary nuclei, hypoplasia of the vermis with a dilated fourth ventricle and partial agenesis of the corpus callosum. In addition, there were internal abnormalities including undescended testes, accessory spleen, hypoplastic gallbladder and abnormal lobulation of the lung. The second son was stillborn with an initial pre-natal ultrasound diagnosis of Pena-Shokeir Syndrome. The phenotype by autopsy included

multiple contractures also consistent with arthrogryposis. The third male was observed by ultrasound at 19 weeks to have cerebellar hypoplasia, underdevelopment of the brain cortex, permanently closed hands, bilateral doriflexion of the foot with rocker-bottom. Autopsy was performed after termination of the pregnancy at 24 weeks by which confirmed features of arthrogryposis, contracted elbows, clenched hands overlapping digits, dorsiflexed ankles and rocker bottom feet. FFPE sections of skeletal muscle were unremarkable and spinal cord anatomy appeared normal with anterior horn cells present. Detailed investigation of the brain was not possible due to the nature of the fetal tissue following the termination procedure. No DNA or tissue was available for study from the deceased affected males. In this family, we identified a novel start loss pathogenic variant p.MET1VAL in *SCML2*. This start loss pathogenic variant was present in the mother in a heterozygous state. We developed a custom TaqMan assay to screen for this pathogenic variant. The two additional family members that were available for this study (the father and maternal uncle of the deceased males) did not have this variant.

Analysis of SCML2 in atypical Crisponi syndrome patients

Some clinical features of the syndrome resembled patients with Crisponi syndrome (CS), related to mutations in *CRFL1*, a neonatal disorder with muscle contractions simulating tetanic spasm, camptodactyly, hyperthermia, as well as feeding and respiratory difficulties and sudden death[7]. Considering these clinical overlapping features, we performed sequencing analysis of the 14 coding exons (including splice sites) of *SCML2* in 8 male patients with atypical CS and negative for mutations in *CRFL1*. No mutations in *SCML2* were identified in these patients (data not shown).

References

1. Cingolani, P. et al. A program for annotating and predicting the effects of single nucleotide polymorphisms, SnpEff: SNPs in the genome of Drosophila melanogaster strain w1118; iso-2; iso-3. Fly (Austin) 6, 80–92 (2012).

2. Adzhubei, I. A. et al. A method and server for predicting damaging missense mutations. Nat Methods 7, 248–249 (2010).

3. Shihab, H. A. et al. Predicting the Functional, Molecular, and Phenotypic Consequences of Amino Acid Substitutions using Hidden Markov Models. Human Mutation 34, 57–65 (2012).

4. Kumar, P., Henikoff, S. & Ng, P. C. Predicting the effects of coding non-synonymous variants on protein function using the SIFT algorithm. Nat Protoc 4, 1073–1081 (2009).

5. Solomon, B. D., Nguyen, A.-D., Bear, K. A. & Wolfsberg, T. G. Clinical genomic database. Proceedings of the National Academy of Sciences 110, 9851–9855 (2013).

6. Kircher, M. et al. A general framework for estimating the relative pathogenicity of human genetic variants. Nat Genet 46, 310–315 (2014).

7. Crisponi, G. Autosomal recessive disorder with muscle contractions resembling neonatal tetanus, characteristic face, camptodactyly, hyperthermia, and sudden death: a new syndrome? Am. J. Med. Genet. 62, 365–371 (1996).

Chapter 4

Published article: EZH2 orchestrates topographic migration and connectivity of mouse precerebellar neurons.

Thomas Di Meglio,* Claudius F. Kratochwil,* Nathalie Vilain, Alberto

Loche, Antonio Vitobello, Keisuke Yonehara, Steven M. Hrycaj, Botond Roska, Antoine H. F. M. Peters, Anne Eichmann, Deneen Wellik, Sebastien Ducret, Filippo M. Rijli

Abstract

We investigated the role of histone methyltransferase Ezh2 in tangential migration of mouse precerebellar pontine nuclei, the main relay between neocortex and cerebellum. By counteracting the sonic hedgehog pathway, Ezh2 represses Netrin1 in dorsal hindbrain, which allows normal pontine neuron migration. In Ezh2 mutants, ectopic Netrin1 derepression results in abnormal migration and supernumerary nuclei integrating in brain circuitry. Moreover, intrinsic topographic organization of pontine nuclei according to rostrocaudal progenitor origin is maintained throughout migration and correlates with patterned cortical input. Ezh2 maintains spatially restricted Hox expression, which, in turn, regulates differential expression of the repulsive receptor Unc5b in migrating neurons; together, they generate subsets with distinct responsiveness to environmental Netrin1. Thus, Ezh2-dependent epigenetic regulation of intrinsic and extrinsic transcriptional programs controls topographic neuronal guidance and connectivity in the cortico-ponto-cerebellar pathway.

Ezh2 Orchestrates Topographic Migration and Connectivity of Mouse Precerebellar Neurons

Thomas Di Meglio,[1*] Claudius F. Kratochwil,[1,2*] Nathalie Vilain,[1] Alberto Loche,[1,2] Antonio Vitobello,[1,2] Keisuke Yonehara,[1] Steven M. Hrycaj,[3] Botond Roska,[1,2] Antoine H. F. M. Peters,[1,2] Anne Eichmann,[3,4] Deneen Wellik,[5] Sebastien Ducret,[1] Filippo M. Rijli[1,2]†

We investigated the role of histone methyltransferase *Ezh2* in tangential migration of mouse precerebellar pontine nuclei, the main relay between neocortex and cerebellum. By counteracting the sonic hedgehog pathway, *Ezh2* represses *Netrin1* in dorsal hindbrain, which allows normal pontine neuron migration. In *Ezh2* mutants, ectopic *Netrin1* derepression results in abnormal migration and supernumerary nuclei integrating in brain circuitry. Moreover, intrinsic topographic organization of pontine nuclei according to rostrocaudal progenitor origin is maintained throughout migration and correlates with patterned cortical input. *Ezh2* maintains spatially restricted *Hox* expression, which, in turn, regulates differential expression of the repulsive receptor *Unc5b* in migrating neurons; together, they generate subsets with distinct responsiveness to environmental *Netrin1*. Thus, *Ezh2*-dependent epigenetic regulation of intrinsic and extrinsic transcriptional programs controls topographic neuronal guidance and connectivity in the cortico-ponto-cerebellar pathway.

In mammals, cortical motor and sensory information is mostly relayed to the cerebellum via the hindbrain precerebellar pontine nuclei (PNs), which include pontine gray and reticulotegmental nuclei. The developing hindbrain is rostrocaudally segregated into progenitor compartments, or rhombomeres (r1 to r8) (*1*), genetically defined by nested *Hox* gene expression (*2*). Mouse PN neurons are generated from r6 to r8 lower rhombic lip progenitors (*3*), undergo a long-distance caudorostral tangential migration via the anterior extramural stream (AES), and settle beside the ventral midline (Fig. 1, A and B) (*4, 5*). Intrinsic expression of transcription factors and guidance receptors and extrinsic distribution of ligands are important for AES migration (*6-8*). However, little is known about the epigenetic regulation of these transcriptional programs. Here, we addressed the role of *Ezh2*, which is member of the Polycomb repressive complex 2 and trimethylates histone H3 at lysine 27 (H3K27me3) (*9*).

Ezh2 transcripts are maintained through late stages in lower rhombic lip progenitors, migratory stream, and PN neurons (fig. S1), whereas H3K27m3 is detected throughout the hindbrain (fig. S2). To conditionally inactivate *Ezh2*, we generated transgenic lines in which *Cre* is driven by rhombomere-specific enhancers in spatially restricted regions tiling the caudal hindbrain (*10*) (figs. S3 and S4). To assess cell-autonomous and/or region-specific non–cell autonomous *Ezh2* function in pontine neuron migration, we first crossed *Krox20::Cre* (*10*) to an *Ezh2*$^{fl/fl}$ allele (*10*) (*Krox20::Cre;Ezh2*$^{fl/fl}$). Inactivation in r3

[1]Friedrich Miescher Institute for Biomedical Research, Maulbeerstrasse 66, 4058 Basel, Switzerland. [2]University of Basel, 4056 Basel, Switzerland. [3]Yale Cardiovascular Research Center, Department of Internal Medicine, Yale University School of Medicine, New Haven, CT 06511–6664, USA. [4]CIRB (Centre Interdisciplinaire de Recherche en Biologie), Inserm U1050, 11 Place Marcelin Berthelot 75005 Paris, France. [5]Department of Cell and Developmental Biology, University of Michigan, Ann Arbor, MI 48109–2200, USA.

*These authors contributed equally to this work.
†To whom correspondence should be addressed. E-mail: filippo.rijli@fmi.ch

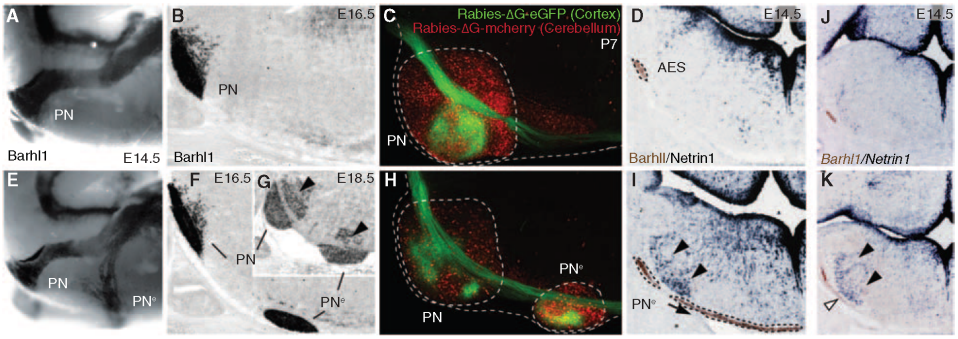

Fig. 1. *Ezh2* non–cell autonomous role in pontine neuron tangential migration. (**A**, **B**, **E**, **F**, and **G**) Migratory phenotypes in control (A) and (B) and *r5-6::Cre;Ezh2*$^{fl/fl}$ mutants (E) to (G). *Barhl1* in situ hybridization in E14.5 whole-mount (A) and (E), E16.5 (B) and (F), and E18.5 (G) sagittal sections. Pontine gray and reticulotegmental [arrowheads (G)] nuclei (PNs) are duplicated (PN^{e}s). (**C** and **H**) Tracings from P7 cortex (rabies-ΔG-eGFP) and cerebellum (rabies-ΔG-mCherry) in controls (C) and *r5-6::Cre;Ezh2*$^{fl/fl}$ mutants (H). PNs and PN^{e}s are connected to cortex and cerebellum. (**D**, **I**, **J**, and **K**) *Barlh1/Netrin1* expression in E14.5 control (D), *r5-6::Cre;Ezh2*$^{fl/fl}$ (I), *r5post::Cre;Ezh2*$^{fl/fl}$*;Shh*$^{fl/+}$ (K), and *r5post::Cre;Ezh2*$^{fl/fl}$*;Shh*$^{fl/fl}$ (J) coronal sections. Ectopic *Ntn1* [arrowheads: (I) and (K)] and PN^e ectopic migration [arrow and white arrowhead, respectively: (I) and (K)] are partially rescued (J).

and r5, which do not contribute to the pontine migratory stream (*3*), resulted in small ectopic PNs in posterior r5 (PN^cs) (fig. S5), which supports an *Ezh2* non–cell autonomous role. Deletion in r5 and r6 (*r5-6::Cre;Ezh2$^{fl/fl}$*) resulted in a more prominent phenotype. A neuronal subset split from the migratory stream, turned ventrally, and generated an ectopic duplication of PNs (PN^cs) (Fig. 1, E to G). PN^c neurons were nonrecombined *Ezh2$^{+/+}$* $H3K27me3^+$ located within the r5- and r6-derived territory mostly devoid of H3K27me3 (fig. S2), which confirmed *Ezh2*'s non–cell autonomous function.

To assess whether PN^cs integrated cortico-cerebellar connectivity, we carried out cortex-to-PN and cerebellum-to-PN tracings. We injected viral constructs expressing green fluorescent protein (GFP) (rabies-ΔG-GFP) and/or mCherry (rabies-ΔG-mCherry) in postnatal day 2 (P2) wild type and *r5-6::Cre;Ezh2$^{fl/fl}$* and *Krox20::Cre;Ezh2$^{fl/fl}$* mutants. At P7, PNs and PN^cs triggered collateralization of corticospinal axons and innervated the cerebellum (Fig. 1, C and H, and fig. S6).

To evaluate *Ezh2* cell-autonomous function, we used the *Wnt1::Cre* deleter (*10*). *Ezh2* transcripts and H3K27me3 were selectively deleted from lower rhombic lip and migratory stream in *Wnt1::Cre;Ezh2$^{fl/fl}$* mutants (figs. S2 and S7). Nonetheless, the mutation was not sufficient to induce ectopic posterior pontine neuron migration (Fig. 2, J and M, and figs. S5 and S7). The most severe phenotype was observed in *Hoxa2::Cre;Ezh2$^{fl/fl}$* mutants, where *Ezh2* was inactivated in both AES neurons and their migratory environment, i.e., throughout r3- to r6- and dorsal r7- to r8-derived structures including the lower rhombic lip (figs. S2 and S3). The whole AES did not migrate anterior to r6 and settled into a single posterior ectopic nucleus (PN^c) (fig. S5). Thus, *Ezh2* has a non–cell autonomous role in AES migration, which is enhanced by a cell-autonomous function in progenitors and migrating neurons.

Netrin1 (Ntn1) and Slit1-3 are attractive or repulsive secreted cues that influence pontine neuron migration (*6, 7*). *Slit1-3* expression was not altered in embryonic day 14.5 (E14.5) *r5-6::Cre;Ezh2$^{fl/fl}$* mutants (fig. S8). In contrast, *Ntn1*, normally expressed in floor-plate and ventral ventricular progenitors (Fig. 1D and fig. S5) (*11*), was ectopically expressed in dorsal progenitors and the mantle layer medially to the AES in *r5-6::Cre;Ezh2$^{fl/fl}$*, *Krox20::Cre;Ezh2$^{fl/fl}$*, *Hoxa2::Cre;Ezh2$^{fl/fl}$*, and *r5post::Cre;Ezh2$^{fl/fl}$* mutants (Fig. 1I and fig. S5). Additional deletion of *Shh* was sufficient to prevent strong ectopic *Ntn1* activation in dorsal progenitors of E12.5 *r5post::Cre;Ezh2$^{fl/fl}$;Shh$^{fl/fl}$* conditional mutants (fig. S5). At E14.5, ectopic *Ntn1* was almost undetectable and the Ezh2 knockout was partially rescued (Fig. 1, J and K, and fig. S5). Therefore, *Ezh2* is required to restrict *Ntn1* expression to ventral progenitors by silencing *Ntn1* in the dorsal neural tube. However, *Ezh2* deletion is not sufficient to ectopically induce *Ntn1*, which additionally requires Shh signaling from the floor plate. Thus, in the dorsal neural tube, *Ezh2*-mediated epigenetic repression of *Ntn1* may normally counteract Shh-mediated activation.

Ectopic and/or increased environmental Ntn1 levels may trigger premature migration toward the midline. In E14.5 *r5-6::Cre;Ezh2$^{fl/fl}$* mutants, only a subset of pontine neurons split from the stream and entered the alternative ventral migratory pathway at the level of the ectopic *Ntn1*$^+$ domain (Fig. 1I and fig. S5), which suggested that AES neurons may display intrinsic differential responsiveness to Ntn1 signaling. To map the contributions of r6 (*r6RL^p*) or r7 and r8 (*r7-8RL^p*) lower rhombic lip–derived neuronal progenies into the pontine stream and nuclei (Fig. 2, B, C and H, and fig. S3), we crossed floxed reporter lines to *r5-6::Cre* or *r7post::Cre* (*Cre* is expressed up to the r6-r7 boundary) (fig. S3H) in which *Cre* is down-regulated before AES migration (fig. S4). *r6RL^p* mapping was confirmed by the tamoxifen-inducible *MafB::CreERT2* transgenic line, whose reporter expression pattern is restricted to r5 and r6, similar to that in *r5-6::Cre* (*10*) (fig. S3). To trace the whole precerebellar lower rhombic lip progeny (*r6-8RL^p*), we used *r5post::Cre* (figs. S3A and S4).

r6-8RL^p contributed to the whole PNs (fig. S3), whereas *r6RL^p* mapped to the most anterior (arrow in Fig. 2H and fig. S3), and *r7-8RL^p* filled the remaining posterior portions of PNs (fig. S3). This topographic organization of pontine neuronal subsets directly correlated with their relative position within the migratory stream. Namely, *r6RL^p* mapped to the dorsalmost AES, whereas *r7-8RL^p* contributed to the remaining portion ventrally to *r6RL^p* (Fig. 2, B and C). Thus, the precerebellar lower rhombic lip is rostrocaudally mapped onto the AES dorsoventral axis (Fig. 3E and fig. S1J) and, in turn, onto the PN rostrocaudal axis (fig. S1K), with neuronal subsets maintaining their relative position throughout migration and settling.

Next, we investigated molecular correlates of this intrinsic cellular regionalization and asked whether *Hox* paralog groups (PG) 2 to 5 maintain their spatially restricted progenitor expression patterns in pontine migratory stream and nuclei (Fig. 2). Indeed, *Hox* PG2 (*Hoxa2*/*Hoxb2*) and PG3 (*Hoxa3*/*Hoxb3*), expressed in the whole precerebellar rhombic lip, were correspondingly maintained throughout the pontine migratory stream and nuclei (*6*) (fig. S1). *Hoxb4* is normally expressed up to the r6-r7 boundary, whereas the *Hox PG5* rostral expression limit is posterior to *PG4* genes (*2*). In the AES and PNs, Hoxb4$^+$ neurons extended just ventrally and posteriorly, respectively, to *r6RL^p* (Fig. 2, C and D, and fig. S1L), whereas *Hoxa5* and *Hoxb5* transcripts and Hoxa5 protein mapped to the ventralmost migratory stream and posteriormost PNs, respectively (Fig. 2, A, F, H and I, and figs. S1 and S2). Simultaneous detection of Hoxa5 and ZsGreen in *r5-6::Cre;R26R^{ZsGreen}* specimens demonstrated rostrocaudal segregation of *r6RL^p* and Hoxa5$^+$ neurons within the PNs (Fig. 2H). To permanently label *Hoxa5*-expressing neurons, we generated a transgenic line in which *Cre* was inserted in-frame at the *Hoxa5* locus (*Hoxa5::Cre*) (*10*) (fig. S3). *Hoxa5::Cre*-expressing neurons segregated to the ventralmost AES and posteriormost PNs, faithfully overlapping endogenous Hoxa5 distribution (Fig. 2, D, E, F and G, and figs. S1F, S3, and S4). Thus, pontine neuron subsets of distinct rostrocaudal origin maintain their relative topographic positions and *Hox* codes throughout migration and settling within the target nucleus (Fig. 4A and fig. S1).

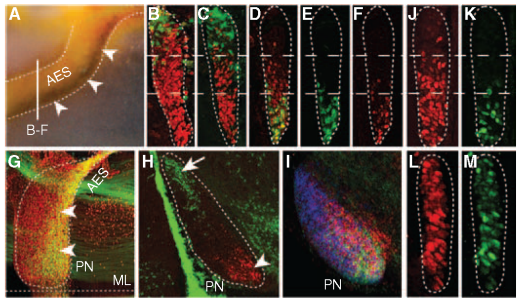

Fig. 2. Intrinsic topography of pontine migratory stream and PNs and *Ezh2*-dependent *Hox* regulation. (**A**) *Hoxb5/Barhl1* in situ hybridization on E15.5 whole-mount brain (lateral view). Arrowheads show Hoxb5$^+$ neuron ventral restriction in AES. (**B** and **C**) E15.5 *r5-6::Cre;R26R^{ZsGreen}* AES coronal sections co-stained with ZsGreen and Pax6 (red) (B) or ZsGreen and Hoxb4 (red) (C) showing complementary dorsal ZsGreen$^+$ and ventral Hoxb4$^+$ cell distributions [bar in (A) shows section level]. (**D** to **F**) E15.5 *Hoxa5::Cre;R26R^{ZsGreen}* AES sections showing partially overlapping ZsGreen and Hoxb4 (red) costainings with offset dorsal limits (D); ZsGreen$^+$ (E) and Hoxa5$^+$ (F) neurons display similar ventral restriction. (**G** and **H**) E15.5 whole-mount *Hoxa5::Cre;R26R^{ZsGreen}* (G) or *r5-6::Cre;R26R^{ZsGreen}* (H) sagittal sections costained with ZsGreen and Pax6 (red) or ZsGreen and Hoxa5 (red), respectively, illustrating posterior PN restriction of Hoxa5$^+$ neurons [arrowheads: (G) and (H)], and anterior restriction of r6-derived neurons [arrow (H)]. ML, ventral midline. (**I**) *Hoxb3/Hoxb4/Hoxb5* nested in situ expression patterns on PN sagittal section (**J** to **M**) Hoxb4 (red) and Hoxa5 (green) immunostaining of E15.5 *Wnt1::Cre;Ezh2$^{fl/+}$* control (J) and (K) and *Wnt1::Cre;Ezh2$^{fl/fl}$* mutant (L) and (M) AES. In (L) and (M), Hoxb4 and Hoxa5 lose their spatial restriction and are ectopically derepressed up to the dorsal edge of the AES.

Is *Ezh2* required to maintain *Hox* nested expression in migrating pontine neurons and PNs? In E14.5 *Wnt1::Cre;Ezh2*$^{fl/fl}$ and *Hoxa2::Cre;Ezh2*$^{fl/fl}$ mutants, Hoxb4, Hoxa5, and *Hoxb5* were ectopically expressed within the anterior lower rhombic lip and spread ventrodorsally throughout the pontine migratory stream (Fig. 2, L and M, and figs. S2 and S7). Thus, by preventing *Hox PG4* and *PG5* expression in anterior precerebellar rhombic lip and migrating neuronal progeny, *Ezh2*-mediated repression contributes to the maintenance of molecular heterogeneity in the migratory stream. This, in turn, may underlie intrinsic differential response of migrating neuron subsets to environmental Ntn1.

Netrin-mediated attraction is counteracted by Unc5 repulsive receptors (*12*), and *Unc5c* inactivation results in variable ectopic migration of AES

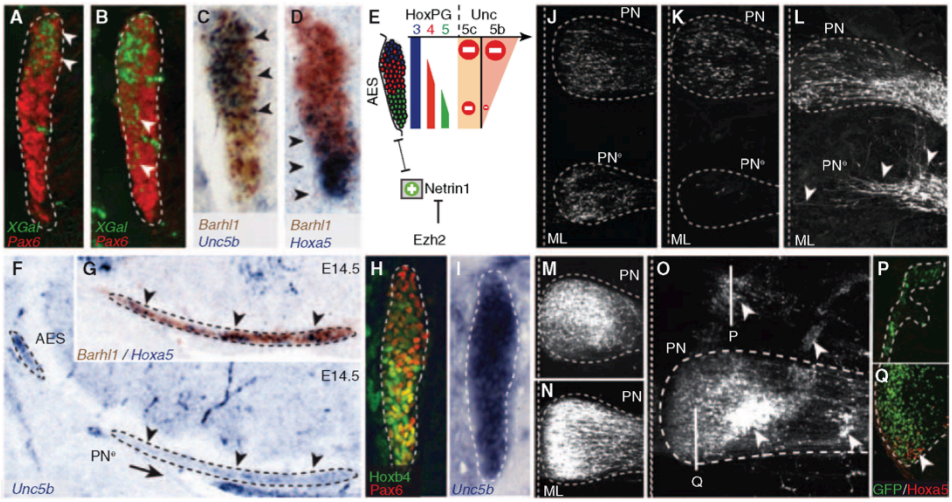

Fig. 3. *Ezh2*- and *Hox*-dependent regulation of *Unc5b* in pontine neuron migration. (**A** and **B**) X-gal (green) and Pax6 (red) costainings of E14.5 *Unc5b*$^{bGal/+}$ heterozygotes (A) and *Unc5b*$^{bGal/bGal}$ homozygotes (B) showing X-gal–stained cell distribution in AES (arrowheads). (**C** to **E**) *Unc5b*/*Barhl1* (C) and *Hoxa5*/*Barhl1* (D) in situ hybridization in E14.5 AES showing complementary dorsoventral expression of *Unc5b* and *Hoxa5* (arrowheads) and summary (E). (**F** and **G**) In *r5-6::Cre;Ezh2*$^{fl/fl}$ mutants, PN^{e} migrating neurons are *Unc5b*-negative (F) and *Hoxa5*$^{+}$/*Barhl1*$^{+}$ (G) (arrowheads). (**H** and **I**) In E14.5 *Hoxa5*$^{-/-}$/*Hoxb5*$^{-/-}$/*Hoxc5*$^{-/-}$ AES, *Unc5b* is up-regulated ventrally (I), whereas Hoxb4 and Pax6 are normally expressed (H). (**J** and **K**) In utero EP in E14.5 *r5-6::Cre;Ezh2*$^{fl/fl}$ mutants of Unc5b/Unc5c/eGFP strongly reduces at E18.5 ectopically migrating PN^{e} neurons (K), as compared with EP of eGFP (J), and partially rescues the phenotype. ML, ventral midline. (**L** to **Q**) In E13.5 wild type, EP of *Ntn1* results in posterior ectopic pontine neuron migration at E17.5, phenocopying *r5-6::Cre;Ezh2*$^{fl/fl}$ mutants [arrowheads (L)]. Although EP at E13.5 of *eGFP* (M) or *Unc5c/eGFP* constructs has no apparent effect on migration at E18.5 (N), EP of *Unc5b/eGFP* results in anterior ectopic migration and/or dorsal-lateral arrest [arrowheads (O)]. Immunostaining on sagittal sections shows that anterior ectopic GFP+/Unc5b^{+} electroporated cells are Hoxa5-negative (P); Hoxa5^{+} cells are normally restricted in posterior PN (Q).

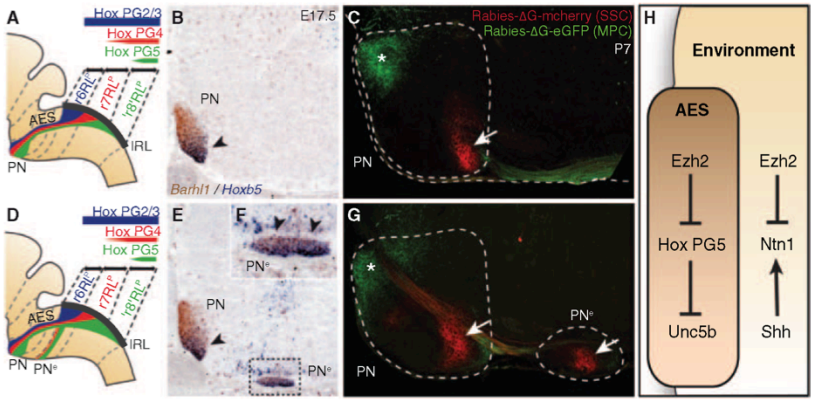

Fig. 4. PN regionalization and patterned cortical input. (**A**, **B**, **D**, **E**, and **F**), *Hox* expression summary in migrating pontine neurons of control (A) and *r5-6::Cre;Ezh2*$^{fl/fl}$ mutants (D). *Barhl1*/*Hoxb5* in situ hybridization on E17.5 sagittal sections (B), (E), and (F). In *r5-6::Cre;Ezh2*$^{fl/fl}$ mutants (E) and (F), Hoxb5^{+} neurons spread throughout the rostrocaudal extent of the ectopic nuclei (PN^{e}s) [arrowheads (F)], whereas, in PNs, they are normally posteriorly restricted as in control [arrowheads: (B) and (E)]. (**C** and **G**) Rabies-ΔG viruses injected in control visual/medioposterior cortex (MPC) and SSC anterogradely trace fibers into anterior (green,*) and posterior (red, arrow) PNs (C), respectively. In *r5-6::Cre;Ezh2*$^{fl/fl}$ mutants (G), PN^{e} lacks innervation by MPC, whereas it is innervated by SSC (arrow). (**H**) *Ezh2*- and *Hox*-dependent genetic circuitry of intrinsic and extrinsic Unc5b/Ntn1 regulation.

neurons (*13*). *Unc5c* is expressed in lower rhombic lip progenitors, down-regulated in migrating neurons, and reactivated upon approaching the midline (fig. S9) (*13*). Thus, *Unc5c* is unlikely to confer a dorsoventrally biased response of the AES to Ntn1. *Unc5b* has been involved in vascular development (*14*), though a role in neuronal development was not explored. We found a dorsoventral high-to-low density of cells expressing *Unc5b* (Fig. 3C and fig. S9) and β-galactosidase activity in $Unc5b^{bGal/+}$ fetuses (Fig. 3A). *Unc5b* expression was, in turn, down-regulated when the migratory stream turned toward the midline (fig. S9C). Dorsoventral *Unc5b* transcript distribution in the migratory stream anti-correlated with *Hox PG5* expression (Fig. 3, C and D). In E14.5 $Hoxa5^{-/-}$;$Hoxb5^{-/-}$;$Hoxc5^{-/-}$ compound mutants, *Unc5b* was up-regulated in ventral $Hoxb4^{+}$/$Pax6^{+}$ AES neurons (Fig. 3, H and I). Thus, Hox PG5 normally represses *Unc5b* in ventral AES neurons originating from posterior precerebellar lower rhombic lip.

In E14.5 $Unc5b^{bGal/bGal}$ null mutants, β-galactosidase^{+} cells partially lost their normal dorsal restriction and spread into ventral AES (Fig. 3B). Thus, *Unc5b* contributes to maintaining topographical organization of dorsal AES subsets. In E16.5 $Unc5c^{-/-}$ fetuses, dorsal *Unc5b*-expressing AES neurons maintained their normal migratory path, whereas ectopic neurons were *Hox* $PG5^{+}$ and mainly *Unc5b*-negative (fig. S9). Therefore, in the absence of *Unc5c*, ventral *Unc5b*-negative AES neurons become more sensitive to Ntn1-mediated attraction than dorsal *Unc5b*-expressing neurons. Similarly, in *r5-6::Cre;*$Ezh2^{fl/fl}$ mutants, *Unc5b*-expressing neurons remain dorsal and pursue their normal migration, whereas *Hox* $PG5^{+}$/*Unc5b*-negative neurons are preferentially influenced by Ntn1 up-regulation and ectopically attracted to the midline (Fig. 3, F and G, and fig. S2). Moreover, in *Hoxa2::Cre;*$Ezh2^{fl/fl}$ mutants, in which all pontine neurons are $Ezh2^{-/-}$/H3K27me3 and migrate through an environment ectopically expressing *Ntn1* (fig. S5), all migrating neurons are prematurely attracted to an ectopic posterior midline position, are *Hox* $PG5^{+}$, and down-regulate *Unc5b* (figs. S2 and S7).

Next, *Unc5b/5c* overexpression by in utero electroporation (EP) of E14.5 lower rhombic lip progenitors was sufficient to cell-autonomously rescue the PN^{e} phenotype in *r5-6::Cre;*$Ezh2^{fl/fl}$ mutants [enhanced GFP–positive (eGFP^{+}) neuron quantification in PN^{e}s compared with PNs: eGFP ($n = 5$) 33.79% ± 0.1060; eGFP/Unc5b/5c ($n = 5$) 0.64% ± 0.0044; $P = 0.00011$] (Fig. 3, J and K), which demonstrated that elevating Unc5 receptor levels counteracts increased Ntn1-mediated attraction. Ntn1 overexpression by EP in E13.5 wild-type fetuses induced ectopic posterior migration of AES neurons (Fig. 3L), partially phenocopying the *r5-6::Cre;*$Ezh2^{fl/fl}$ mutant phenotype and showing that increasing Ntn1 is sufficient to cause ectopic ventral migration of neuronal subsets.

Furthermore, although overexpression of *Unc5c* in E13.5 wild-type fetuses had no apparent effect on AES migration (Fig. 3, M and N), *Unc5b* EP triggered ectopic anterior migration and/or a block in dorsal position of Hoxa5-negative pontine neuron subsets (Fig. 3, O to Q). Therefore, maintaining constitutively high Unc5b levels in migrating neurons prevents or delays turning toward the midline; the latter results in ectopic anterior migration. Conditional *Hoxa2* overexpression in rhombic lip derivatives by mating *Wnt1::Cre* with a *ROSA26::(lox-STOP-lox)Hoxa2*-internal ribosome entry site (*IRES*)-*eGFP* (*Wnt1::Cre;*$R26R^{Hoxa2}$) allele (*10*) also resulted in anterior ectopic migration generating rostrally elongated PNs, which maintained high *Unc5b* expression, unlike in control mice (fig. S9). Therefore, although *Hox PG5* are involved in negatively regulating *Unc5b* in the ventral migratory stream, *Unc5b* expression in dorsal AES may be under *Hox PG2*-positive regulation and generates differential responses to environmental Ntn1.

Finally, we investigated whether the PN and PN^{e} patterning differences in *r5-6::Cre;*$Ezh2^{fl/fl}$ mutants result in distinct cortical inputs. In P7 *Pcp2::Cre;*$R26R^{tdTomato}$ animals (*10*) expressing *Cre* in medioposterior (including visual) cortex (MPC), *tdTomato*$^{+}$ axons projected onto the rostral PN, in agreement with (*15*), including the $r6RL^{p}$ neuron subset (fig. S6). Coinjection of rabies-ΔG-GFP and rabies-ΔG-mCherry into visual and/or MPC and medial somatosensory cortex (SSC) resulted in rostral GFP^{+} and caudal mCherry^{+} axonal inputs onto the PNs, respectively (Fig. 4C). In *r5-6::Cre;*$Ezh2^{fl/fl}$ mutants, PN was targeted both by visual or MPC-derived GFP^{+} (rostrally) and SSC-derived mCherry^{+} (caudally) axons, whereas PN^{e} was innervated by SSC-derived though not visual/MPC-derived axons (Fig. 4G), correlating with their posterior *Hox* $PG5^{+}$ profile (Fig. 4, A, B, and D to F).

During radial migration, correlation to rostrocaudal position of origin is maintained through interaction with glial progenitors (*16*). How long-range tangentially migrating neurons (*17*) maintain information about their origin is less well understood. We show that the topographic migratory program of r6- to r8-derived pontine neurons is largely established in progenitor pools according to rostrocaudal origin and maintained in migrating neurons. We found similar organizational principles during lateral reticular nucleus migration (fig. S10). Moreover, the r2 to r5 rhombic lip also gives rise to neurons that migrate tangentially along a short dorsoventral extramural path and populate distinct brainstem cochlear nuclei with a rostrocaudal topography (*3*). On its caudorostral route, the precerebellar stream migrates ventrally to the cochlear stream (*3*), although they do not mix despite close cellular proximity, which suggests that rhombomere-specific programs may control appropriate precerebellar neuron position during tangential migration. Indeed, we show that the topography of r6 versus r7 versus r8 origin is preserved throughout migration, mapped along the dorsoventral axis of the pontine stream, and eventually within rostrocaudal subregions of the PNs, correlating with patterned cortical input. The transcriptional regulation of this tangential migratory program is epigenetically maintained (Fig. 4H). *Ezh2*-mediated repression maintains dorsoventrally restricted environmental distribution of attractive and/or repulsive cues, such as *Ntn1*, and an intrinsically heterogeneous *Hox* transcriptional program in the migratory stream that, in turn, provides neuronal subsets with distinct Unc5b-dependent responses to environmental Ntn1, and thus contributes to maintaining the neuronal position during migration.

References and Notes

1. A. Lumsden, R. Krumlauf, *Science* **274**, 1109 (1996).
2. S. Tümpel, L. M. Wiedemann, R. Krumlauf, *Curr. Top. Dev. Biol.* **88**, 103 (2009).
3. A. F. Farago, R. B. Awatramani, S. M. Dymecki, *Neuron* **50**, 205 (2006).
4. J. Altman, S. A. Bayer, *J. Comp. Neurol.* **257**, 529 (1987).
5. C. I. Rodriguez, S. M. Dymecki, *Neuron* **27**, 475 (2000).
6. M. J. Geisen *et al.*, *PLoS Biol.* **6**, e142 (2008).
7. K. T. Yee, H. H. Simon, M. Tessier-Lavigne, D. M. O'Leary, *Neuron* **24**, 607 (1999).
8. S. Nóbrega-Pereira, O. Marín, *Cereb. Cortex* **19** (Suppl. 1), i107 (2009).
9. R. Margueron, D. Reinberg, *Nature* **469**, 343 (2011).
10. Materials and methods are available as supplementary materials on *Science* Online.
11. E. Bloch-Gallego, F. Ezan, M. Tessier-Lavigne, C. Sotelo, *J. Neurosci.* **19**, 4407 (1999).
12. K. Hong *et al.*, *Cell* **97**, 927 (1999).
13. D. Kim, S. L. Ackerman, *J. Neurosci.* **31**, 2167 (2011).
14. X. Lu *et al.*, *Nature* **432**, 179 (2004).
15. T. B. Leergaard, J. G. Bjaalie, *Front. Neurosci.* **1**, 211 (2007).
16. P. Rakic, *Science* **241**, 170 (1988).
17. M. E. Hatten, *Annu. Rev. Neurosci.* **22**, 511 (1999).

Acknowledgments: We thank K. Balint, F. Boukhtouche, Y.-Y. Lee, C.-Y. Liang, D. Kraus, T. Mathivet, F. Santagati, J. F. Spetz, and A. Yallowitz for technical support and discussion. We are grateful to M. Tessier-Lavigne, S. H. Orkin, E. Callaway, V. Castellani, P. Mehlen, O. Nyabi, and J. Haigh for gifts of mouse lines, probes, or reagents. The mouse transgenic lines *r5-6::Cre*, *Hoxa2::Cre*, *r5post::Cre*, *r7post::Cre*, *MafB::CreERT2*, *Hoxa5::Cre*, *ROSA26::(lox-STOPlox) Hoxa2-IRES-EGFP* generated in this research and their respective DNA constructs are available from F.M.R. under a material transfer agreement with the Friedrich Miescher Institute for Biomedical Research, Basel, Switzerland. The SAD G-eGFP and SAD G-mCherry G–deleted rabies viruses used in this research are available from E. M. Callaway under a material transfer agreement with Salk Institute for Biological Studies, La Jolla, CA, USA. T.D. is the recipient of a European Molecular Biology Organization Long-Term Fellowship. Work in F.M.R.'s laboratory is supported by the Swiss National Science Foundation (Sinergia CRSI33_127440), Association pour la Recherche sur la Sclérose en Plaques, and the Novartis Research Foundation.

Supplementary Materials

www.sciencemag.org/cgi/content/full/339/6116/204/DC1
Materials and Methods
Figs. S1 to S10
References (*18*–*37*)

27 August 2012; accepted 7 November 2012
10.1126/science.1229326

www.sciencemag.org/cgi/content/full/338/6116/204/DC1

Supplementary Materials for

Ezh2 Orchestrates Topographic Migration and Connectivity of Mouse Precerebellar Neurons

Thomas Di Meglio, Claudius F. Kratochwil, Nathalie Vilain, Alberto Loche, Antonio Vitobello, Keisuke Yonehara, Steven M. Hrycaj, Botond Roska, Antoine H. F. M. Peters, Anne Eichmann, Deneen Wellik, Sebastien Ducret, Filippo M. Rijli*

*To whom correspondence should be addressed. E-mail: filippo.rijli@fmi.ch

Published 11 January 2012, *Science* **338**, 204 (2012)
DOI: 10.1126/science.1229326

This PDF file includes

Materials and Methods
Figs. S1 to S10
Full References

Materials and Methods

Generation of Hoxa5::Cre BAC line

The BAC clone RP23-20F21 (BACPAC Resources Center at Children's Hospital Oakland Research Institute, Oakland, Calif., USA) containing the entire *Hoxa* cluster was used as a template for bacterial recombination as described previously (*18*). The plasmid pN21-Cre was used to amplify a Cre-SV40polyA-Frt-Kanamycin-Frt cassette with 70-mer primers containing 50 nucleotides of homology (indicated as caps) surrounding the coding sequence of the *Hoxa5* first exon, such that *Cre* is inserted in-frame with the *Hoxa5* ATG codon. Forward primer: 5'ACGCACAAACGACCGCGAGCCACAAATCAAGCACACATATCAAAAAACAA atgtccaatttactgaccgt3'; reverse primer:, 5'CAAGACCCGCGCCCCCACGGACGCGTGGATCAGAAAACGGCTGGCTTTACt attccagaagtagtgagga3'. To obtain the *Hoxa5::Cre* BAC construct, EL250 bacteria containing the BAC RP23-20F21 were induced for recombination at 42°C and then electroporated with the Cre-SV40polyA-Frt-Kanamycin-Frt cassette. Bacteria were subsequently arabinose-induced for *Flpe* expression in order to remove the kanamycin cassette. Correct recombination and removal of the resistance gene in the *Hoxa5::Cre* BAC were tested by PCR, restriction enzyme digestion and sequencing. Before microinjection, the modified BAC was linearized by PI-SceI digestion. One founder was obtained that displayed the expected *Cre* expression pattern.

Generation of the MafB::CreERT2 line and tamoxifen treatment

The same approach as above was taken using the BAC clone BAC clone RP23-33A18 (BACPAC Resources Center at Children's Hospital Oakland Research Institute, Oakland, CA). The plasmid pN21-CreERT2 was used to amplify a CreERT2-SV40polyA-Frt-Kanamycin-Frt cassette by using 70-mer primers containing 50 nucleotides of homology (indicated as caps) surrounding the coding sequence of the *MafB* gene, such that the Cre is inserted in-frame with the *MafB* ATG codon.

Forward primer:

5'GGCCGCAAAGTTTTCCCCGCGGCAGCGGCGGCTGAGCCTCGCTTTTAGCGA TGtccaatttactgaccgt3';

reverse primer:

5'GAATAGGGAGTCTGGGCCAGGGCAAGGGCGGGGGCCGGACCCGCCAGGAC ctattccagaagtagtgagga3'.

Tamoxifen was dissolved in corn oil and administered by oral gavage at E7.5 (1mg; 100μl of 10mg/ml stock solution).

Generation of r5post::Cre, r5-6::Cre and r7post::Cre lines

We generated transgenic mice in which *Cre* is driven by rhombomere-specific enhancers of *Hoxb3* (*19*) (*r5-post::Cre*), *Hoxa3* (*20*) (*r5-6::Cre*), or *Hoxb4* (*21*) (*r7post::Cre*) (figs. S3 and S4), which were mated to Gt(ROSA)26Sor (*R26R*)^{lacZ} (*22*), *R26R*^{tdTomato} (*23*), or *R26R*^{ZsGreen} (*23*) reporter lines.

The mouse lines were created by replacing the LacZ gene of the pKS-ß-globin-lacZ vector (BGZ40) (*24*) with a Cre cassette (Clontech) using homologous recombination. Enhancers for *Hoxb3* (*19*) (*r5-post::Cre*, 483 bp), *Hoxa3* (*20*) (*r5-6::Cre*, 629 bp) and

Hoxb4 (*21*) (*r7-post::Cre*, 400 bp) were amplified by PCR from genomic DNA using the following primers: *r5-post::Cre:* forward, 5`ATATCCGCGGGATCGGAGAGGAGAGGGCAA; reverse, 5` CGCGACTAGTGATCTCCAAGGTCCCCTTTCA. *r5-6::Cre:* forward, 5`ATATCCGCGGCAACTTGAAAGGGAAGAGCC; reverse, 5` CGCGACTAGTGATATCAAATAGCAGCGAATCTTC. *r7-post::Cre:* forward, 5`ATATCCGCGGTCCTTGGAAGGTATGAATAG; reverse, 5` CGCGACTAGTTGTTACCTCTGAGCCTCTTG. The PCR bands were purified and inserted 5` of the ß-globin promoter using restriction sites FslI and XhoI (*r5-6::Cre*) and BglI and PvuII (*r5-post::Cre, r7-post::Cre*), thus generating constructs consisting of an enhancer, a ß-globin minimal promoter and Cre recombinase encoding sequence. The constructs were linearized, purified and microinjected into the pronuclei of blastocyst embryos. Founders were identified by PCR and screened at P0 after crossing with *R26R*^{lacZ} animals. 72 animals were genotyped (19 for *r5post::Cre*; 38 for *r5-6::Cre*; 15 for *r7post::Cre*). 19 were positive for Cre (8 for *r5post::Cre*; 8 for *r5-6::Cre*; 3 for *r7post::Cre*). 3/8 showed the expected recombination pattern at P0 for *r5post::Cre*; 2/8 for *r5-6::Cre* and 1/3 for *r7post::Cre*, while the other founders showed no, ubiquitous or ectopic patterns of recombination.

Generation of Hoxa2::Cre line

For the generation of the *Hoxa2::Cre* transgenic line a 3.5kb EcoRI fragment upstream to the *Hoxa2* promoter (from -3585 to -1) was obtained from the plasmid p314R (*25*) and subcloned in a native orientation upstream to a β-globin minimal promoter, the Cre gene and a SV40 polyA signal. The transgene fragment was excised by digestion with SalI and

NotI, and purified before microinjection.

Generation of the ROSA::(lox-STOP-lox)Hoxa2-IRES-EGFP mouse line

The conditional Hoxa2 overexpression mouse line was generated by using the Gateway-compatible *ROSA26* locus targeting vector as previously described (*26*). LR reactions were performed between the plasmid pENTR-FLAG-Hoxa2 (containing the Hoxa2 cDNA coding sequence with a 5'FLAG tag) and the destination vector pROSA26-DV1 to obtain the targeting vector pROSA26-FLAG-Hoxa2-IRES-EGFP. This vector was linearized with PvuI and electroporated into the E14 ES cell line. The positive ES cell clones, selected by G418 resistance and screened by PCR, were aggregated with morula-stage embryos obtained from inbred (C57BL/6 x DBA/2) F1 mice. Germline transmission of the *ROSA26::(lox-STOP-lox)Hoxa2-IRES-EGFP* allele was obtained. Heterozygous and homozygous mice were viable and fertile.

Other mouse lines used in the study

Wnt1::Cre (*27*), $R26R^{lacZ}$ (*22*), $Ezh2^{fl/fl}$ (kind gift from S.H. Orkin) (*28*), *Hoxa5, Hoxb5, Hoxc5* knockout mice (*29*), $Unc5b^{bGal/bGal}$ knockout mice (kind gift from M. Tessier-Lavigne) (*14*) and $Unc5c^{rcm}$ (embryos kindly obtained from V. Castellani) (*30*) were as described. *Pcp2::Cre* (*31*), $R26R^{tdTomato}$, $R26R^{ZsGreen}$ (*23*) and Shh^{tm2Amc} (Shh^{fl}) mice (*32*) were obtained from Jackson Laboratory.

Circuit tracing

G-deleted rabies virus vectors encoding mCherry (SADΔG-mCherry) or eGFP (SADΔG-eGFP) were harvested from BHK-B19G cells (kind gift from E. Callaway) and centrifuged as described previously (*33*). Stereotaxic injections of viruses to different

areas of neocortex or cerebellum were performed via pulled-glass pipettes using a microinjector (Narishige, IM-9B). Pups were anesthetized by hypothermia, injected at P2 and perfused at P7.

In utero electroporation

In utero electroporation was performed on embryos at E13.5 or E14.5 as described previously (*34*) using different combinations of *eGFP* (pCX-eGFP (*35*)), *Unc5b* (pcDNA- *ratUnc5b* (*36*)), *Unc5c* (pcDNA 3.1-*mouseUnc5c*; kind gift from P. Mehlen) and *Netrin1* (pcDNA 3.1-*humanNetrin1*; kind gift from P. Mehlen) expressing vectors diluted to 1 mg/ml in 1x phosphate buffer (PBS1x). Electroporated brains between E16.5 and P0 were fixed for 30 min in paraformaldehyde (PFA, Merck) 4%/ PBS1x. For rescue experiments on *r5-6::Cre;Ezh2*$^{fl/fl}$ embryos, the proportions of ectopic neurons were quantified by Imaris (Bitplane). A Student's t-test was used for statistical analysis.

Histological analysis, immunostaining, and *in situ* hybridization

Prenatal or postnatal brains, dissected when necessary, were fixed in 4% PFA diluted in phosphate buffer (PBS 1x) from 30 minutes to overnight. For cryostat sections, tissues were cryoprotected in 10% sucrose (Fluka) / PBS1x and embedded in gelatine 7.5% (Sigma) / 10% sucrose / PBS1x before being frozen at -80°C. Cryostat sections (20 μm and 30 μm) were cut (Microm HM560) in coronal and sagittal orientations, respectively. Vibratome sections (80 μm or 35 μm for reconstruction) were prepared from postnatal brains after embedding in 4% agarose (Promega)/0.1 M phosphate buffer (pH 7.4). Immunohistochemistry was performed as described in (*6*, *29*) using rabbit anti-mouse

Pax6 (Millipore; AB2237; 1/1000^{em}), anti-Hoxa5 antibody (Sigma; HPA029319; 1/200^{em}), rat anti-mouse Hoxb4 (developed by A. Gould and R. Krumlauf; obtained from the Developmental Studies Hybridoma Bank developed under the auspices of the NICHD and maintained by The University of Iowa, Department of Biology, Iowa City, IA 52242; 1/100^{em}) or rabbit anti-mouse trimethyl-histone H3 Lys27 (07-449; Millipore; 1/250^{em}), followed by species-specific fluorochrome-coupled secondary antibody staining, including donkey anti-rabbit A546 (Invitrogen; 1/1000^{em}) and the donkey anti-rat A488 (Invitrogen; 1/1000^{em}) diluted in solutions containing DAPI (Invitrogen). Simple and double *in situ* hybridizations were performed as described previously(*6*). The following probes were used: *Barhl1; Hoxa2; Hoxb3; Hoxb4; Hoxb5*, *Hoxa5* (*6*, *29*), *Ntn1* (*6*, *11*), *Unc5b and Unc5c* (*37*). X-galactosidase staining on whole embryos, whole brains or cryostat sections was performed as described in (*6*).

Imaging and Picture Processing

Imaging of fluorescent signals was performed using an Axio imager Z2 upright microscope coupled to a LSM700 Zeiss laser scanning confocal 5x lens (NA 0.25), 10x lens (NA 0.45) or oil/glycerol/water immersion lens 25x (NA 0.8). Stitching of whole-mounts (electroporated brains) was performed using Zen Software at postnatal stages, and using Xuvtools (http://www.xuvtools.org) at prenatal stages. Chromogenic staining was examined by classical wide-field or binocular microscopy (Nikon). Fig. 2I is an inverted artificial superposition of chromogenic signals from adjacent sections. In Fig. 3A, B inverted X-Gal signal is artificially projected onto Pax6 immunohistochemistry.

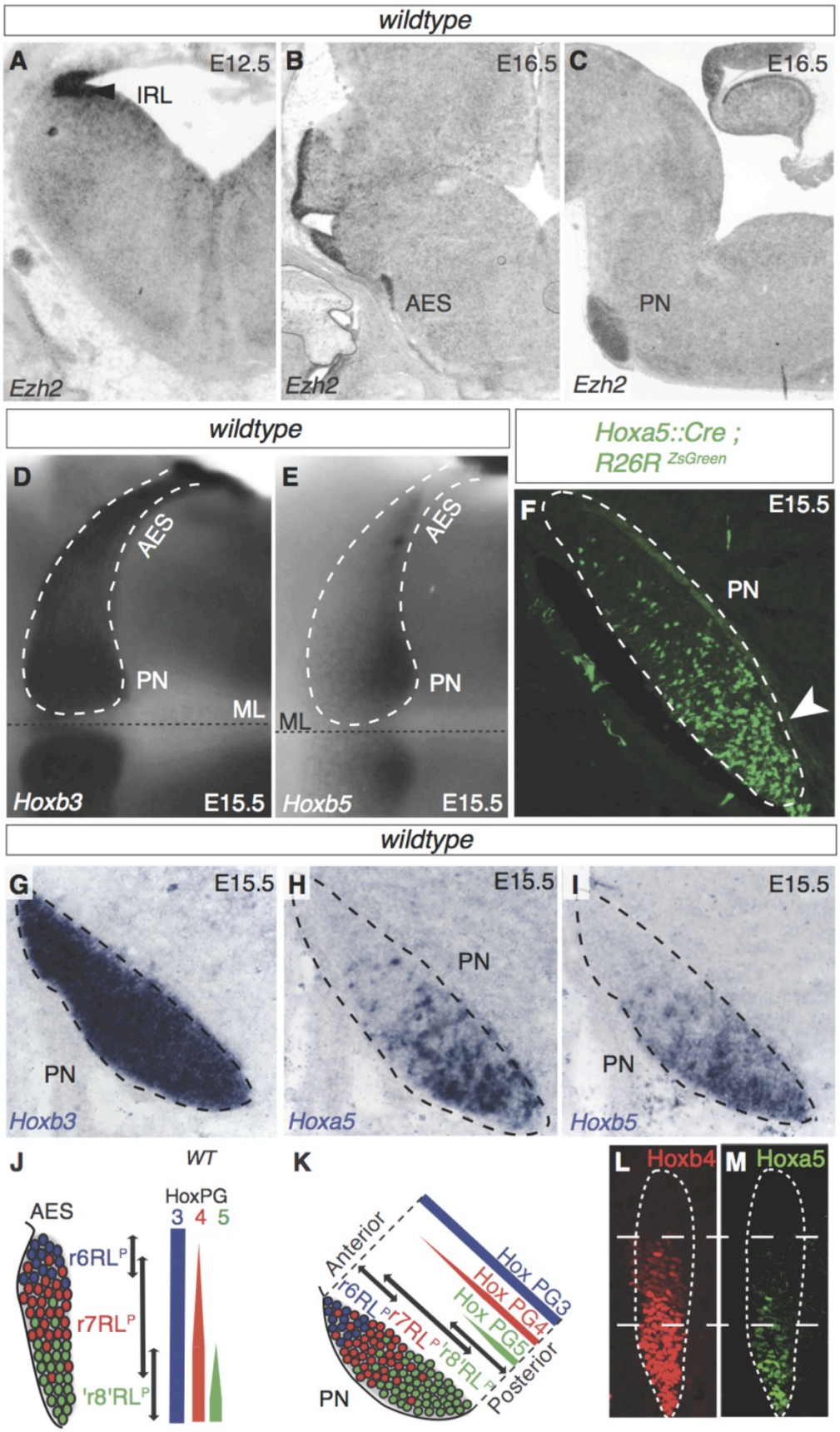
wildtype
A
E12.5
IRL
Ezh2
B
E16.5
AES
Ezh2
C
E16.5
PN
Ezh2
wildtype
Hoxa5::Cre ;
R26R ZsGreen
D
AES
PN
ML
Hoxb3
E15.5
E
AES
PN
ML
Hoxb5
E15.5
F
E15.5
PN
wildtype
G
E15.5
PN
Hoxb3
H
E15.5
PN
Hoxa5
I
E15.5
PN
Hoxb5
J
WT
AES
HoxPG
3 4 5
r6RL^P
r7RL^P
'r8'RL^P
K
Anterior
Hox PG3
Hox PG4
Hox PG5
r6RL^P
r7RL^P
'r8'RL^P
Posterior
PN
L
Hoxb4
M
Hoxa5

8

Fig. S1. *Ezh2* and *Hox* gene expression in precerebellar rhombic lip derivatives. (**A** to **C**) *Ezh2 in situ* hybridization on coronal (A, B) and sagittal sections (C). At E12.5 *Ezh2* is expressed in lower rhombic lip (lRL, A) and maintained in E16.5 anterior extramural stream (AES, B) and pontine nuclei (PN, C). (**D** to **E**) E15.5 whole-mount hindbrains show *Hoxb3* expression in all pontine neurons (D) and *Hoxb5* restriction to the posterior PN (E). (**F**) Sagittal section of E15.5 *Hoxa5::Cre;R26R*^{ZsGreen} specimen revealing the localization of ZsGreen^{+} neurons to the posterior PN (arrowhead). (**G** to **I**) E15.5 PN sagittal sections show *Hoxb3* expression in all pontine neurons (G) and restriction of *Hoxa5*$^{+}$ (H) and *Hoxb5*$^{+}$ (I) cells to the posterior PN. (**J** to **K**) Summaries of Fig. 2A-I and fig. S1D-I. (**L** to **M**) Hoxb4 (L) and Hoxa5 (M) immunostaining on a coronal section of a E14.5 wildtype embryo. ML: ventral midline.

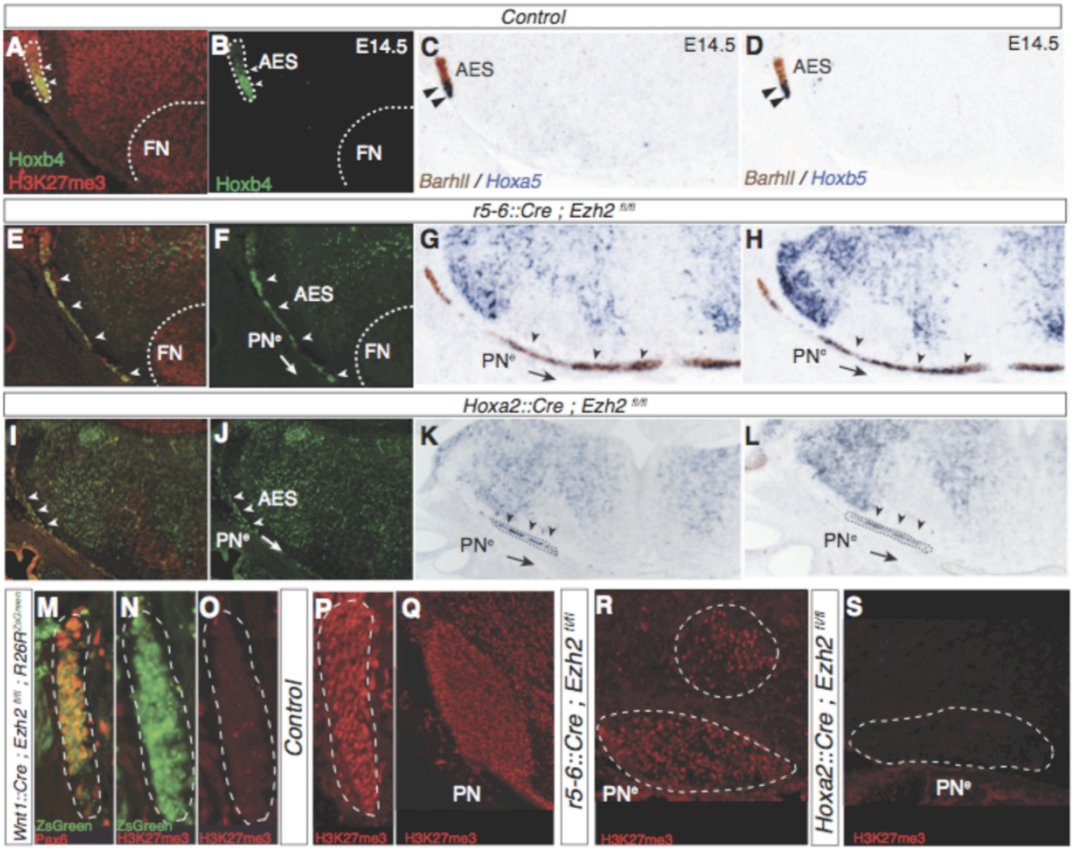

Fig. S2. Hox gene expression in migrating pontine neurons of *Ezh2* conditional mutants. (**A** to **L**) H3K27me3/Hoxb4 immunostaining (A,B,E,F,I,J), *Hoxa5*/*Barhl1* (C,G,K) and *Hoxb5*/*Barhl1* (D,H,L) *in situ* hybridization on coronal sections at r5-r6 level in control (A-D), *r5-6::Cre;Ezh2*$^{fl/fl}$ (E-H) and *Hoxa2::Cre;Ezh2*$^{fl/fl}$ (I-L) E14.5 fetuses. Strong reduction of H3K27me3 in the r5-r6 environment of *Ezh2* conditional knockouts (E,F,I,J). In control (A-D), arrowheads show restricted ventral expression of Hoxb4 (A,B), *Hoxa5* (C) and *Hoxb5* (D) in the anterior extramural stream (AES). In *r5-6::Cre;Ezh2*$^{fl/fl}$ embryos, Hoxb4^{+} pontine neurons migrate to ectopic pontine nuclei (PN^{e}), are Ezh2$^{+/+}$ (co-labeled by H3K27me3/Hoxb4 double immunostaining (arrowheads, E,F)), and express both *Hoxa5* and *Hoxb5* (arrowheads, G,H). In *Hoxa2::Cre;Ezh2*$^{fl/fl}$ embryos, Hoxb4^{+} pontine neurons migrate ectopically to PN^{e} are *Ezh2*$^{-/-}$ as shown by the lack of H3K27me3 (arrowheads, I,J), and express both *Hoxa5* and *Hoxb5* (arrowheads, K,L). The neurons of the facial nucleus (FN), a r4 derivative, still carry the H3K27me3 mark in *r5-6::Cre;Ezh2*$^{fl/fl}$ embryos, showing the specificity of the knockout (E). (**M** to **P**) Pax6 (M) and H3K27me3 (N,O,P) immunohistochemistry of *Wnt1::Cre;Ezh2*$^{fl/fl}$*;R26R*^{ZsGreen} (M-O) and control AES (P) on coronal sections. In the conditional knockout, ZsGreen^{+} pontine neurons express Pax6 (M), but lack the H3K27me3 mark (N,O) in contrast to controls (P). (**Q to S**) H3K27me3 immunohistochemistry on sagittal sections at E18.5 showing loss of the H3K27me3 mark in environment only (R, *r5-6::Cre;Ezh2*$^{fl/fl}$) or environment and PN^{e} (S, *Hoxa2::Cre;Ezh2*$^{fl/fl}$) unlike in controls (Q).

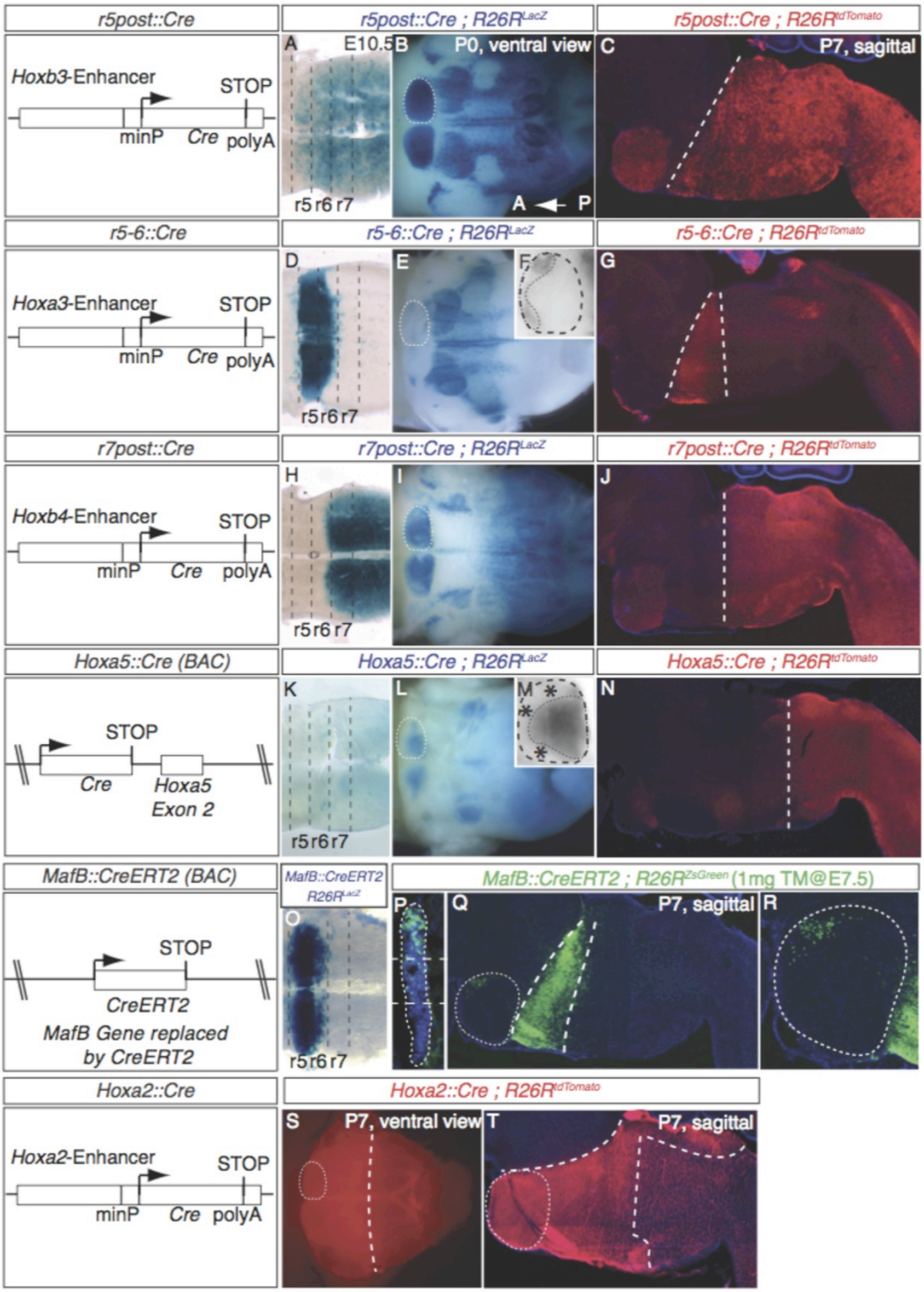

Fig. S3. Generation and characterization of posterior hindbrain Cre-expressing lines. (**A,D,H,K,O**) Embryos carrying *r5post::Cre* (A), *r5-6::Cre* (D), *r7post::Cre* (H)

and *MafB::CreERT2* (1mg Tamoxifen@E7.5) (O) transgenes crossed to the *R26R*^{lacZ} floxed reporter and expressing *β-galactosidase* (*βGal*) at E10.5 in a rhombomere-specific manner, with *r5post::Cre* expression spanning r5 to spinal cord (A), *r5-6::Cre* and *MafB::CreERT2* spanning r5 and r6 (D, O), and *r7post::Cre* spanning r7 to spinal cord (H). *Hoxa5::Cre* is not expressed in the hindbrain before E10.5 (K). (**B,E,I,L,S**) Detection of the *βGal* on whole-mount hindbrains (ventral views) at P0 show the spatially-restricted progeny of these rhombomeres traced after recombination of the *R26R*^{LacZ} locus in each of these Cre or CreERT2 expressing lines (B,E,I,L) or in (S) using the *R26R* ^{tdTomato} reporter line at P7 for *Hoxa2::Cre*. (**F,M**) High magnifications show the segregation of r6 (*r5-6::Cre*, (F)) (rostrally) and *Hoxa5* (i.e. 'r8') (caudally) progenies (M) in the pontine nuclei. (**C,G,J,N,T**) Sagittal sections at P7 show recombined, *tdTomato*$^{+}$ rhombomere progenies of indicated genotypes; segregation of rhombomere-derived territories persists up to postnatal stages. (**P** to **R**) Coronal (P, E15.5) and sagittal sections (Q,R, P7) of *Mafb::CreERT2; R26R*^{ZsGreen} show the dorsal restriction of r5-6 progeny in the anterior extramural stream (P) and the restriction of ZsGreen^{+} cells to the anterior pontine nuclei (R). r: rhombomere; minP: minimal promoter.

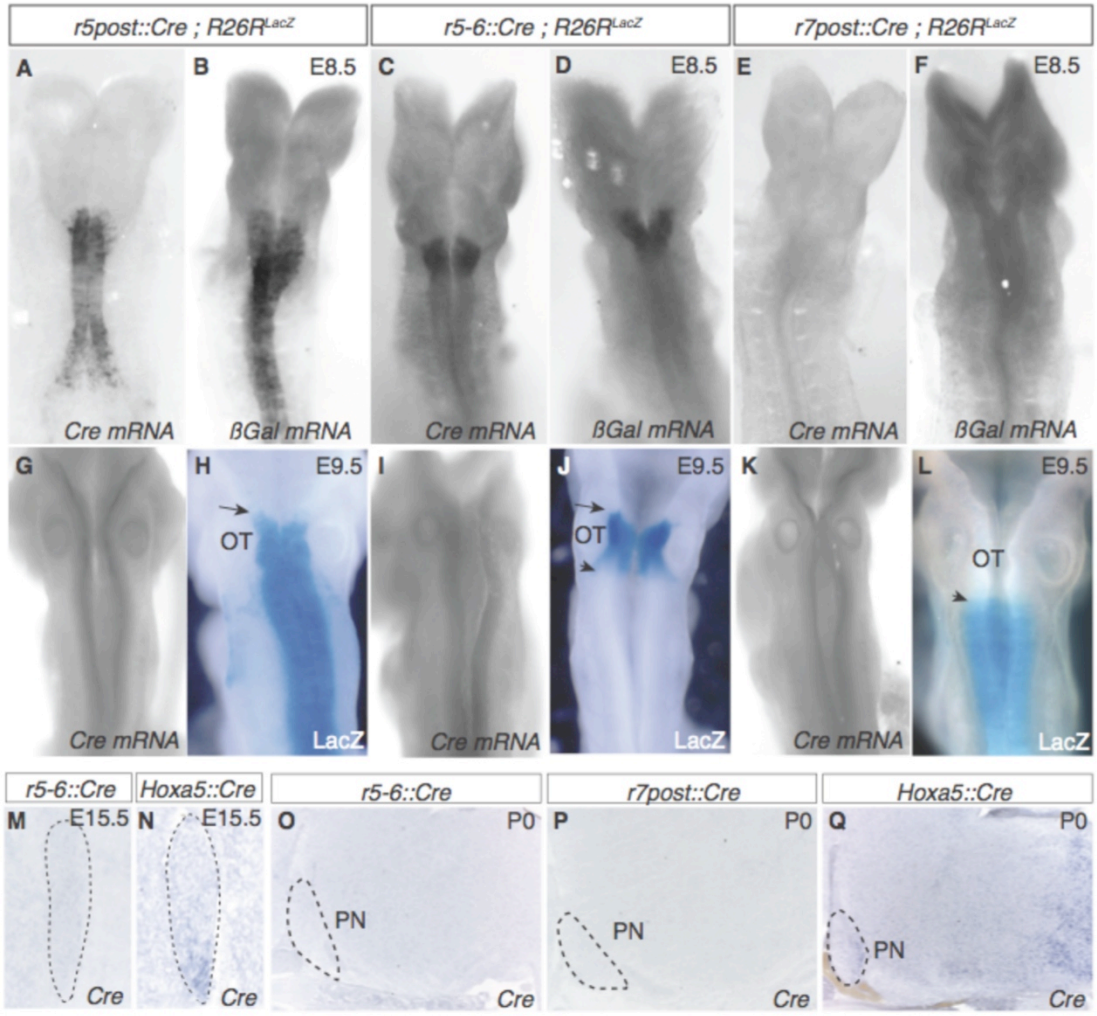

Fig. S4. *Cre* expression patterns in transgenic lines. (**A** to **D**) At E8.5, *Cre* (A,C) and *ß-galactosidase* (*ßGal*) (B,D) are expressed in *r5post::Cre* (A,B) and *r5-6::Cre* (C,D) whole-mount embryos. (**E** to **F**) In *r7post::Cre*, neither *Cre* nor *ß-Gal* are expressed at E8.5. (**G, I, K**) At E9.5, *Cre* transcripts were not detectable in any of the *Cre* transgenics. (**H, J, L**) LacZ signals reveal that the $R26R^{LacZ}$ locus has recombined in all three *Cre* transgenics at E9.5. *r5post::Cre* (H) and *r5-6::Cre* (J) share the same *ßGal* anterior boundary (arrow), while *r5-6::Cre* (J) and *r7post::Cre* (L) have their posterior and anterior expression boundaries, respectively, at the r6/r7 border with no overlap (arrowhead). Note that *r7post::Cre;*$R26R^{lacZ}$ show LacZ restricted activity at E9.5 (L), although *Cre* and *ßGal* transcript levels are below *in situ* hybridization detection at E8.5 and E9.5 (E,F,K). (**M** to **N**) *In situ* hybridizations on coronal sections of E15.5 AES show no expression of *Cre* in *r5-6::Cre* (M), while in *Hoxa5::Cre* embryos *Cre* expression faithfully recapitulates endogenous *Hoxa5* expression (N). (**O** to **Q**) On P0 sagittal sections, *Cre* transcripts are not present at detectable levels in *r5-6::Cre* (O) and *r7post::Cre* (P), while *Hoxa5::Cre* newborns show *Cre* expression in posterior hindbrain and posterior PN (Q). OT: otic capsule; PN: pontine nuclei.

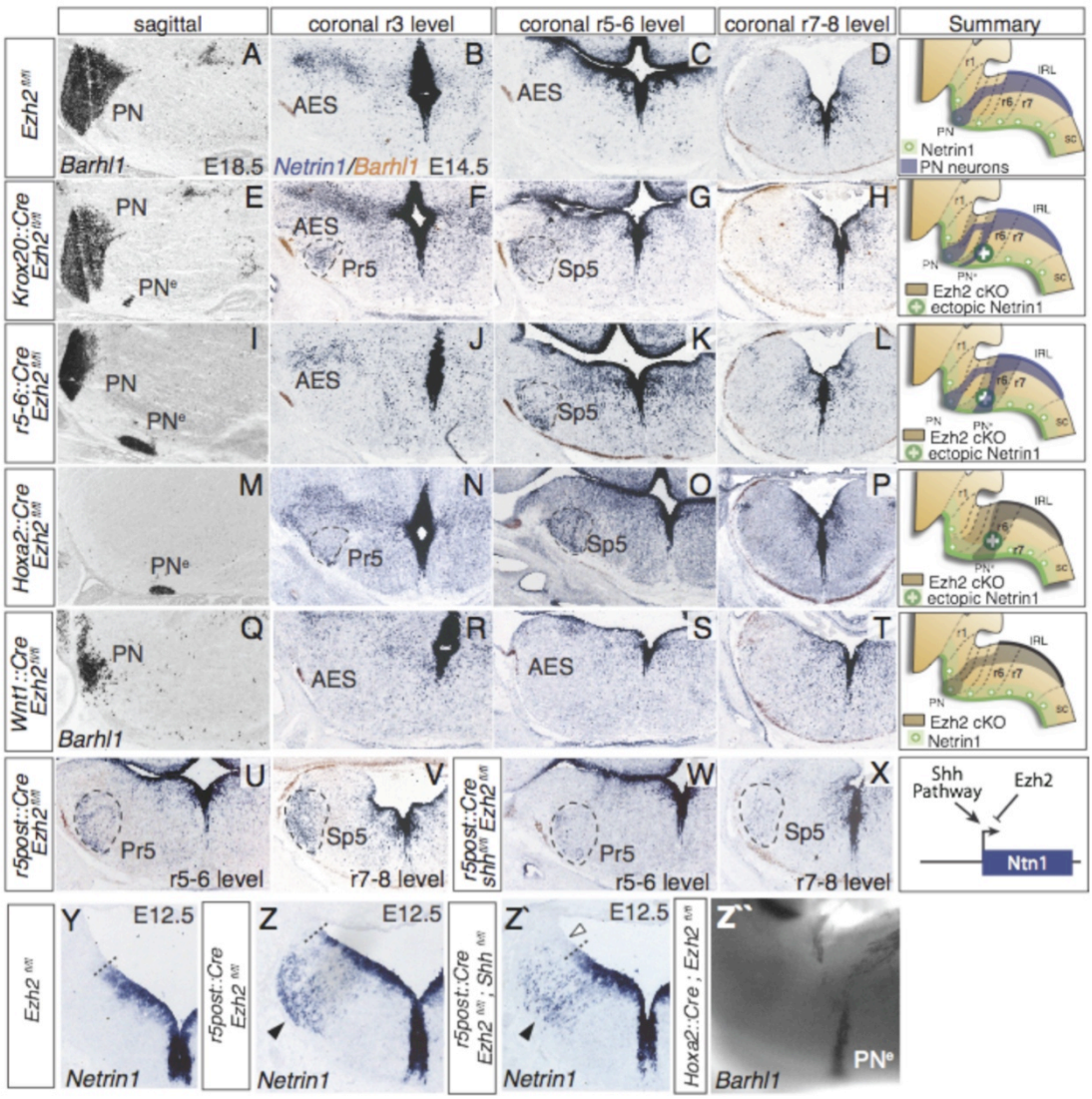

Fig. S5. Analysis of pontine neuron migratory phenotypes in *Ezh2* conditional mutants. (**A** to **T**), PN migratory phenotype in control *Ezh2*$^{fl/fl}$ (A-D), *Krox20::Cre;Ezh2*$^{fl/fl}$ (E-H), *r5-6::Cre;Ezh2*$^{fl/fl}$ (I-L), *Hoxa2::Cre;Ezh2*$^{fl/fl}$ (M-P) and *Wnt1::Cre;Ezh2*$^{fl/fl}$ (Q-T) fetuses. *In situ* hybridization on sagittal sections show rostrocaudal distribution of normal (PN) and ectopic (PN^{e}) *Barhl1*$^{+}$ pontine neurons at E18.5 in the different genotypes (A,E,I,M,Q). Co-detection of *Netrin1* and *Barhl1* transcripts on serial coronal sections taken at the r3, r5/r6 and r7/r8 levels show ectopic expression of *Netrin1* in *Krox20::Cre;Ezh2*$^{fl/fl}$, *r5-6::Cre;Ezh2*$^{fl/fl}$ and *Hoxa2::Cre;Ezh2*$^{fl/fl}$ (dashed lines, F,G,K,N,O) but not in *Wnt1::Cre;Ezh2*$^{fl/fl}$ and *Ezh2*$^{fl/fl}$ embryos at E14.5. (**U** to **X**) Expression of *Netrin1* and *Barhl1* in *r5post::Cre;Ezh2*$^{fl/fl}$ (U, V) and *r5post::Cre;Ezh2*$^{fl/fl}$*;Shh*$^{fl/fl}$ (W,X) at r5/r6 (U, W) and r7/r8 (V, X) levels at E14.5. Ectopic *Netrin1* expression is strongly reduced in *Shh/Ezh2* double cKO (W,X) partially rescuing the *Ezh2* cKO phenotype (U,V). (**Y** to **Z`**) At E12.5, ectopic *Netrin1* expression (black arrowheads) observed in *r5post::Cre;Ezh2*$^{fl/fl}$ mutants (Z) is absent in controls

Ezh2$^{fl/fl}$ (Y) and partially rescued in *r5post::Cre;Ezh2*$^{fl/fl}$*;Shh*$^{fl/fl}$ compound mutants (white and black arrowheads, Z`). (**Z``**) Migratory phenotypes in *Hoxa2::Cre;Ezh2*$^{fl/fl}$ shown by *Barhl1 in situ* hybridization on E14.5 whole-mount. Summaries show the migratory pathways of wildtype and mutants as well as the proposed genetic interaction between Shh, Ezh2 and Netrin1 in the last column. AES: anterior extramural stream; lRl: lower rhombic lip; r: rhombomere; sc: spinal cord; Pr5: principal trigeminal nucleus; Sp5: spinal trigeminal nucleus; cKO: conditional knockout.

15

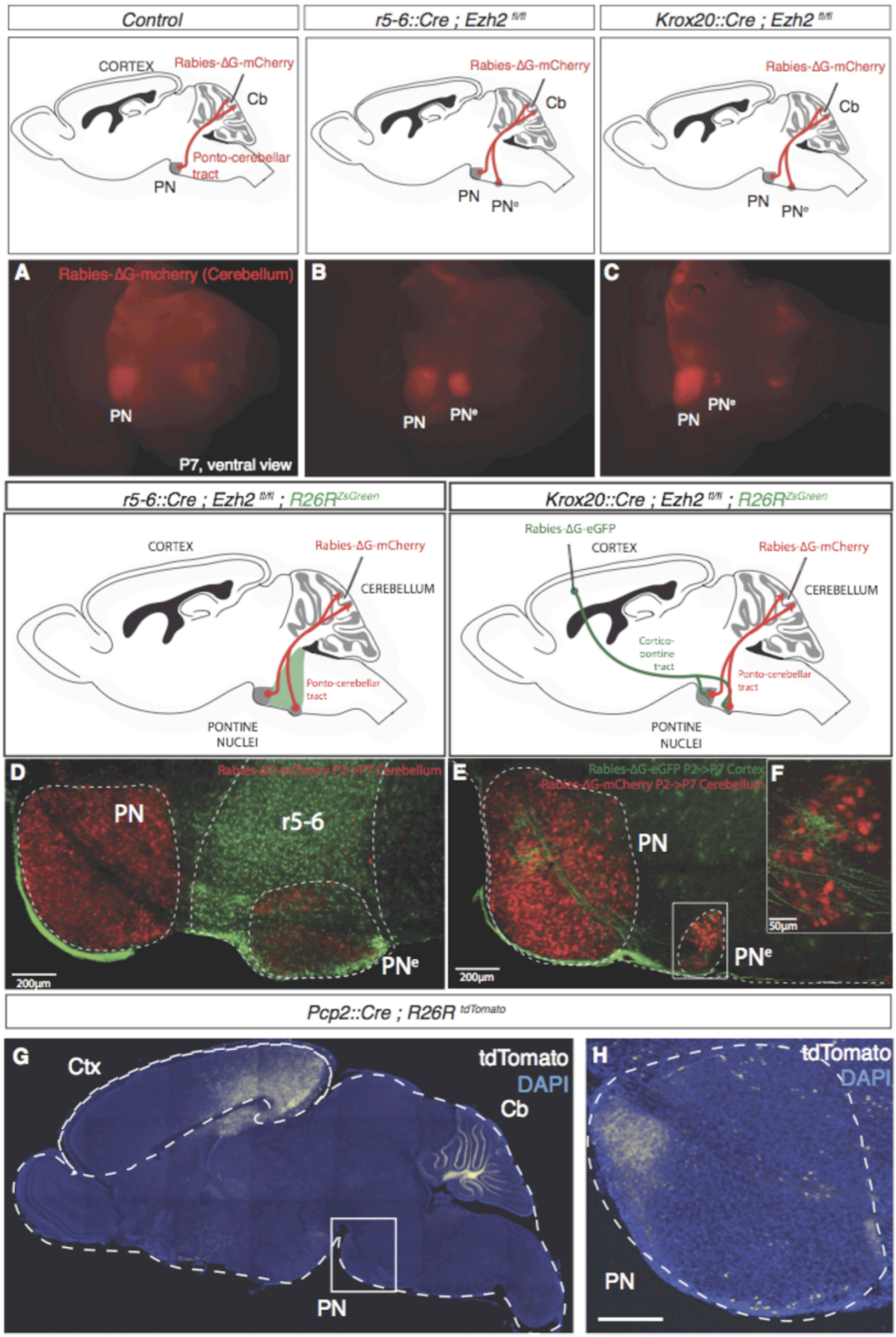
Control
r5-6::Cre ; Ezh2 fl/fl
Krox20::Cre ; Ezh2 fl/fl
CORTEX
Rabies-ΔG-mCherry
Cb
Ponto-cerebellar tract
PN
PNe
A
Rabies-ΔG-mcherry (Cerebellum)
P7, ventral view
B
C
r5-6::Cre ; Ezh2 fl/fl ; R26RZsGreen
Krox20::Cre ; Ezh2 fl/fl ; R26RZsGreen
Rabies-ΔG-eGFP
CEREBELLUM
Cortico-pontine tract
PONTINE NUCLEI
D
Rabies-ΔG-mCherry P2->P7 Cerebellum
r5-6
200µm
E
Rabies-ΔG-eGFP P2->P7 Cortex
F
50µm
Pcp2::Cre ; R26R tdTomato
G
Ctx
tdTomato
DAPI
H

16

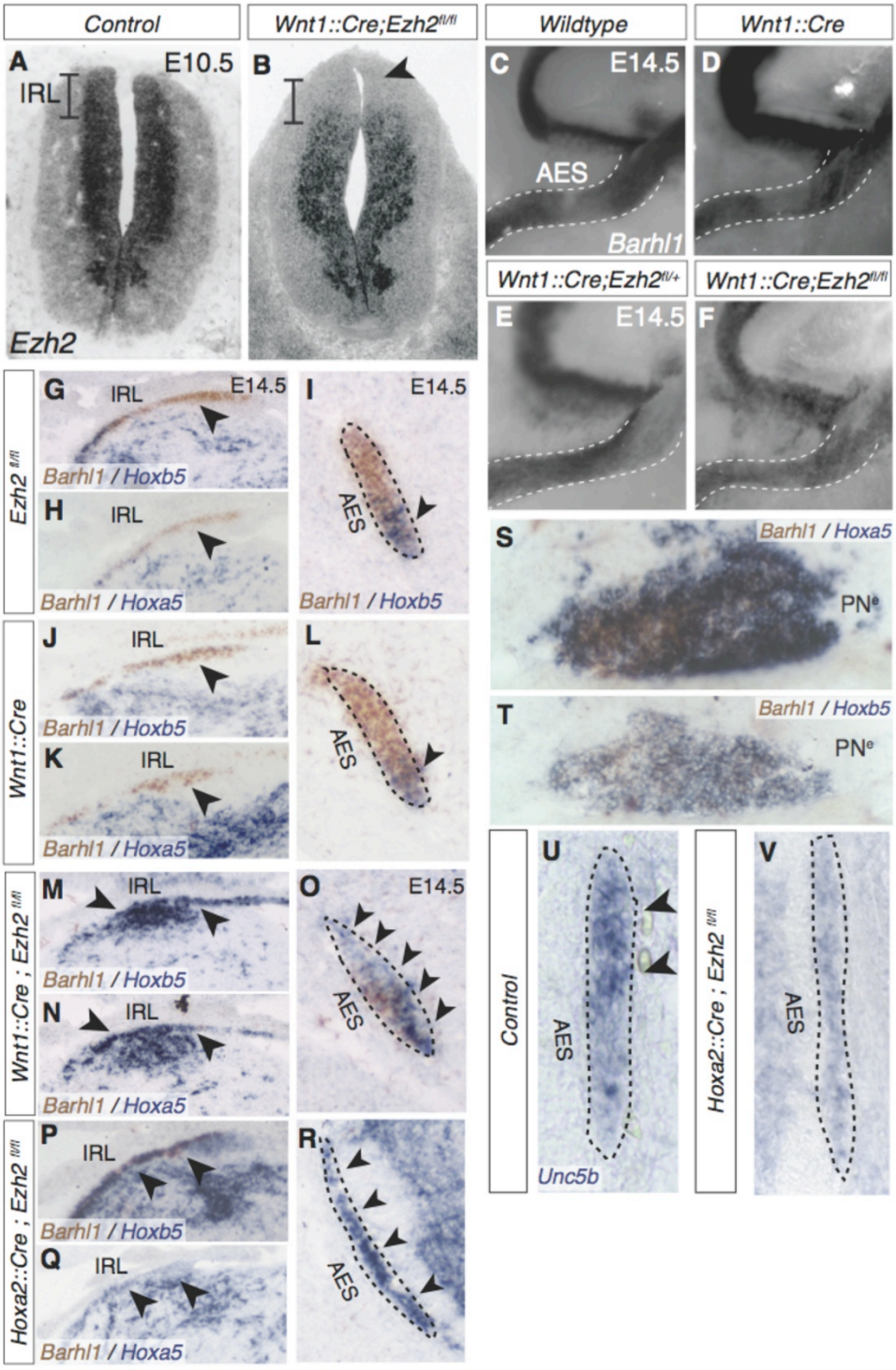

Fig. S7. ***Ezh2*** **cell-autonomous role in rhombic lip and pontine neurons**. (**A** to **B**) *Ezh2* is downregulated in the lower rhombic lip (lRL) of *Wnt1::Cre Ezh2*$^{fl/fl}$ embryos at E10.5 (B, arrowhead) compared to controls (A). (**C** to **F**) Lateral views of *Barhl1*$^{+}$

Fig. S6. Cortico-ponto-cerebellar connectivity in *Ezh2* conditional mutants. (**A** to **C**) Ventral views of P7 whole-mount hindbrains after retrograde tracing with rabies-ΔG-mCherry from cerebellum (Cb) show that Cb is innervated by normal pontine nuclei (PN) in control (A) and both PN and ectopic pontine nuclei (PN^e) in *Krox20::Cre;Ezh2$^{fl/fl}$* (B) and *r5-6::Cre;Ezh2$^{fl/fl}$* (C) mutants. (**D**) Retrograde injections in P7 *r5-6::Cre;Ezh2$^{fl/fl}$;R26R^{ZsGreen}* animals show that PN^e is included within the $ZsGreen^+$ domain demonstrating PN^e localization in posterior r5/r6 as well as the duplication of both parts of the PN, i.e. reticulotegmental nucleus (inner nucleus) and pontine gray nucleus (outer nucleus). (**E** to **F**) Cortical injections of rabies-ΔG-GFP combined with retrograde cerebellar tracing (rabies-ΔG-mCherry) illustrate that in P7 *Krox20::Cre;Ezh2$^{fl/fl}$* pups, PN^e (F) is also integrated into cortico-ponto-cerebellar connectivity. Injections were carried out at P2 and analyzed at P7. (**G** to **H**) Restricted *tdTomato$^+$* cells in posterior/visual cortex (Ctx) in P7 *Pcp2::Cre;R26R^{tdTomato}* pups (G) and *tdTomato$^+$* axon projection to anterior PN in sagittal sections (H).

anterior extramural stream (AES) in E14.5 wild type (C), *Wnt1::Cre* (D), *Wnt1::Cre*;*Ezh2*$^{fl/+}$ (E), and *Wnt1::Cre*;*Ezh2*$^{fl/fl}$ (F) conditional mutant whole-mount hindbrains. (**G** to **R**) Co-detection of *Hoxb5* and *Barhl1* (G,I,J,L,M,O,P,R) and *Hoxa5* and *Barhl1* (H,K,N,Q) expression on coronal sections from E14.5 embryos (G-I, *Ezh2fl/fl*; J-L, *Wnt1::Cre*), *Wnt1::Cre:Ezh2*$^{fl/fl}$ (M-O) and *Hoxa2::Cre:Ezh2*$^{fl/fl}$ (P-R) at anterior precerebellar lRL (G,H,J,K,M,N,P,Q) and AES levels (I,L,O,R). In controls *Hoxa5* and *Hoxb5* transcript is absent from the anterior precerebellar lRL (arrowheads, G,H,J,K) and restricted to the ventral AES (I,L). In both *Wnt1::Cre:Ezh2*$^{fl/fl}$ and *Hoxa2::Cre:Ezh2*$^{fl/fl}$ conditional knockouts, *Hoxa5* and *Hoxb5* are expressed ectopically in the anterior precerebellar lRL (arrowheads, M,N,P,Q) and throughout the AES (arrowheads, O,R), while expression is regionalized in controls (arrowheads, H,J). (**S** to **T**) Co-detection of *Hoxa5 (S), Hoxb5 (T)* and *Barhl1 (S,T)* transcripts in E18.5 *Hoxa2::Cre:Ezh2*$^{fl/fl}$ ectopic pontine nuclei (PN^{e}) on sagittal sections. (**U** to **V**) Dorsal *Unc5b* expression at E14.5 in coronal control AES (U), as compared to *Hoxa2::Cre Ezh2*$^{fl/fl}$ AES (V) showing *Unc5b* downregulation. PN: pontine nuclei.

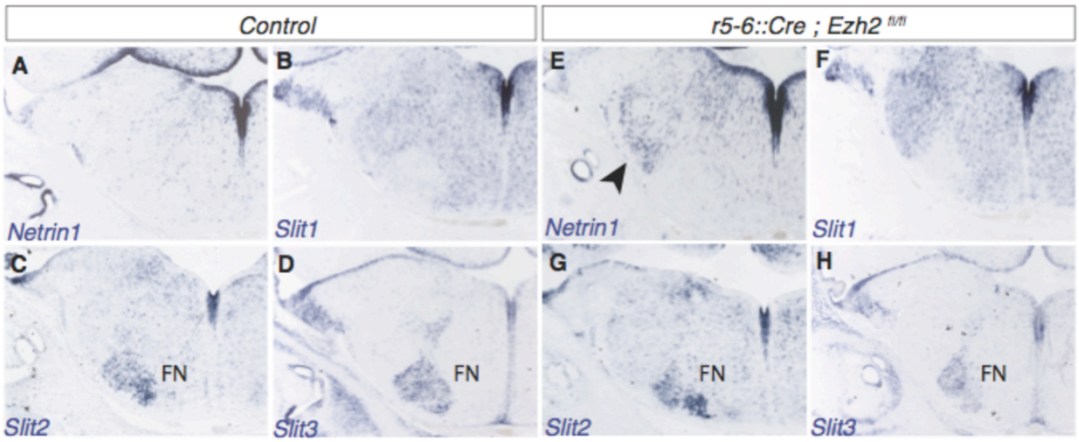

Fig. S8. ***Slit1-3*** **expression patterns in conditional** ***Ezh2*** **mutants.** (**A** to **H**) *In situ* hybridization for *Netrin1* (A,E), *Slit1* (B,F), *Slit2* (C,G) and *Slit3* (D,H) on adjacent coronal sections at r5-r6 level in E14.5 control (A-D) and *r5-6::Cre;Ezh2*$^{fl/fl}$ (E-H). *Netrin1* is ectopically expressed in *r5-6::Cre;Ezh2*$^{fl/fl}$ (arrowhead, E). FN: facial motor nucleus

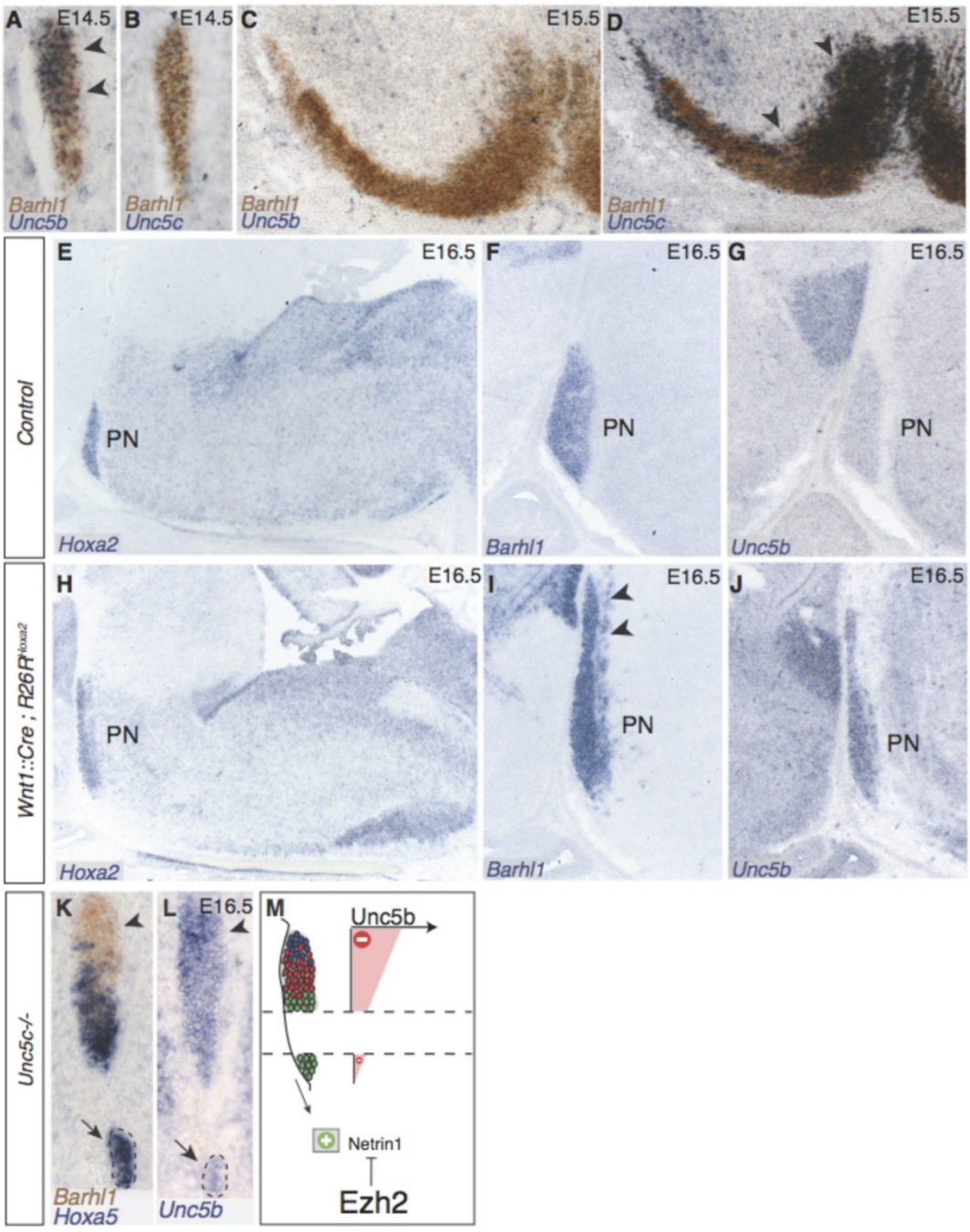

Fig. S9. *Unc5b* and *Unc5c* expression during normal pontine neuron migration and in *Wnt1::Cre;R26R*^{Hoxa2} mutants. (**A** to **D**) Double *in situ* hybridizations for *Barhl1*/*Unc5b* (A,C) and *Barhl1*/*Unc5c* (B,D) on coronal sections at E14.5 (A,B) and E15.5 (C,D). *Unc5b* transcripts are detected in the dorsal part of the anterior extramural stream (AES) (arrowheads, A) and become undetectable in *Barhl1*$^{+}$ neurons reaching the ventral midline (C). On the contrary, *Unc5c* transcript expression is undetectable in AES neurons (B) while is reactivated during the second phase of ventral migration

(arrowheads, D). (**E** to **J**) *In situ* hybridization for *Hoxa2* (E,H), *Barhl1* (F,I) and *Unc5b* (G,J) on E16.5 sagittal sections in controls (E-G) and *Wnt1::Cre;R26R*^{Hoxa2} embryos (H-J). In the latter, pontine nuclei (PN) are anteriorly extended (arrow, I) and overexpress *Unc5b* (J), which is undetectable in control E16.5 PN (G). (**K** to **M**) *Hoxa5*/*Barhl1* (K) and *Unc5b* (L) expression in E16.5 *Unc5c*$^{-/-}$ AES. Ectopically migrating neurons (arrows) strongly express *Hoxa5* while do not express *Unc5b*, as summarized in (M).

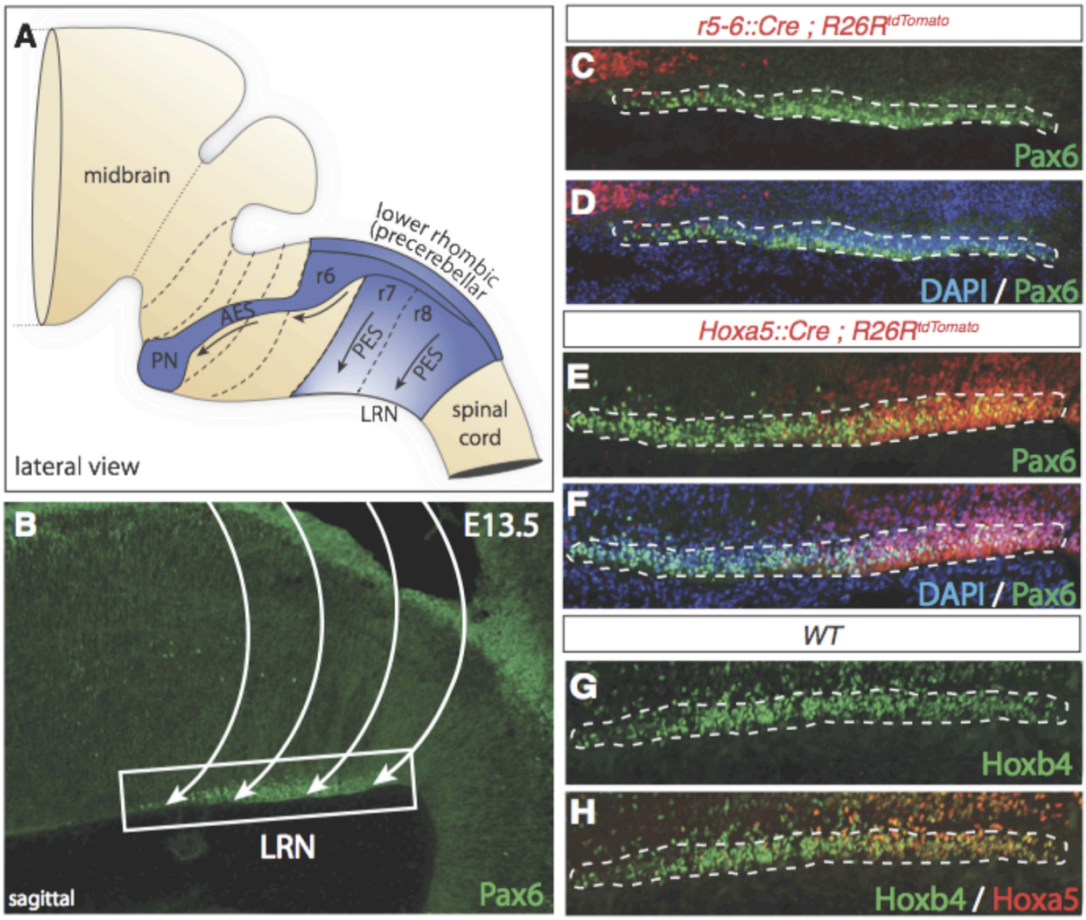

Fig. S10. Topographic organization of migrating lateral reticular nucleus. (**A** to **B**) Lateral reticular nucleus (LRN) neurons originate as the pontine nuclei (PN) from the lower rhombic lip (A) and migrate extramurally to the contralateral side. The migratory stream can be visualized by Pax6 immunostaining on E13.5 sagittal sections (B). (**C** to **D**) Pax6/DAPI double immunohistochemistry on sagittal sections of *r5-6::Cre;R26R*^{tdtomato} embryos at E13.5 showing that LRN neurons lack r5-6 derived progeny. (**E** to **F**) Pax6/DAPI double immunohistochemistry on sagittal sections of *Hoxa5::Cre;R26R*^{tdtomato} embryos at E13.5 showing that posterior LRN neurons are contributed by *Hoxa5::Cre;R26R*^{tdtomato} positive cells. (**G** to **H**) Immunohistochemistry for Hoxb4 (G) and Hoxa5 (H) in migrating LRN neurons on sagittal sections show the posterior restriction of Hoxa5 (H) positive cells. PES: posterior extramural stream; AES: anterior extramural stream.

References and Notes:

1. A. Lumsden, R. Krumlauf, Patterning the vertebrate neuraxis, *Science* **274**, 1109–1115 (1996).

2. S. Tümpel, L. M. Wiedemann, R. Krumlauf, Hox genes and segmentation of the vertebrate hindbrain, *Curr. Top. Dev. Biol.* **88**, 103–137 (2009).

3. A. F. Farago, R. B. Awatramani, S. M. Dymecki, Assembly of the brainstem cochlear nuclear complex is revealed by intersectional and subtractive genetic fate maps, *Neuron* **50**, 205–218 (2006).

4. J. Altman, S. A. Bayer, Development of the precerebellar nuclei in the rat: IV. The anterior precerebellar extramural migratory stream and the nucleus reticularis tegmenti pontis and the basal pontine gray, *J Comp Neurol* **257**, 529–552 (1987).

5. C. I. Rodriguez, S. M. Dymecki, Origin of the precerebellar system, *Neuron* **27**, 475–486 (2000).

6. M. J. Geisen *et al.*, Hox paralog group 2 genes control the migration of mouse pontine neurons through slit-robo signaling, *PLoS Biol* **6**, e142 (2008).

7. K. T. Yee, H. H. Simon, M. Tessier-Lavigne, D. M. O'Leary, Extension of long leading processes and neuronal migration in the mammalian brain directed by the chemoattractant netrin-1, *Neuron* **24**, 607–622 (1999).

8. S. Nóbrega-Pereira, O. Marín, Transcriptional control of neuronal migration in the developing mouse brain, *Cerebral Cortex* **19**, i107–13 (2009).

9. R. Margueron, D. Reinberg, The Polycomb complex PRC2 and its mark in life, *Nature* **469**, 343–349 (2011).

10. Materials and methods are available as supplementary material on Science Online.

11. E. Bloch-Gallego, F. Ezan, M. Tessier-Lavigne, C. Sotelo, Floor plate and netrin-1 are involved in the migration and survival of inferior olivary neurons, *J Neurosci* **19**, 4407–4420 (1999).

12. K. Hong *et al.*, A ligand-gated association between cytoplasmic domains of UNC5 and DCC family receptors converts netrin-induced growth cone attraction to repulsion, *Cell* **97**, 927–941 (1999).

13. D. Kim, S. L. Ackerman, The UNC5C netrin receptor regulates dorsal guidance of mouse hindbrain axons, *J Neurosci* **31**, 2167–2179 (2011).

14. X. Lu *et al.*, The netrin receptor UNC5B mediates guidance events controlling morphogenesis of the vascular system, *Nature* **432**, 179–186 (2004).

15. T. B. Leergaard, J. G. Bjaalie, Frontiers: Topography of the complete corticopontine projection: From experiments to principal maps, *Frontiers in neuroscience* **1**, 211–223 (2007).

16. P. Rakic, Specification of cerebral cortical areas, *Science* **241**, 170–176 (1988).

17. M. E. Hatten, Central nervous system neuronal migration, *Annu Rev Neurosci* **22**, 511–539 (1999).

18. E. C. Lee *et al.*, A highly efficient Escherichia coli-based chromosome engineering system adapted for recombinogenic targeting and subcloning of BAC DNA, *Genomics* **73**, 56–65 (2001).

19. T. O. Yau *et al.*, Auto/cross-regulation of Hoxb3 expression in posterior hindbrain and spinal cord, *Dev Biol* **252**, 287–300 (2002).

20. M. Manzanares *et al.*, Conserved and distinct roles of kreisler in regulation of the paralogous Hoxa3 and Hoxb3 genes, *Development* **126**, 759–769 (1999).

21. A. Gould, N. Itasaki, R. Krumlauf, Initiation of rhombomeric Hoxb4 expression requires induction by somites and a retinoid pathway, *Neuron* **21**, 39–51 (1998).

22. P. Soriano, Generalized lacZ expression with the ROSA26 Cre reporter strain, *Nat Genet* **21**, 70–71 (1999).

23. L. Madisen *et al.*, A robust and high-throughput Cre reporting and characterization system for the whole mouse brain, *Nat Neurosci* **13**, 133–140 (2010).

24. M. Studer, A. Lumsden, L. Ariza-McNaughton, A. Bradley, R. Krumlauf, Altered segmental identity and abnormal migration of motor neurons in mice lacking Hoxb-1, *Nature* **384**, 630–634 (1996).

25. F. M. Rijli *et al.*, A homeotic transformation is generated in the rostral branchial region of the head by disruption of Hoxa-2, which acts as a selector gene, *Cell* **75**, 1333–1349 (1993).

26. O. Nyabi *et al.*, Efficient mouse transgenesis using Gateway-compatible ROSA26 locus targeting vectors and F1 hybrid ES cells, *Nucleic Acids Res* **37**, e55–e55 (2009).

27. P. S. Danielian, D. Muccino, D. H. Rowitch, S. K. Michael, A. P. McMahon, Modification of gene activity in mouse embryos in utero by a tamoxifen-inducible form of Cre recombinase, *Curr Biol* **8**, 1323–1326 (1998).

28. M. Puschendorf *et al.*, PRC1 and Suv39h specify parental asymmetry at constitutive heterochromatin in early mouse embryos, *Nat Genet* **40**, 411–420 (2008).

29. D. C. McIntyre *et al.*, Hox patterning of the vertebrate rib cage, *Development* **134**, 2981–2989 (2007).

30. S. L. Ackerman *et al.*, The mouse rostral cerebellar malformation gene encodes an UNC-5-like protein, *Nature* **386**, 838–842 (1997).

31. P. M. Lewis, A. Gritli-Linde, R. Smeyne, A. Kottmann, A. P. McMahon, Sonic hedgehog signaling is required for expansion of granule neuron precursors and patterning of the mouse cerebellum, *Dev Biol* **270**, 393–410 (2004).

32. P. M. Lewis *et al.*, Cholesterol modification of sonic hedgehog is required for long-range signaling activity and effective modulation of signaling by Ptc1, *Cell* **105**, 599–612 (2001).

33. K. Yonehara *et al.*, Spatially asymmetric reorganization of inhibition establishes a motion-sensitive circuit, *Nature* **469**, 407–410 (2011).

34. H. Taniguchi, D. Kawauchi, K. Nishida, F. Murakami, Classic cadherins regulate tangential migration of precerebellar neurons in the caudal hindbrain, *Development* **133**, 1923–1931 (2006).

35. T. Okada, K. Keino-Masu, M. Masu, Migration and nucleogenesis of mouse precerebellar neurons visualized by in utero electroporation of a green fluorescent protein gene, *Neurosci Res* **57**, 40–49 (2007).

36. F. Llambi *et al.*, The dependence receptor UNC5H2 mediates apoptosis through DAP-kinase, *EMBO J* **24**, 1192–1201 (2005).

37. E. D. Leonardo *et al.*, Vertebrate homologues of C. elegans UNC-5 are candidate netrin receptors, *Nature* **386**, 833–838 (1997).

Conclusion and outlook

The regulatory mechanisms establishing and modulating the epigenome at a system level represent a remarkable example of complexity and importance in nearly all biological processes. It is therefore not surprising that genetic mutations compromising the function of key epigenetic regulators result in a disruption of properly ordered neuronal migration, or insults to the brain severe enough to precipitate epilepsy produce major changes. The epigenetic of epilepsy and homeostatic synaptic scaling is at the very beginning of its long way. Aberrant patterns of epigenetic modification could, and most likely do, affect gene expression and play an important role into disease pathogenesis or with the inability to cope with sustained increased levels of excitation, both at a micro-circuit level and within long range circuitries, such as talamo-cortical or cortico-spinal projections. These disregulated mechanisms could therefore be important in the maintenance of the chronic status epilepticus. Affected genes are likely to be involved in normal neuronal homeostasis, excitability, cell survival, and inflammatory processes (Henshall)[1]. There is in fact evidence to support each of the major epigenetic processes as being possibly involved in epilepsy. Research has also shown that these are causally important in some cases, contributing to both beneficial adaptive changes to reduce excitability as well as maladaptive pathogenic changes. As extensively discuss in the introductory chapter of this work, it is of note that a number of genetic disorders that arise because of mutations in genes encoding epigenetic proteins have clinical phenotypes that include epilepsy. Remarkable for the analogy to our work, is the recent discovery that Auts2 is able to reverse PRC1 activity, turning this classically believed repressive complex into an activator of transcription. In testis, Scml2 has

shown a similar potential by its association with Usp7. Together in fact this complex counteracts the ubiquitilation of histone 2A at lysine 119. Much work still has to be done to understand SCML2 function in the brain. Nevertheless, our work on excitability, plus the discovery that *L3MBTL1* is responsible for homeostatic synaptic downscaling in excitatory neurons (Mao and Futai, Proceedings of the Society for Neuroscience, SfN 2015 Abstract), and together with the discovery that several genes, including *SCML2* and *L3MBTL1,* are found mutated in glioblastoma, provide a solid ground for future discoveries. It indeed seems that Polycomb protein role in epileptogenesis has been surprisingly ignored, althought leads exist now since several years on their involvement in such processes. Given the broad function of this class of epigenetic regulators, changes in their expression and function in epilepsy cannot be always assumed to relate to their role in epigenetic processes[1]. Notably, several neurological disorders related to errors or failure of genetic imprinting feature high rates of epilepsy, including Angelman syndrome, making the possible role of these proteins as fascinating as hard to be fully understood.

Most importantly, a key open question remains unsolved and should be the very next one to be tackled: to which extent do altered epigenetic states causally lead to impaired inhibition excitation balance, rather than being a pure consequence, at the cellular level, of a disregulated circuit disorder? Or in other words, can we experimentally separate the causal versus the neuroprotective components of epigenetic adaptation to neuronal excitability?

Unraveling the combinatorial complexity of the altered brain epigenome in epilepsyis a task of enormous complexity. These challenges are not unique to epilepsy and must be determined in the field of neuroepigenetics[2], along with the potential to realize therapeutic manipulation of epigenetics for brain disorders, such as epilepsy.

References

1. Henshall, D. C. & Kobow, K. Epigenetics and Epilepsy. *Cold Spring Harb Perspect Med* (2015). doi:10.1101/cshperspect.a022731
2. Sweatt, J. D. Perspective. *Neuron* **80,** 624–632 (2013).